GLOBAL INVERSION TECHNIQUE FOR GEOTECHNICAL ENGINEERING APPLICATIONS

By

KHIEM TAT TRAN

A DISSERTATION PRESENTED TO THE GRADUATE SCHOOL
OF THE UNIVERSITY OF FLORIDA IN PARTIAL FULFILLMENT
OF THE REQUIREMENTS FOR THE DEGREE OF
DOCTOR OF PHILOSOPHY

UNIVERSITY OF FLORIDA

2010

To my parents, whose lifetimes of hard work have made mine easier

ACKNOWLEDGMENTS

First of all, I would like to express my sincere gratitude to my advisor, Dr. Dennis R. Hiltunen. His valuable support, encouragement, and guidance during my doctoral research were what made this possible. I have benefited tremendously from his experience and research methodology. He has provided for me not only his knowledge but also his kind consideration. I thank the other members of my committee, Dr. Reynaldo Roque, Dr. Michael McVay, and Dr. Ashok V. Kumar for their valuable comments and suggestions.

I would like to thank my parents for encouraging my studies. I deeply thank my wife who has supported my decisions and the results of those decisions for the past few years, and my son who has given me emotion to overcome all difficulties of my studies. Lastly, I extend thanks to all of my friends who treated me like family.

TABLE OF CONTENTS

LIST OF FIGURES

Abstract of Dissertation Presented to the Graduate School
of the University of Florida in Partial Fulfillment of the
Requirements for the Degree of Doctor of Philosophy

GLOBAL INVERSION TECHNIQUE FOR GEOTECHNICAL ENGINEERING APPLICATIONS

By

Khiem Tat Tran

August 2010

Chair: Dennis R. Hiltunen
Major: Civil Engineering

Standard methods using seismic waves, which are routinely used for shallow subsurface investigation in engineering, have limitations in characterizing challenging profiles that include low-velocity layers and embedded cavities. The limitations are often due to insensitivity of data used for inversion and pitfalls of local inversion schemes employed in these methods. This research focuses on overcoming these limitations by developing two new methods using both sensitive data and a global inversion scheme, simulated annealing.

The first method is an inversion technique to invert travel times for a wave velocity profile. The technique is based on an extremely fast finite-difference solution of the Eikonal equation to compute the first-arrival time through the velocity models by the multi-stencils fast marching method. The core of the simulated annealing, the Metropolis sampler, is applied in cascade with respect to shots to significantly reduce computer time. In addition, simulated annealing provides a suite of final models clustering around the global solution and having comparable least-squared error to allow determining uncertainties associated with inversion results. The capability of this inversion technique is tested with both synthetic and real experimental surface data sets. The inversion results show that this technique successfully maps 2-D velocity profiles with high

variation. The inverted wave velocity from the real data appears to be consistent with cone penetration test (CPT), geotechnical borings, and standard penetration test (SPT) results.

Employed for site characterization of deep foundation design, the developed technique is applied to combined surface and borehole data. Using the combined travel time data, the technique enables to provide credible information of material at the socket and partially detect anomalies near the socket. This becomes very important because the material at and near the socket often carries a majority of load from foundations. The inversion results of the combined data, including inverted profiles and associated uncertainties, enable to characterize spatial variability in geotechnical engineering physical parameters of subsurface formations useful in the design of deep foundations. This will be particularly useful in implementing the new LRFD design methodology that can explicitly account for spatial variability and uncertainty in design parameters.

The second method is an inversion technique to invert full waveforms for a wave velocity profile. The full waveform inversion scheme is based on a finite-difference solution of 2-D elastic wave equation in the time distance domain. The strength of this approach is the ability to generate all possible wave types (body waves and surface waves, etc.) and thus to simulate and accurately model complex seismic wave fields that are then compared with observed data to infer complex subsurface properties. The capability of this inversion technique is also tested with both synthetic and real experimental data sets. The inversion results from synthetic data show the ability of detecting reverse models that are hardly detected by traditional inversion methods that use only dispersion property of Rayleigh waves. The inversion result from the real data is generally consistent with the cross-hole, SPT N-value, and material log results.

CHAPTER 1
INTRODUCTION

1.1 Problem Statement

Near surface soil conditions control the responses of foundations and structures to earthquake and dynamic motions. To get the optimum engineering design, the modulus of underlying layers must be determined correctly. A popular method to obtain modulus is nondestructive in situ testing. The measured elastic wave fields carry substantial information about characteristics of media they propagate in, and wave evaluation techniques use this information to infer the properties of media. There are many techniques that are routinely used for shallow subsurface investigation, such as techniques using wave velocity dispersion, including spectral analysis of surface waves (SASW) (Nazarian, 1984), multi-channel analysis of surface waves (MASW) (Park, et al., 1999), refraction microtremor (ReMi) (Louie, 2001), and passive-source frequency-wavenumber (f-k), and techniques using travel times, including conventional seismic refraction and seismic refraction tomography (SRT). However, these standard techniques utilized in current engineering evaluations have limitations in dealing with challenging profiles, which include anomalies such as low-velocity zones and cavities. The limitations of these methods are generally caused by: 1) insensitivity of data used for inversion, and 2) shortcomings of local inversion techniques often employed in these methods.

Regarding the insensitivity of data, standard techniques usually use only a limited portion of information carried by elastic wave fields, such as travel times or wave velocity dispersion. Synthetic tests in this research prove that surface travel times are not very sensitive to the anomalies. Thus, the anomalies are not well detected if using only surface travel times. For the techniques using wave velocity dispersion, O'Neill (2003) found that a low-velocity layer (LVL) of few meters thickness buried at depth of a few meters can not be inverted with confidence, due

to loss of sensitivity with depth. In addition, the dispersion property is absolutely insensitive to lateral variation, thus techniques using wave velocity dispersion are only for 1-D problems and can not be applied in regions with high lateral variation.

Regarding the shortcomings of local inversion techniques, geotechnical inversion problems are typically highly non-linear, non-unique, and influenced by inherent noise in measured data. Results from any local inversion technique heavily depend on the initial model and priori information. In order to obtain a good inversion result, these local techniques require both a reasonable initial model and priori information that are not always available. In addition, it does not guarantee that the model corresponding to the smallest error (best fitting) is closest to the true model because of the noise and non-uniqueness of inverted solutions. Any of many thousand models that have a similar degree of fitting can be the inversion result. The question here is how to decide which model is the best and the uncertainty associated with that model.

This research focuses on overcoming the aforementioned limitations by developing new methods using both sensitive data and global inversion schemes. Firstly, data sensitive to anomalies, such as borehole data will be utilized to improve resolution of travel time inversion results. By using borehole data, it is possible to increase depth of investigation, to reduce the uncertainty associated with inversion result, and to improve resolution of inverted profiles. Secondly, full waveform data will be also utilized to solve 2-D reverse problems when the borehole data is not available. The reason to use the full waveform data instead of the wave velocity dispersion is that it is more sensitive to the anomalies. Lastly, global optimization schemes based on simulated annealing will be employed in both travel time and full waveform inversions. These global techniques do not depend on the initial model and become important in regions where no prior information about subsurface profiles is available.

1.2 Hypothesis

Global inversion techniques using sensitive data such as borehole travel times or full waveforms can characterize subsurface profiles better than traditional techniques that use only surface travel times or dispersion property.

1.3 Objectives

The primary objective of the research is to develop inversion techniques that can well characterize challenging profiles with requirement of a little or no priori information, and can also evaluate the uncertainties associated with the inverted profiles. Specific objectives of this research include the following:

- Develop a global inversion technique to invert travel times for a velocity structure. The technique is independent of initial model, and thus can be applied in regions where no priori information is available.
- Determine the uncertainty associated with the inverted profile from travel times. This uncertainty represents the influence of noise in measured data and non-uniqueness of inversion solution.
- Incorporate borehole data into a travel time inversion to improve the resolution of the inverted profile and reduce the associated uncertainty.
- Develop another global inversion technique using a full waveform. This technique is primarily used when borehole data is not available, particularly for cases of reverse velocity structures.

1.4 Scope

Non-destructive tests including refraction test, full waveform test and/or invasive tests including con penetration test (CPT), geotechnical borings, standard penetration test (SPT), and cross-hole test were conducted at three test sites:

- A National Geotechnical Experiment site (NGES) at Texas A & M University (TAMU).
- A Florida Department of Transportation (FDOT) storm water runoff retention basin in Alachua County off of state road 26, Newberry, Florida.
- A test site near Ft. McCoy, Ocala, Florida.

Two inversion techniques, which use travel times and full waveforms, have been developed and intensively tested on synthetic models before being applied to real test data. For the technique using travel times, it is first tested on many synthetic models that were previously tested on three commercial refraction tomography codes by Sheehan et al. (2005) to verify its capability, and then applied to many real data sets. The inverted profiles from non-destructive data are compared to CPT, SPT, and geotechnical borings results to appraise its feasibility for geotechnical engineering applications.

Similarly, the technique using full waveforms is first tested on challenging 1-D and 2-D synthetic models that include low- and high-velocity layers to verify its capability of dealing with reverse profiles, and then applied to real test data. The inverted results from the real test data are also compared to SPT, cross-hole test, and refraction test results for partially appraising the accuracy of those inverted results.

1.5 Organization of Dissertation

An overview of the following chapters follows. Chapter two provides an overview of site characterization methods using seismic waves, limitations of these standard methods, and suggested improvements.

Chapter three presents a global inversion technique to invert travel times using simulated annealing. The technique is described in details including forward modeling, optimization method, and its applications to synthetic and real test data sets. In this chapter, only travel times measured on the surface are used for inversion, and inverted results are compared to invasive test results to appraise the capability of the inversion technique.

Chapter four demonstrates the coupling of so-called down-hole and refraction tomography technique, which uses combined bore-hole and surface travel times. Comparisons of inversion results utilizing the combined data against results developed using just the surface data are

presented to both quantitatively and qualitatively appraise the benefit when adding data from a borehole. The focus here is to detect voids in rock that may be filled by air, water or soil.

Chapter five presents another inversion technique to invert full waveforms using simulated annealing. This technique is also described in details including forward modeling, optimization method, and its applications to synthetic and real test data sets. The primary applications of this technique are for reverse profiles when the borehole data is not available.

CHAPTER 2
SITE CHARACTERIZATION METHODS USING SEISMIC WAVES

2.1 Seismic Waves

A wave is a perturbation that travels in a medium and carries energy (Doyle, 1995). Waves propagate in a medium can be divided into two categories: body waves and surface waves, whose particle motions are presented in Figure 2-1. Body waves that propagate in the interior of a medium include longitudinal waves (P-wave) and shear waves (S-wave). P-waves generate compression or dilatational particle motions parallel to the direction of propagation, and S-waves generate particle motions perpendicular to the direction of propagation. Unlike body waves, surface waves only propagate in a shallow zone near a free surface. They are essentially of two different kinds: Love waves and Rayleigh waves. Love waves only exist when a medium consists of a soft superficial zone over a stiffer zone, and the particle motions associated with them are transversal with respect to the direction of propagation. Rayleigh waves always exist near a free surface, and their particle motions consist of vertical and horizontal components that are exactly 90^0 out of phase, and thus the particle motion path is an ellipse.

Many techniques for soil characterization at very small strain levels are based on measurements of particle motions associated to wave propagation. This is made possible because of strong links existing between wave propagation characteristics and mechanical properties of the medium that need to be characterized. These links are between wave velocities and elastic moduli as:

$$G \equiv \mu = \rho V_S^{\ 2} \tag{2-1}$$

$$\lambda = \rho(V_P^{\ 2} - 2V_S^{\ 2}) \tag{2-2}$$

$$E = \frac{\mu(3\lambda + 2\mu)}{\lambda + \mu} \tag{2-3}$$

where V_P, V_S are P-wave and S-wave velocities, μ, λ are Lame's parameters, G, E are shear and young's moduli, and ρ is density.

2.2 Site Characterization Methods Using Seismic Waves

2.2.1 Goals of Seismic Wave Methods

The primary goal of site characterization methods using seismic waves is to determine elastic modulus of subsurface materials. The modulus is used either directly in design of engineering substructures or as an indication to delineate anomalies such as voids, low-velocity zones embedded in the subsurface profiles.

2.2.2 Borehole Methods

Borehole methods include seismic down-hole and cross-hole methods (Figure 2-2). Down-hole tests can perform in a single borehole. In the down-hole test, an impulsive source is located on the surface, a single receiver that can move or a string of receivers are fixed to the walls of the borehole to measure the wave fields from the source. A plot of travel time versus depth can be generated, and the slope of the travel time curve represents the wave velocity at depth for a 1-D soil profile.

Cross-hole tests use two (three) boreholes. A source and one (two) receiver are located at the same depth in the boreholes, and the wave propagation velocity of the material between the boreholes at that depth is measured. By testing at various depths, a 1-D velocity profile is obtained.

The borehole methods can be used to obtain credible 1-D velocity profiles. However, these methods are not popular as surface methods because of the requirement of boreholes and difficulties in measurements.

2.2.3 Surface Methods

Unlike borehole methods, surface methods are attractive to researchers because the measurements on the surface are relatively easy, and the measured signals carry important information about the mechanical properties of the medium. These methods have been intensively developed and routinely used for geotechnical site characterization in last few decades. They are roughly categorized into two groups: methods using travel times and methods using wave velocity dispersion.

2.2.3.1 Methods using surface travel times

Methods using surface travel times are often referred as seismic refraction methods including conventional methods and seismic refraction tomography (SRT). The seismic refraction methods consist of measuring data at a test site, picking travel times from the measured data, and doing inversion to invert the travel times for a subsurface wave velocity profile. Figure 2-3 presents a test setup, picked travel times, and inverted velocity tomogram of a typical seismic refraction tomography.

A data measurement is conducted at known points along the surface to obtain a seismic wave field generated by an energy source. The energy source is usually generated by a small explosive charge or accelerated weight drop, such as a sledgehammer. Energy that propagates out from the source, either travels directly through the upper layer, known as a direct arrival, or travels down to and laterally along a lower high velocity layer, known as a refracted arrival. This energy is detected on the surface using receivers arranged in a linear array, and travel times are derived by manually picking the first-arrival signals. The travel times are then used in an inversion to generate a velocity profile of the subsurface along the length of the refraction profile relying upon the assumption that the velocity of the subsurface material increases with depth.

During the inversion, while the conventional methods divide the model into continuous layers of constant velocity, SRT divides the model into a large number of smaller constant velocity grid cells or nodes. The model is adjusted each iteration in attempt to match the calculated travel times with the measured as closely as possible. This is repeated until the pre-defined stop criterion is achieved, and the inverted profile is then derived.

2.2.3.2 Methods using surface wave dispersion

Two most popular methods using dispersion property of measured wave fields are spectral analysis of surface waves (SASW) (Nazarian, 1984) and multi-channel analysis of surface waves (MASW) (Park, et al., 1999). They both consist of three steps: measuring data from a test site, processing the measured data to obtain a dispersion curve, and doing inversion to invert the dispersion curve for a subsurface shear wave velocity profile. Figure 2-4 presents a test setup, a typical dispersion curve, and an inverted velocity profile of SASW. For MASW, multiple geophones are used instead of two; the dispersion data and inverted velocity profile are similar to those of SASW.

For the first step, a wave field from an active source is measured by two geophones (SASW) or multiple geophones (MASW). The geophones are located far enough from the source in order to get dominant components of Rayleigh waves in the measured wave field. For the second step, a cross power spectrum analysis (SASW) or a multi-channel data processing method (MASW) is applied to the measured wave field to obtain dispersion property. The measured wave field is here decomposed into components of different frequencies, and phase velocity of each component is calculated to establish a dispersion curve that is used as experimental data for an inversion in the last step.

Inversion of the dispersion curve is a process for determining a shear wave velocity profile from frequency-phase velocity dispersion relationship. This process consists of evaluation of a

theoretical dispersion curve for an assumed profile and comparison with the experimental dispersion curve. When the theoretical dispersion curve and the experimental dispersion relatively match, the assumed profile is the desired solution. The assumed profile is composed of horizontal layers that are homogeneous, isotropic and the shear velocity in each layer is constant and does not vary with depth. The theoretical dispersion curve calculation is often based on the matrix formulation of wave propagation in layered media given by Thomson (1950).

Besides methods using the dispersion property of active wave fields, there are also methods using the dispersion property of passive wave fields. Among those, refraction microtremor method (ReMi) (Louie, 2001) and passive-source frequency-wavenumber (f-k) method are more popular. Passive methods also require three steps as those in active methods. First, a wave field that is ambient vibrations is measured by a linear geophones array (ReMi) or a two-dimensional geophones array (f-k). Second, a signal processing method, which is a slowness-frequency transformation (ReMi) or frequency-wavenumber transformation (f-k), is applied to the measured signal to obtain an experimental dispersion curve. Lastly, an inversion technique, which is exactly the same as that of active methods, is used to invert the experimental dispersion curve for a subsurface shear wave velocity profile.

2.3 Overview of the Surface Methods

2.3.1 Overview of Methods Using Surface Travel Times

Conventional refraction methods are useful for a simple profile consisting of a few constant velocity layers with linear interfaces (Sheehan et al., 2005). In this case of sharp contrasts in velocity at the interfaces, the conventional method is more suitable than SRT because of two reasons. First, SRT will always model a sharp contrast in velocity with a gradient in velocity, and second SRT requires that more shots and receivers be used than conventional techniques. This increase in field data collected significantly increases the amount of time

necessary to perform the field testing. The time required to process this data, i.e., make first-arrival picks, and the time required for inversion is also significantly increased.

Seismic refraction tomography is able to resolve velocity gradients and lateral velocity changes within the subsurface with greater ability than conventional methods. As such, SRT may be applied in settings where conventional refraction methods fail, such as areas of compaction, karst, and zone faults (Zhang and Toksoz, 1998).

Carpenter et al. (2003) used SRT programs on sites known to be karstic in Illinois and Kentucky, to determine their accuracy by comparing with known subsurface geology from outcrops, borehole logs, other geophysical methods, and synthetic travel time data. The tomograms seemed to indicate consistency with known geology and borehole information. However, the authors mention problems with artifacts appearing such as pinnacles or cutters in the lower third of the model when too many velocity elements are used. These artifacts may be due to the insensitivity of the surface measured travel times to the deep and small velocity elements. These small elements can be assigned any velocity without changing the surface travel times, thus the artifacts are created as a product of inversion.

Sheehan et al. (2005) investigated the ability of SRT programs for karst terrains that frequently contain sinkholes, irregular and gradational bedrock interfaces, and voids in rocks that may be filled by air, water or soil. They found that SRT performs well in many situations where conventional methods fail, e.g., where vertical and lateral gradients compose a significant component of the velocity structure, and however SRT fails to detect embedded cavities. Again, the surface travel times are not sensitive to the embedded cavities, thus these cavities are hardly detected by surface-based SRT methods.

Hiltunen and Cramer (2008) used SRT to characterize the subsurface at Pennsylvania bridge sites in mantled karst terrain. Refraction profiles generated by commercial software SeisImager were compared with pile tip elevations at driving refusal and drilling data. They found that SRT appears to be able to characterize the soil/rock interface. However, there exists a zone where pile tip elevations are much deeper than the soil/rock interface depth from SRT. This discrepancy is due to the presence of a low-velocity zone, which SRT fails to detect by just using the surface measurements. The failure of detecting the low-velocity zone can be possibly explained as following. The inversion technique of SeisImager is a deterministic method that depends on an initial model, which has velocity increasing with depth. During the inversion, travel times and ray paths of each assumed model are calculated, and only cells having ray paths are updated. It is likely no ray paths go through the area where the low-velocity zone supposes to be, and thus this area is not frequently updated and has the velocity similar to that of the initial model.

2.3.2 Overview of Methods Using Surface Wave Dispersion

For active surface wave methods, SASW and MASW have become very popular in recent years for shallow non-destructive testing of both layered natural (soil and rock) and artificial (pavement and concrete) structures. They typically perform well on normal profiles that have velocity increasing with depth. However, for reverse profiles consisting of both high-velocity and low-velocity layers, these methods need to be used with particular care.

O'Neill (2003) intensively investigated inversion using surface wave dispersion of multiple modes on a variety of models. He found that the most difficult parameters to accurately interpret with the surface wave dispersion are layers below a high-velocity layer (HVL), and a deep (a few meters) buried low-velocity layer (LVL) with a thickness of a few meters can not be inverted with confidence. He also found that for a case of real data from a well characterized test

site, a 5 m thick stiff silt-sand layer at 20 m depth, in a mostly soft, clay background cannot be interpreted with any surface wave dispersion method, due to loss of sensitivity with depth. The main reason behind these limitations is that the surface wave dispersion is not very sensitive to thin (relatively to depth) embedded LVL or HVL.

Jin et al. (2009) studied the role of forward model in surface-wave inversion to delineate a HVL of 1.5 m thickness, 2 m depth, and 1500 m/s shear velocity (Vs). They found that the HVL can be detected by an inversion technique consisting of simulated annealing followed by a linearized inversion, using only the fundamental mode. However, even though using simulated annealing to search over a large parameter space at the beginning of inversion, it still requires relatively strict constraints for the HVL such as thickness, 0 to 2 m; depth, 1 to 5 m; Vs, 1000 to 2000 m/s. That means the strictly priori information about the HVL are needed to delineate it, and the technique would fail if the priori information is not available.

For passive surface wave methods, ReMi and f-k methods have been routinely used recently for deep shear wave velocity profiles. The most important advantage of testing methods using passive waves is the ability to obtain deep depths of investigation with very little field effort. Desired Rayleigh waves from passive seismic arrivals are relatively pure plane waves at low frequencies allow determining Vs profiles up to hundreds meter depth.

Li (2008) applied ReMi and f-k methods on real data sets measured from eleven test sites distributed over a distance of about 180 km in the upper Mississippi Embayment in the central United States to obtain Vs profiles up to depth of hundreds of meters. The Vs profiles are compared to those from SASW and MASW, which used a new developed low-frequency vibrator to generate wave fields at very low frequencies down to 1 Hz. He found that the active surface wave methods are more reliable than passive wave methods for deep Vs profiling.

2.4 Limitations of the Standard Methods Using Seismic Waves

As reviewed in section 2.3, the limitations of the standard methods using seismic waves are generally caused by insensitivity of data used for inversion and the shortcomings of local inversion techniques.

2.4.1 Limitations due to Insensitivity of Data

The standard seismic wave methods using either surface travel times or surface wave dispersion interpret subsurface velocity structures. The travel time from a shot to a receiver on the surface is measured from the fastest ray that starts from the shot and travels through a medium to the receiver. This fastest ray tends to go through stiffer material (high velocity zones), and avoids softer material (low velocity zones). Thus the surface travel times are not sensitive to these low velocity zones, and consequently these zones can not be well characterized with only travel times.

Surface wave dispersion data is more sensitive to a low velocity layer than surface travel times. However, the dispersion property is developed by taking accounts of whole material within a depth of approximately one wavelength for each frequency, and more sensitive to a shallow stiff layer than to a deep soft layer. When the depth of investigation increases, lower frequency or longer wavelength components are required, larger volumes of material are utilized to derive the dispersion property, and the dispersion data becomes insensitive to a deep and thin low-velocity layer. Hence, the low-velocity layer is hardly detected by just using the surface wave dispersion. In addition, the dispersion property is absolutely insensitive to lateral variation, thus techniques using wave dispersion are only for 1-D problems and can not be applied in regions with high lateral variation.

2.4.2 Limitations due to Local Inversion Techniques

The main goal of inversion is to find earth models that explain the seismic observations. The inversion involves finding an optimal value of a misfit function of several variables. The misfit function characterizes the differences between the observed and synthetic data calculated by using an assumed earth model. The earth model is described by physical parameters that characterize properties of soil/rock layers such as compression and shear wave velocities, density, etc.

For many geotechnical applications, the misfit function is highly complicated, and its surface consists of multiple hills and valleys. Thus such a function will have many maxima and minima; the minimum of all the minima is called the global minimum and all other minima are called the local minima. Local inversion techniques such as gradient descent methods typically attempt to find a local minimum in the close neighborhood of the starting solution. They use the local properties of the misfit function (gradients) to calculate the update to the current position and search in the downhill direction that only accepts a model having a smaller misfit value. Thus, these techniques will miss the global minimum if the starting solution is nearer to one of the local minima than the global minimum.

2.5 Suggested Improvements

2.5.1 Improvements by Using Sensitive Data

The capability of the seismic wave methods will be significantly improved by using sensitive data for inversion. The target of this research is to develop techniques that can characterize anomalies such as low-velocity layers, voids in rocks that may be filled by air, water, or soil. For this purpose, combined travel times measured both on the surface and in a borehole will be utilized to obtain high resolution inverted profiles. In addition, full waveforms will be employed to characterize reverse profiles when the borehole data is not available. The

full waveform has been used by authors for the deep (> 1 km) subsurface investigation, in both the time domain (Shipp and Singh [2002], Sheen et al. [2006]) and the frequency domain (Pratt [1999]). In all of these applications, body waves are dominant components in wave fields used for inversion. Unlike these methods, this research uses Rayleigh waves as dominant components in wave fields. Because, Rayleigh waves are more sensitive to shear wave velocity and less sensitive to Poison's ratio or density of a medium, they are useful for geotechnical applications where the shear wave velocity primarily controls properties of soil particles.

The following chapters will prove that the borehole travel times and full waveforms are more sensitive to the anomalies than surface travel times and wave velocity dispersion, respectively.

2.5.2 Improvements by Employing Global Inversion Techniques

The capability of the seismic wave methods will be also improved by employing global inversion techniques. Although, these techniques require much more computer time than local techniques, they are feasible for geotechnical engineering problems with the advent of fast computers.

Unlike local inversion techniques, global inversion techniques such as simulated annealing, genetic algorithm, and other importance sampling approaches attempt to find the global minimum of the misfit function by searching over a large parameter space. They have recently been applied in evaluation of various geophysical data sets (Sen and Stoffa [1991, 1995], Pullammanappallil and Louie [1994], Sharma and Kaikkonen [1998]). Most of the global inversion techniques are stochastic and use more global information to update the current position, thus they likely converge to the global minimum. In this study, simulated annealing will be employed for inversion problems in geotechnical engineering because it can be used in cases

where the model-data relationship is highly nonlinear and produces multimodal misfit functions (Sambridge and Mosegaard, 2000).

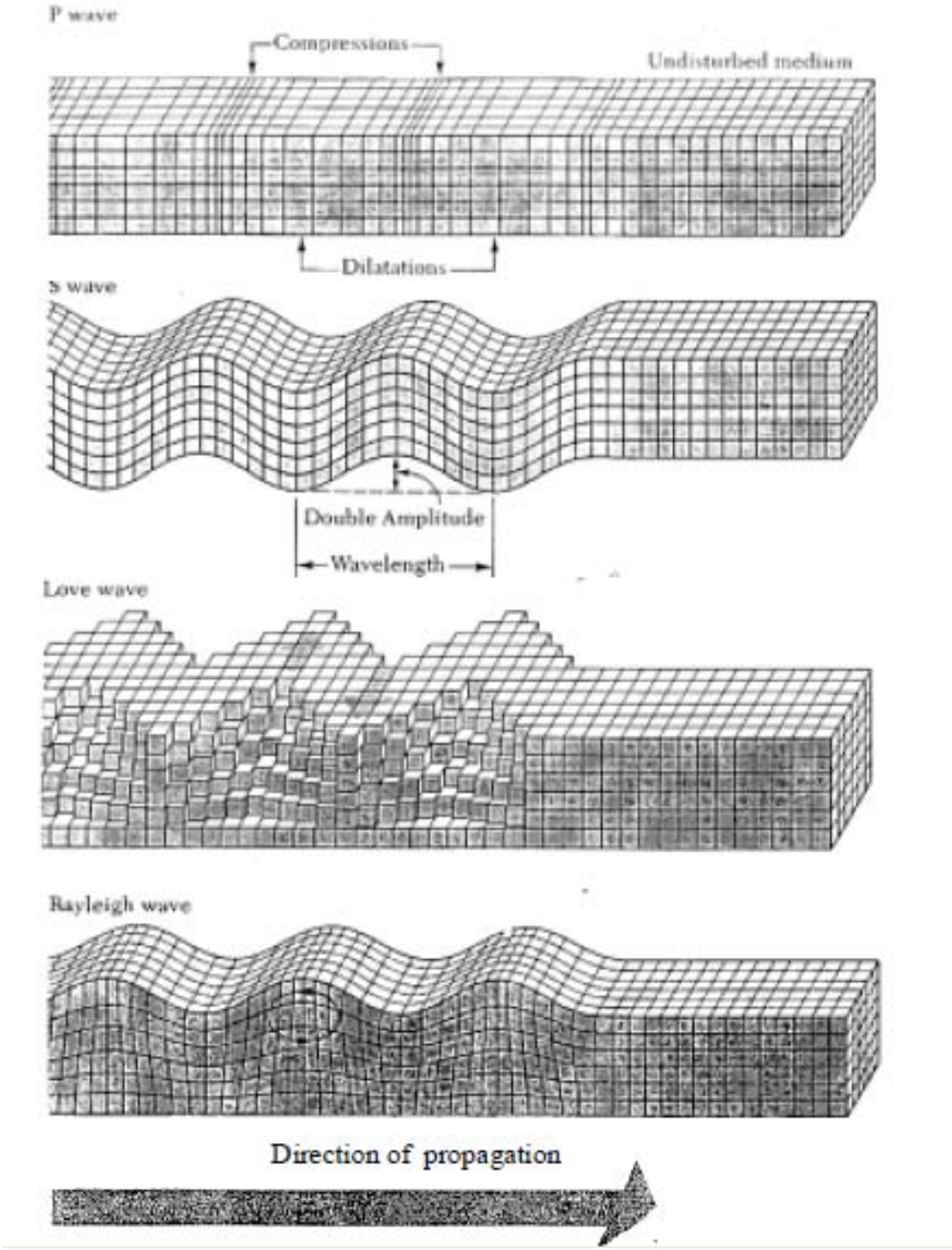

Figure 2-1. Particle motions associated with body waves and surface waves (from Bolt 1976)

a)

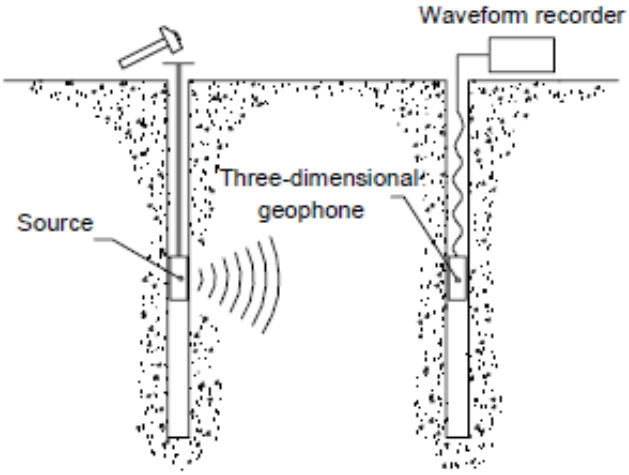

b)

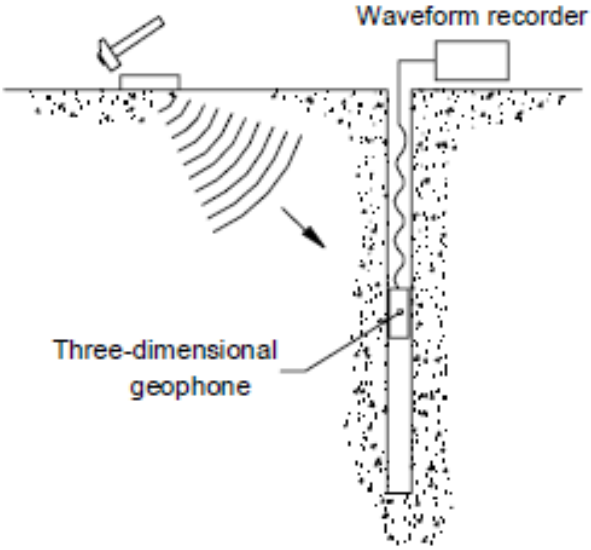

Figure 2-2. Bore-hole methods: a) cross-hole test and b) down-hole test (from Foti 2000)

a)

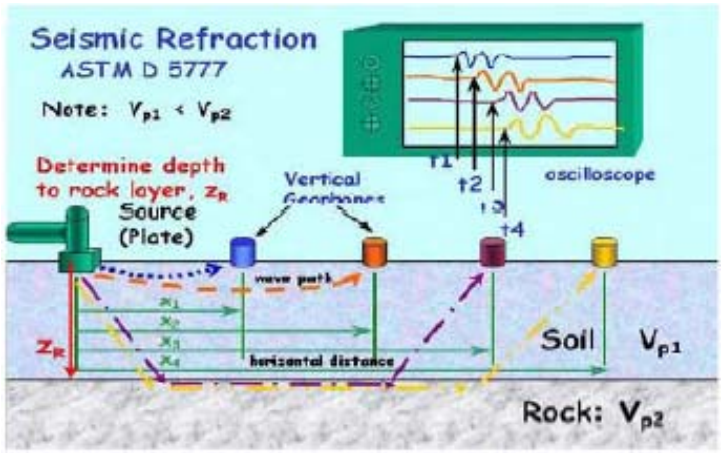

b)

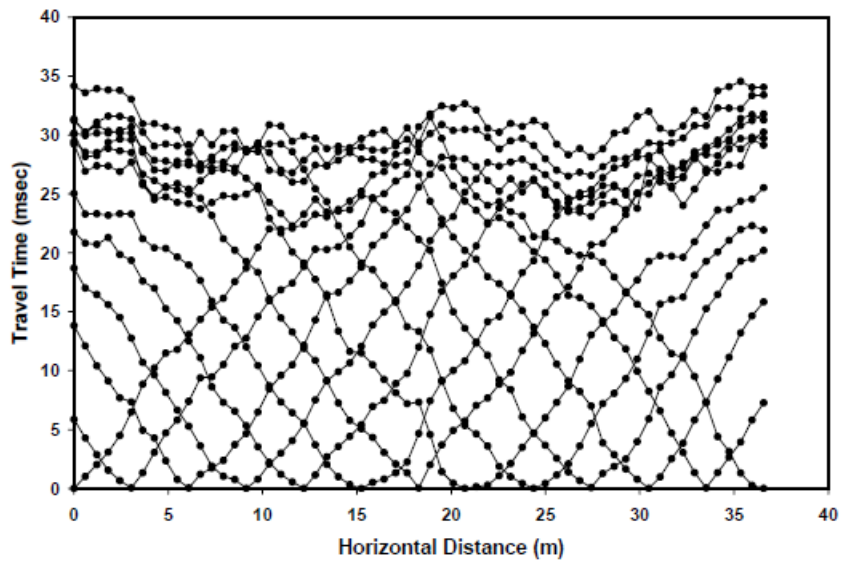

c)

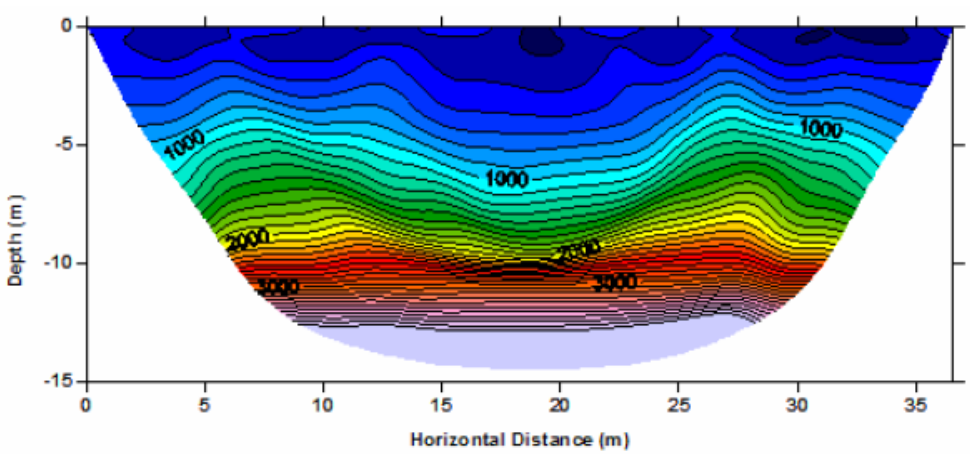

Figure 2-3. Seismic refraction tomography: a) test setup, b) travel times, and c) inverted velocity tomogram

a)

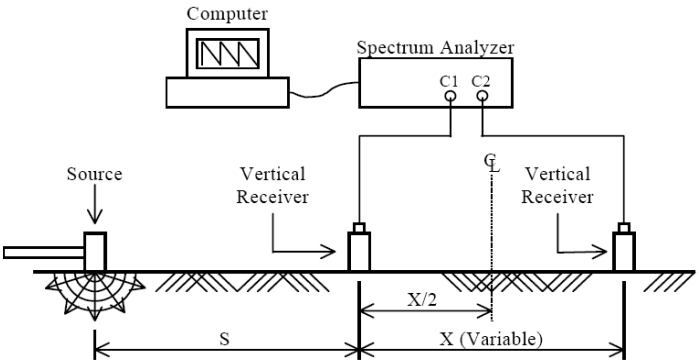

b)

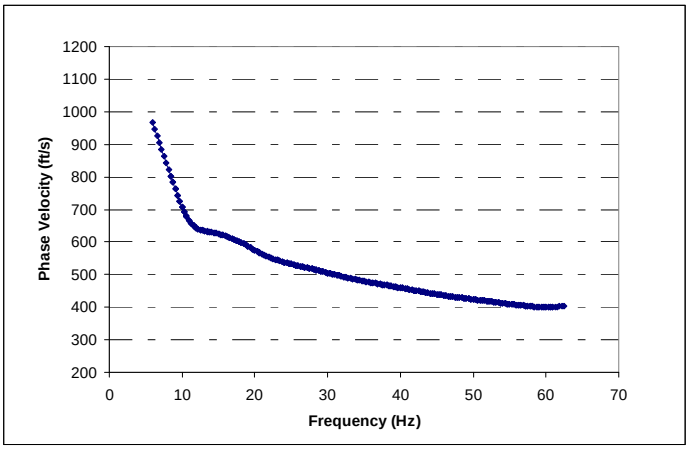

c)

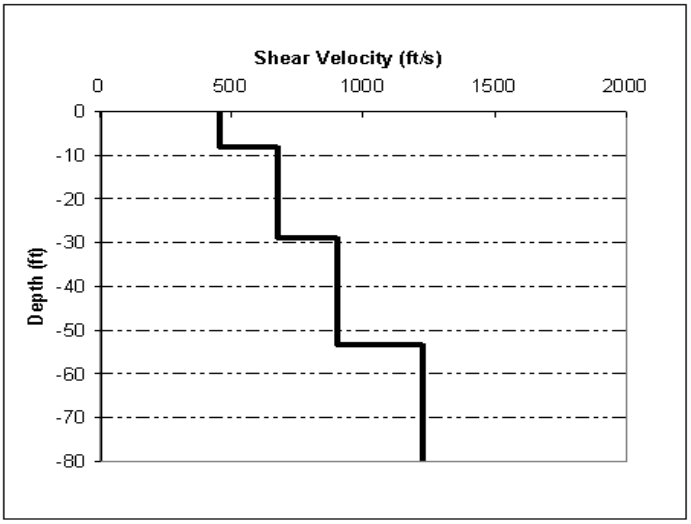

Figure 2-4. SASW: a) test setup, b) dispersion data, and c) inverted velocity profile

CHAPTER 3
INVERSION OF FIRST-ARRIVAL TIMES USING SIMULATED ANNEALING

3.1 Introduction

This chapter presents an inversion technique to invert first-arrival time using simulated annealing. The scheme is based on an extremely fast finite-difference solution of the Eikonal equation to compute the first-arrival time through the velocity models by the multi-stencils fast marching method. The core of the simulated annealing, the Metropolis sampler, is applied in cascade with respect to shots to significantly reduce computer time. In addition, simulated annealing provides a suite of final models clustering around the global solution and having comparable least-squared error to allow determining uncertainties associated with inversion results.

Global inversion techniques such as simulated annealing, genetic algorithms, and other importance sampling approaches have recently been applied in evaluation of various geophysical data sets (Sen and Stoffa [1991, 1995], Pullammanappallil and Louie [1994], Sharma and Kaikkonen [1998]). Unlike local inversion techniques, global inversion techniques attempt to find the global minimum of the misfit function by searching over a large parameter space. Most of the global inversion techniques are stochastic and use more global information to update the current position, thus they likely converge to the global minimum. In this study, simulated annealing is employed for engineering problems because it can be used in cases where the model-data relationship is highly nonlinear and produces multimodal misfit functions (Sambridge and Mosegaard [2000]). In addition, simulated annealing enables to provide a suite of final models clustering around the global solution and having comparable least-square error. This allows getting the inversion result by averaging all of these models to mitigate the influence of noise and the non-uniqueness of the inversion solutions.

The most important advantage of global inversion techniques is to avoid being trapped in local minima, and thus to allow final inversion results to be independent of the initial model. However, these global inversion techniques can require significant computer time, especially if the model contains a large number of model parameters. This disadvantage is reduced herein by using an extremely fast forwarding model solution, and by sampling in cascade with respect to shot position. First-arrival time inversions usually require many shots to obtain a high-resolution profile and each shot needs a forwarding model solution. Meanwhile, global optimization methods sample over a large number of trial models, and only accept a small part of them. Using an acceptance rule in cascade, forwarding model solutions for only a few shots are often required to reject the biased models. For the cases presented herein, a saving in computer time of 70% is achieved when utilizing the acceptance rule in cascade.

The technique is presented herein for synthetic data sets created from models that were previously tested on three commercial refraction tomography codes by Sheehan et al. (2005), and two experimental data sets from a well documented test site. The inversion results show that this technique successfully maps 2-D velocity profiles with high variation. The inverted wave velocity from the real data appears to be consistent with cone penetration test (CPT), geotechnical borings, and standard penetration test (SPT) results.

3.2 Methodology

3.2.1 Forward Modeling

Two main approaches that have been routinely used to calculate first-arrival times are the shortest path method (SPM) and the Eikonal equation solution. SPM originated in network theory (Dijkstra [1959]) and was applied by Nakanishi and Yamaguchi (1986) and Moser (1991) to seismic ray tracing. The main advantage of SPM are its simplicity and capacity for simultaneous calculation of both the first arrival time and the associated ray path, but it takes

more time for calculation and is not very efficient to use for the global optimization methods. The Eikonal equation shown below has been solved by many authors, including (Vidale [1988], Van Trier and Symes [1991], Nichols [1996], Sethian [1996, 1999], Kim [1999], Chopp [2001], Hassouna and Farag [2007]).

$$\left(\frac{\partial u}{\partial x}\right)^2 + \left(\frac{\partial u}{\partial z}\right)^2 = \frac{1}{V(x,z)^2} \tag{3.1}$$

In this equation, u=u(x,z) and V(x,z) are the arrival time and velocity at point (x,z), respectively. Among these methods, the fast marching method (FMM) is typically considered the fastest and most stable and consistent method for solution of the Eikonal equation. It was first presented by Sethian (1996) and has been improved by other authors. In this study, the improved version of FMM by Hassouna and Farag (2007), the so called multistencils fast marching (MSFM), is utilized to compute first-arrival times for forward modeling. MSFM computes the solution at each point by solving the Eikonal equation along several stencils, and then picks the solution that satisfies the upwind condition.

3.2.2 Optimization Method

Simulated annealing was first proposed by Metropolis et al. (1953) and significantly improved by Kirkpatrick et al. (1983). The basic concepts are borrowed from a physical annealing process. The annealing process occurs when a solid in a heat bath is initially heated by increasing the temperature such that all the particles are distributed randomly in a liquid phase. This is followed by a slow cooling such that all particles arrange themselves in the low energy ground state where crystallization occurs.

Simulated annealing has recently been applied in evaluation of various geophysical data sets. Rather than discussing the analogy of simulated annealing that has been well described by

Sen and Stoffa (1995), a brief description of the process used in this study is presented in the following:

1. Select an initial velocity model V, and then calculate the least-squared error E_i, for the *ith* shot, and average error E_{mean}, as:

$$E_i = \frac{1}{N}\sum_{k=1}^{N}\left[d_{k,i} - g_{k,i}(V)\right]^2 , \tag{3.2}$$

$$E_{mean} = \frac{1}{M}\sum_{i=1}^{M} E_i , \tag{3.3}$$

   where $d_{k,i}$ and $g_{k,i}$ are the *kth* observed and computed travel times from the *ith* shot, respectively, N is the number of observation points, and M is the number of shots.

2. Following the idea of Pullammanappallil and Louie (1994), perturb the velocity model by randomly selecting a box within the medium and randomly assign all of the cells within the box a new velocity between the minimum and maximum velocities chosen by the user. Next, to avoid unusual artifacts and high velocity gradients that would violate the assumption of an Eikonal equation solution, the model is smoothened. The smoothing is accomplished by adjusting the velocity of each cell in contact with and just outside the boundary of the box. The adjusted velocity for each of these perimeter cells is established by averaging the velocities of the four cells in contact with the four edges of the perimeter cell. Following the process described, a new model is now obtained.

3. Apply the acceptance rule in cascade with respect to shots for the new model. The travel times from one shot at a time are used to test the new model. For the *ith* shot, the least-squared error E_i corresponding to the new model is calculated as equation (2). The new model unconditionally passes the *ith* shot if its least-squared error is smaller than that from the previous model, and conditionally passes the *ith* shot if its least-squared error is bigger with the following probability:

$$p_i = \exp\left(-\frac{\Delta E_i}{T}\right), \tag{3.4}$$

   where ΔE_i is the positive difference between the least-squared errors of the two models. If the new model passes the first shot, then it is tested for the second shot and so on. It is immediately rejected if failing at a certain shot, i.e., the new model is only accepted if it passes all of the shots.

4. Repeat steps 2 and 3 until a desired number of accepted models are completed, then reduce the temperature to the next level according to a schedule:

$$T(k) = \frac{T(k-1)}{2} , \tag{3.5}$$

   where $T(k)$ and $T(k-1)$ are the temperatures at the *kth* level and the *(k-1)th* level.

The criterion for convergence requires that the relative difference between the maximum and minimum average errors E_{mean} from all accepted models at a particular temperature become

very small (empirically say between 0.1% and 0.5%). If the criterion for convergence is not satisfied, the temperature is reduced to the next level. At a sufficiently low temperature, the accepted models are in the vicinity of the global minimum and the optimization converges.

The selection of a correct initial temperature is very important. Selecting a very high value leads to unnecessary computations, whereas starting from a low value can lead to a local solution. Based on the idea of Sharma and Kaikkonen (1998), in this study, the initial temperature is taken to be the nearest lower power of ten to the least-squared error; for example, if the least-squared error is 50.59, then the initial value is 10. In this way, the initial temperature is usually higher than the critical temperature, and any bias created by the initial model will be destroyed.

The cooling schedule is another important parameter in the global optimization. Many schedules have been investigated herein for inversion problems up to 1500 cells, and it has been found that the number of accepted models at each temperature level should be at least 10,000, and the temperature needs to reach a very low value to obtain the global solution. In the studied cases, the final temperature was about 10^{-3} to 10^{-4} when the initial temperature was 10. When the number of cells increases, the procedure needs a slower schedule, i.e., more accepted models at each temperature or a smaller change in temperature, and hence the time of computation increases in order to get the global solution. Therefore, the cooling schedule should be selected with care.

3.3 Applications

3.3.1 Applications on Synthetic Data

Synthetic models refer to earth models whose velocity profile is assumed or known a priori. Using a known velocity structure, travel time data is calculated for an assumed test

layout. This travel time data is then input to the inversion program as if it were data collected from a field test, and velocity structure is calculated from travel time data. Theoretically, the interpreted velocity profile should be the same as the model assumed at the start.

Synthetic model studies were conducted for at least two reasons. The first objective was to assess ability of the inversion technique to identify and delineate subsurface features that are routinely present in test sites. It was important to determine prior to actual field testing whether the system is sensitive to these features, otherwise there was no point in conducting an actual field test. Second, in conducting model studies in which the "answer" is known, an analysis protocol can be developed to systematically and consistently analyze travel time data to develop believable velocity tomograms. In order to be confident of results interpreted from actual field data, one has to develop confidence that the program and analysis procedures are reputable. Synthetic model studies help build this confidence since interpreted velocity profiles can be compared to the known starting profile.

The technique presented was intensively tested on many synthetic models, and three of them with high lateral variation are presented herein in Figure 3-1. These three synthetic models (1, 2, and 3) are models 3, 5, and 6 from Sheehan et al. (2005), respectively. They include a notch (model 1), a stair step (model 2), and broad epikarst (model 3). For all three models, 25 shots into 48 geophones were used to create synthetic first-arrival times. The geophone spacing was 1 m for models 1 and 2, and 2 m for model 3. For all models, all 25 shots were within the geophone spread and the shot spacing was twice the geophone spacing. With the so arrangement, the number of shots, the number of geophones, and the geophone spacing are the same as those used in Sheehan et al. (2005).

To run the inversion, the medium sizes were kept the same as the true models, and discretized with a grid size of 1 m for ease in picking the first-arrival times from the forward modeling. The velocity constraints were assigned by slightly increasing the maximum true value and decreasing the minimum true value, and thus the velocity was allowed to vary between 100 m/s and 4000 m/s for models 1, and 2, and between 100 m/s and 5000 m/s for model 3. All initial models were specified with a constant velocity of 2000 m/s, which leads to an initial temperature of 10. Velocities of cells were then perturbed, models were updated, and temperature was reduced after each 10,000 accepted models until the criterion of convergence was satisfied. Because of the non-uniqueness of the inversion problem and to further avoid unusual artifacts, in all three cases, 50,000 accepted models from the last five temperature levels and that have least-squared errors within a few percent from the smallest error are averaged to derive the final inverted model, and the associated uncertainty in the form of a coefficient of variation (COV).

First, consider the results for model 1 presented in Figure 3-1. A primary feature of refraction tomography is delineation of both vertical and horizontal changes in seismic wave velocity, e.g., detection of anomalies. Here it is observed that the inversion is able to reasonably characterize the presence, location, and general shape of the notch. However, it is also observed that the inverted model is not identical to the true model. Most notably, as discussed by Sheehan et al. (2005) and others, refraction tomography will always model a sharp contrast in velocity with a gradient in velocity (this is usually a result of some method of smoothing of the velocity model such as utilized herein). This reality largely accounts for the differences in the two models. In addition, refraction tomography is not able to characterize zones of material outside of the ray coverage. Here is where the uncertainty results (Figure 3-1c) are helpful. The uncertainty is low in zones with good ray coverage, such as zones near the surface, and high in

zones with poor ray coverage, such as zones near the bottom corners of the medium. In zones of high uncertainty, the inversion routine simply reports the velocity as the average value from all values randomly and uniformly withdrawn between the minimum and maximum velocity constraints selected by the user. Otherwise, in the zones of low uncertainty, the inverted velocity is independent of the constraints, and thus more reliable. From these results, it appears that the delineation between low and high uncertainty is reasonably established at a COV value of approximately 20%. Finally, the result from the presented technique seems better than that shown in Sheehan et al. (2005) for commercial codes GeoCT-II, SeisImager, and Rayfract because the results from these codes all show a high velocity artifact under the notch, and the notch is not well detected.

Second, the results for model 2 are presented in Figure 3-2. Similar to model 1, the anomaly (stair step) is reasonably recovered for both the location and general shape. The primary difference between the true and inverted models is again due to the gradient. The gradient is mostly inserted at the interface between layers, and the interface can be interpreted from areas of maximum gradient in the inverted model, such as the contour line of 2000 m/s shown in Figure 3-2b. In addition, the result from the presented technique seems better than that from GeoCT-II, and similar to those from SeisImager and Rayfract.

Last, the results for model 3 are presented in Figure 3-3. It is observed that the inverted model is an excellent recovery of the true model. Both velocities and interfaces between layers are very well inverted. The result from the presented technique is consistent with that obtained from all three commercial codes.

3.3.2 Applications on Real Test Data

The results from the synthetic models have shown the capability of the presented technique in dealing with high lateral and vertical variation profiles. In the end, to gain acceptance and

wide-spread application, it must be demonstrated that results from the technique compare well with ground truth information obtained from real test sites. Thus, it has been applied to a well-documented test site.

The University of North Florida (UNF) and the University of Florida (UF) have developed a Florida Department of Transportation (FDOT) dry retention pond into a karstic limestone geophysical/ground proving test site in Alachua County, Florida. The site contains a number of survey lines and five PVC-cased boreholes extending to approximately 15 m. The test site is unique because the northern portion of the retention pond commonly experiences sinkhole activity, whereas the southern portion rarely experiences sinkhole activity.

The geophysical/ground proving test site is located outside of Newberry, Florida on State Road 26 in Alachua County. The site is approximately 29 km from Gainesville, and approximately 150 km from Jacksonville. The test site is a dry retention pond, approximately 1.6 ha in size. The northern portion of the site has been susceptible to sinkhole formation and a number of large sinkholes have formed and been repaired. However, the southern portion has been relatively free of sinkholes and is an ideal location for characterizing karst limestone sites. The southern portion of the test site was subdivided into 26 north-south survey lines equally spaced a distance of 3.0 m apart. The lines were labeled A through Z from west to east across the site, and each line was 85.3 m long, with station 0 m located at the southern end of the site. Two 36.6-m long refraction tests were conducted end-to-end along lettered site lines A, F, K, P, U, and Z, and beginning at station 0. Thus, the 12 refraction tests covered six of the site lines from station 0 to 73.2 m.

Each 36.6-m long refraction test was conducted with 4.5 Hz vertical geophones spaced equally at 0.61 m, for a total of 61 measurements. Seismic energy was created by vertically

striking a metal ground plate with an 89 N sledgehammer, thus producing compression wave (P-wave) first arrivals. Shot locations were spaced at 3.0-m intervals along the 36.6-m line and starting at 0 m, for a total of 13 shots. Since a 32-channel dynamic signal analyzer was used to collect time records, and each line required 61 measurements, each line was conducted in two stages. In stage one, 31 geophones were placed at 0.61-m intervals from station 0 m to station 18.3 m. In stage two, 31 geophones were placed at 0.61-m intervals from station 18.3 m to station 36.6 m. Since there was a designed overlap between the two stages at station 18.3 m, a total of 61 measurement locations were collected. For each stage, time records were collected at each of the 13 shot locations, and then the data were combined to produce a complete shot gather for the survey line from station 0 m to station 36.6 m. Data from gridline A is chosen to present herein because these data displayed the most variable condition along the line. The measured travel time is presented in Figures 3-4 and 3-5. Cone penetration tests (CPT), geotechnical borings, and standard penetration tests (SPT) were also conducted on gridline A for partially verifying the inverted P-wave tomograms.

To run the inversion, the velocity constraints and the medium depth need to be established. Even though the inversion technique does not require strict velocity constraints for convergence, required computer time can be reduced significantly if they are available. To save computer time, an estimate of the minimum and maximum layer velocities must be determined. For these estimates, results from a simple two-layer velocity profile determined via traditional refraction analysis procedures (Burger [1992] and Redpath [1973]) were employed. These simple velocity models were generated using travel time curves from only the two outside source locations (e.g., 0 and 36.6 m for data set A_0-36.6) of the refraction surveys. From the simple profile thus determined, the first layer velocity was used to determine the minimum velocity constraint, and

the second layer velocity was used to determine the maximum velocity constraint. For both data sets presented herein, the minimum and maximum velocities were determined as 300 m/s and 3000 m/s, respectively.

It is very important to determine a reasonable medium depth to get credible inversion results. If one assigns a very large medium, new models will be easily accepted because models are highly perturbed at less sensitive zones, or zones outside of ray coverage, and the inversion may not well characterize the velocity structure. For cases without any prior information, one can assign a large depth such as equal to the geophone spread, and run a trial inversion. This run with a large medium may not give a high resolution of velocity structure, but the uncertainty result will provide rational information about the depth of investigation. The delineation between low and high uncertainty zones can then be used to determine the depth of the medium for an improved inversion run. Alternatively, the depth of the medium can also be estimated from experience from 1/3 to 1/2 of the geophone spread. For both data sets presented herein, the depth of the medium was simply taken as 1/3 of the geophone spread.

In the inversion process, for convenience of calculating the first-arrival time in the forward modeling, the medium was discretized with a grid size equal to the geophone spacing of 0.61 m. The initial models were specified the same for both tests with a constant velocity of 1000 m/s, and the initial average least-squared errors were 63.0082 ms2 for data set A_0-36.6, and 30.1335 ms2 for data set A_36.6-73.2, thus the initial temperature was 10 for both. Velocities of cells were perturbed by randomly assigning values between the constraints, models were updated with the number of accepted models at each temperature level equal to 10,000, and the temperature was lowered until the criterion of convergence was reached at which the least-squared errors were 0.8652 ms2 for data set A_0-36.6, and 0.8927 ms^2 for data set A_36.6-73. The criterion of

convergence was not satisfied until the estimated first-arrival times from the final accepted model were very close to the observed travel times (shown in Figures 3-4 and 3-5). In order to reach the criteria of convergence, both inversion runs were required to test more than one million trial models, and each run took a few hours on a standard laptop computer.

Because of noise, subjective judgments in manually picking first arrival times, and non-uniqueness of inverted solutions, there is no guarantee that the model corresponding to the smallest error is closest to the true model. Therefore, the inversion results should be inferred from many accepted models clustering around the global minimum and having similar errors, instead of from only one model that has the smallest error. As with the synthetic models, the last 50,000 accepted models were used to derive the final inversion results and the associated uncertainties.

Figures 3-6a and 3-7a present two-dimensional compression (P) wave refraction tomograms determined from test data collected along the surface. These tomograms indicate that the P-wave velocity at this site generally increases with depth, and that the specific pattern of increase depends on lateral location across the site. Figures 3-6b and 3-7b show the uncertainties associated with the inverted P-wave profiles. Again, the uncertainty is consistent with expectations: low uncertainty in zones with good ray coverage (zones near the surface), and high uncertainty in zones with poor ray coverage (zones near the bottom corners of the medium). With the confidence gained from running synthetic models, the depth of investigation is about 10 m at the middle of the model where the COV from surface to that depth is less than 20 percent.

Following refraction data collection and analysis, invasive ground proving information was collected at the site to provide partial verification of the refraction test result interpretations, and these data are presented in the following paragraphs.

Cone Penetration Tests (CPT):

Ten CPT soundings were conducted at strategic locations across the site. Because line A displayed the most lateral variability along the line, four of the 10 soundings were conducted along line A. These four tests were located at the following horizontal stations: 19.8, 39.6, 44.2, and 65.5 m. The measured tip resistance results are shown in Figure 3-8, and the length of each test run is shown atop the tomograms in Figures 3-6a and 3-7a. These results are compared with the refraction tomograms from Figures 3-6a and 3-7a as follows:

- At station 19.8 m, the CPT tip resistance approached a large value of 30 MPa, and the test was terminated at a depth of about 9.2 m. Station 19.8 m is near the middle of a valley feature on the tomograms (Figure 3-6a), and the CPT tip terminates at a P-wave velocity of ±2000 m/s.

- The sounding at 39.6 m was terminated before the tip resistance approached a large value because the CPT rod system was bending seriously to the south as penetration was attempted. It is interesting to note on the tomograms (Figure 3-7a) that station 39.6 m is slightly to the left of a block/pinnacle feature, and bending of the CPT rod to the south at the site (to the left or lower station number on tomogram) is consistent with this block feature.

- At stations 44.2 and 65.5 m the tests were terminated at shallow depths less than 0.5 m because the CPT tip resistance approached a large value of 30 MPa. Stations 44.2 and 65.5 m are both located near the top of block/pinnacle features on the tomograms (Figure 3-7a). However, in contrast to station 19.8 m, the CPT tips terminated at P-wave velocities less than 1000 m/s at stations 44.2 and 65.5 m.

- It is reported that small, rock outcrops were visible near stations 62.5-64 m and 66.1-67.1 m, which are on both sides of the CPT sounding at 65.5 m.

Geotechnical Borings and Standard Penetration Tests (SPT):

Eight geotechnical borings and SPT soundings were conducted at strategic locations across the site. Similar to above, the refraction tomograms and CPT results were used to select these locations. All of the borings included drilling and recovery of rock cores through a minimum of 3 m of material, and in one core, through 11 m of material. The following information is provided:

- Three of the eight borings were located along line A at the following stations: 19.8, 35.6, and 65.5 m. These borings coincided with CPT tests at 19.8 and 65.5, while the boring at 35.6 m was slightly to the left of the CPT sounding at 39.6 m.

- At station 19.8 m, the boring was advanced through predominantly sand overburden soil having SPT N-values less than 10 to a depth of 9.0 m. Below 9.0 m, coring was conducted to a depth of 12.5 m, and the material was reported to be tan limestone with fossils throughout. The recovery of this material was 100% throughout, and the rock quality designation (RQD) was reported as 100, except for the first 0.5 m which was broken at the top (RQD approximately 85).

- At station 35.6 m, the boring was advanced through sandy clay and sand overburden soil having SPT N-values between 7 and 10 to a depth of 2.3 m. Below 2.3 m, coring was conducted to a depth of 11.0 m, and the material was reported to be predominantly light tan to white limestone with fossils throughout.

- At station 65.5 m, the boring was advanced through sand overburden soil to a depth of only 0.3 m. Below 0.3 m, coring was conducted to a depth of 9.4 m, and the material was reported to be predominantly light tan to white limestone with fossils throughout. The recovery of this material varied between 80-100%, with approximately 60% of the run reported at the 100% recovery level. The boring notes report that several zones appeared to be weak and broken, and the RQDs varied widely between 30 and 100. Nearly half the run indicated an RQD between 60 and 80, a short distance (10%) at RQD of 100, and the remaining 40% reported a RQD between 30 and 60.

These results are compared with the refraction tomograms from Figs. 6a and 7a, and the

CPT results from Figure 3-8 as follows:

- The CPT and boring information at stations 19.8 and 65.5 m appear to be in good agreement. At 19.8, CPT testing was terminated upon approaching a limiting large value at a depth of 9.2 m, while boring information reported the overburden soil/rock interface at a depth of 9.0 m. Similarly, at 65.5, CPT testing was terminated at a depth less than 0.5 m, while the top of rock was reported at 0.3 m.

- The undulating, valley/bowl to block/pinnacle features noted along the P-wave velocity tomograms appear to be the result of lateral variation in the overburden soil/rock interface along the length of the refraction line. At 19.8, a valley/bowl feature appears, and the top of rock is found at 9.0 m, while at 65.5, a block/pinnacle feature appears, and the top of rock is found at 0.3 m.

- While the undulating features in the velocity tomograms are generally indicative of the soil/rock interface, the top of rock does not appear along a constant contour of P-wave velocity. Within a valley (station 19.8), the top of rock is found at approximately 2000 m/s, while at the top of a block (station 65.5), the top of rock is found at a velocity of approximately 500 m/s. However, the rock under station 19.8 m was reported competent and intact, with 100% recovery and RQD of 100 throughout all but a short length at top of

core run, while the rock under station 65.5 m was reported to be of lower quality. Velocity differences between these two materials should be expected.

- Finally, it is interesting to note that the CPT appears to penetrate a particulate, sand material of higher velocity (station 19.8) easier than it will a rock of lower velocity (station 65.5). A possible explanation is as follows. Velocity is related to the small-strain modulus of the material, while CPT tip resistance is related to bearing capacity or strength of the material. Even though the rock at station 65.5 has a relatively low velocity as measured through a large volume of material, the local strength beneath the cone tip is still large. A large, broken mass of this material under low confinement near the ground surface has low velocity. However, the local, broken pieces are still an intact, cemented material, and highly resistant to local CPT penetration. Alternatively, the particulate, sand material under large confinement at 9 m is considerably stiffer, yet will undergo local shear failure under CPT penetration. Thus, these results reinforce the premise that good site characterization practice should include measurement of multiple parameters to fully understand expected behavior.

In summary, it would appear that the invasive site characterization results provide excellent corroborating evidence for the refraction tomograms presented herein, and suggest that the refraction tomograms provide valuable information regarding subsurface characteristics.

3.4 Conclusion for Chapter 3

A global optimization scheme based on simulated annealing is presented to obtain near-surface velocity profiles from travel times. Although the presented technique requires more computer time than the three mentioned commercial packages, it has the own superiorities. First, this inversion technique does not depend on the initial model and becomes important in regions where prior information about subsurface profiles is not available. Second, simulated annealing provides a suite of final models clustering around the global solution and having comparable least-squared error. This provides an inversion result by averaging all of these models to mitigate the influence of noise and the non-uniqueness of the inversion solutions. Last, the technique also enables to determine the uncertainties associated with inverted results. In cases, the inversion results of subsurface formations are used for the design of engineering structures such as foundations, the uncertainty will be particularly useful in implementing the new LRFD design

methodology that can explicitly account for spatial variability and uncertainty in design parameters.

By using an extremely fast forwarding model solution and an acceptance rule in cascade to reduce the computer time to a few hours on a standard laptop, the technique is feasible for practical engineering inversion problems.

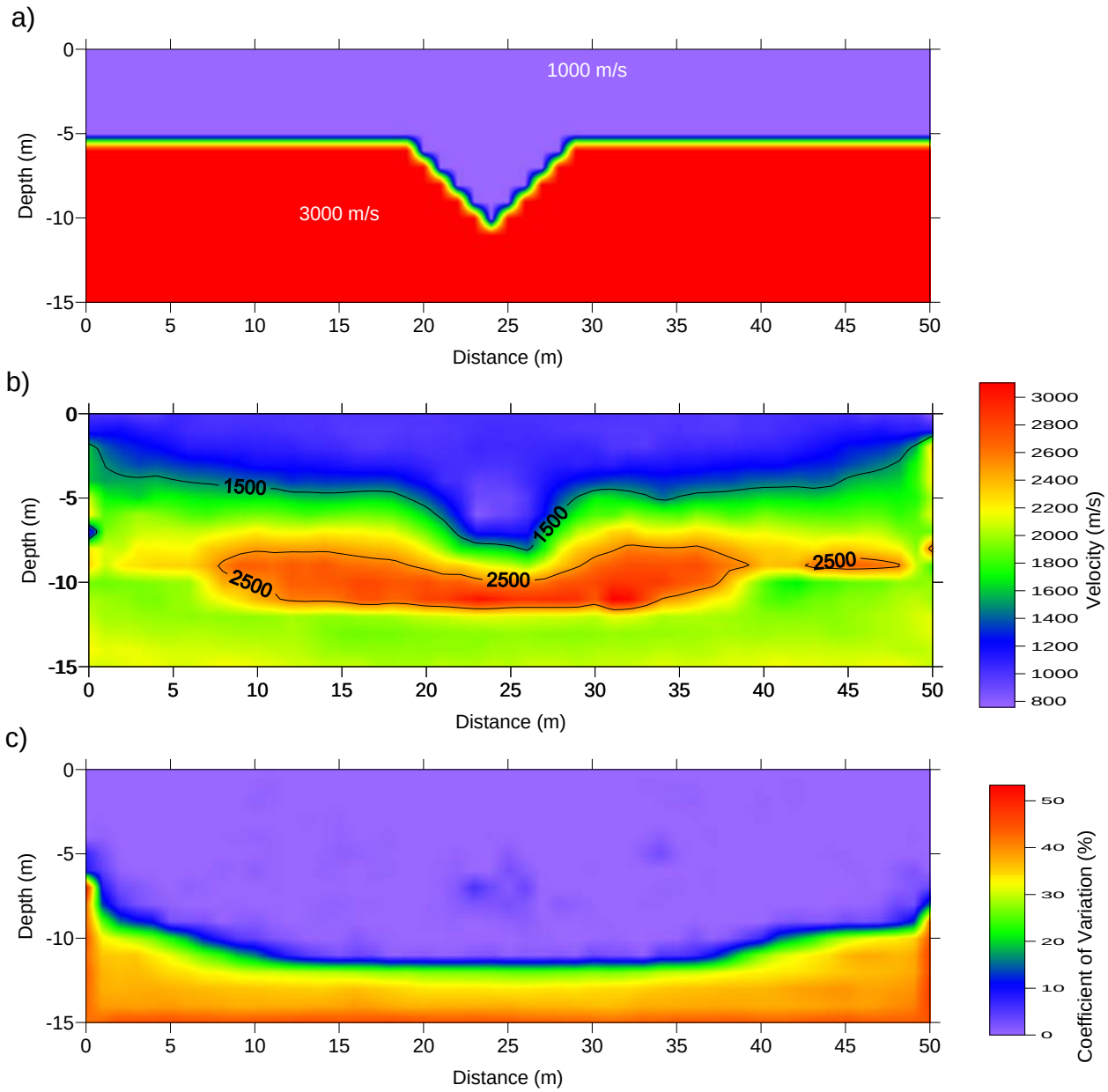

Figure 3-1. Synthetic model 1: a) true model, b) inverted model, and c) uncertainty associated with the inverted model

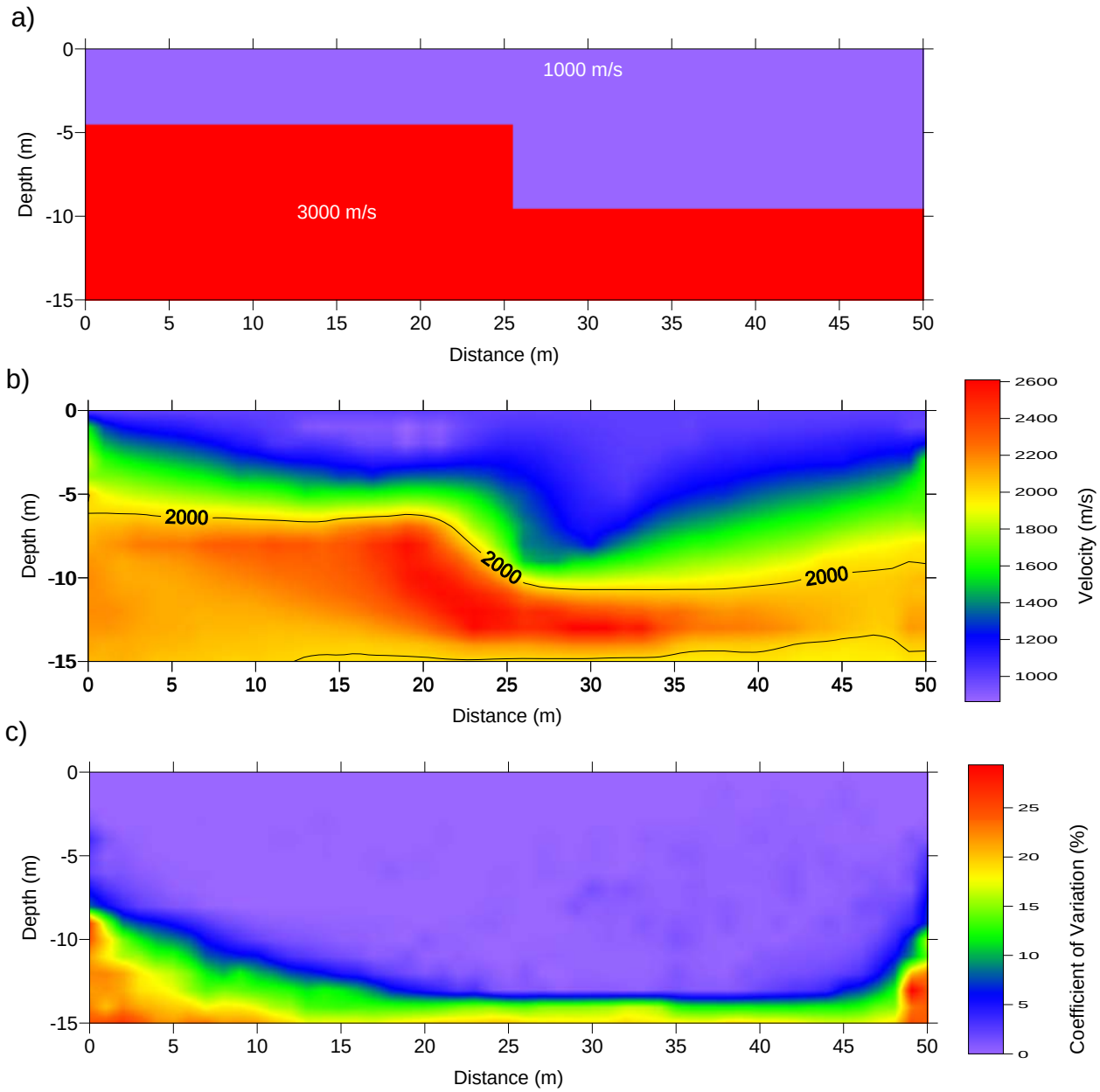

Figure 3-2. Synthetic model 2: a) true model, b) inverted model, and c) uncertainty associated with the inverted model

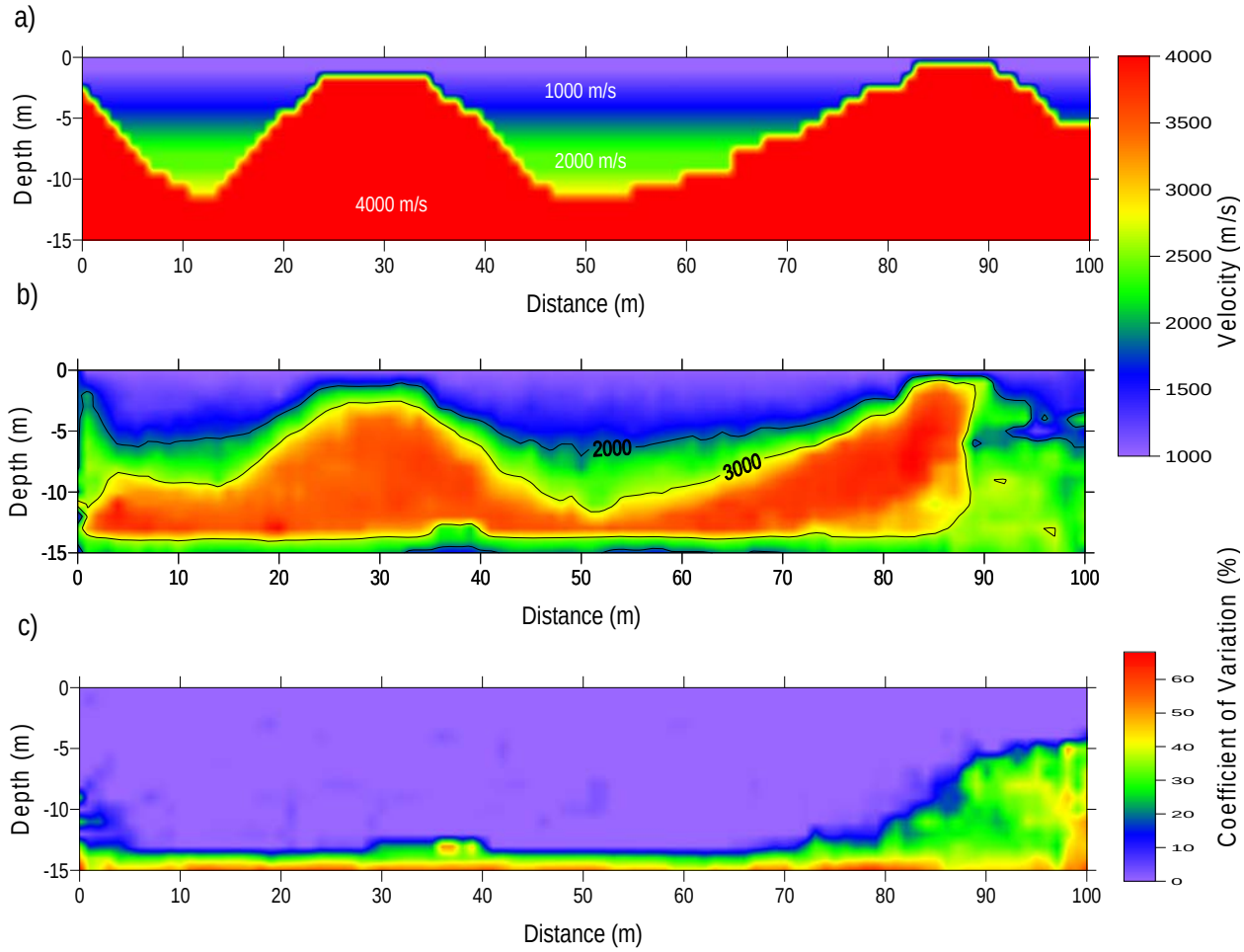

Figure 3-3. Synthetic model 3: a) true model, b) inverted model, and c) uncertainty associated with the inverted model

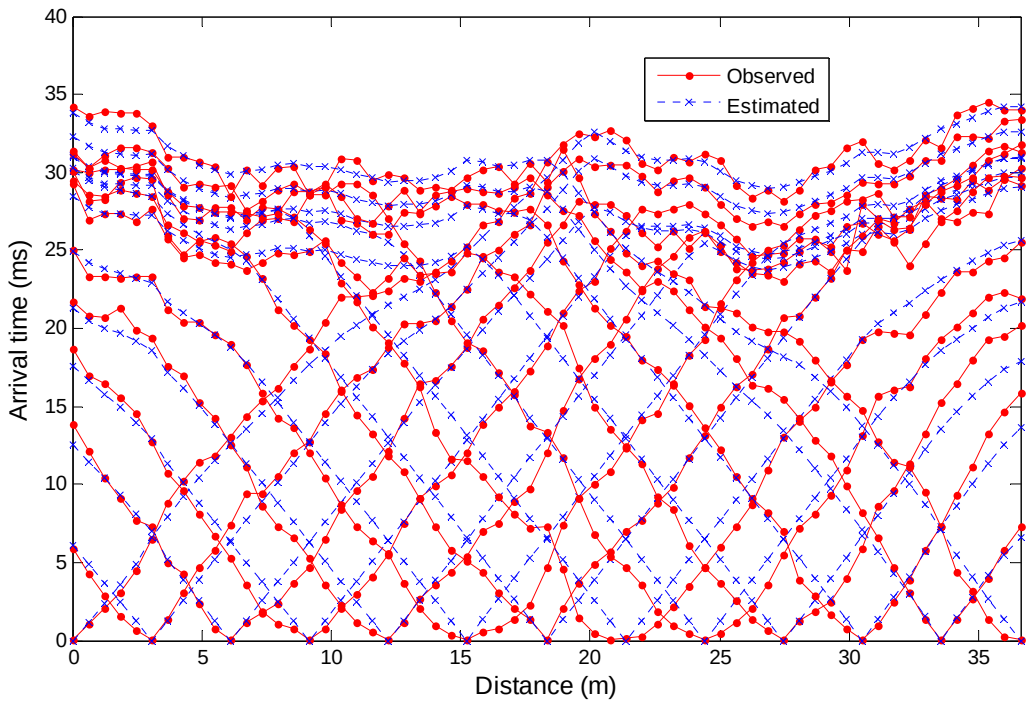

Figure 3-4. Comparison between the estimated and observed first-arrival time for the real data A_0-36.6

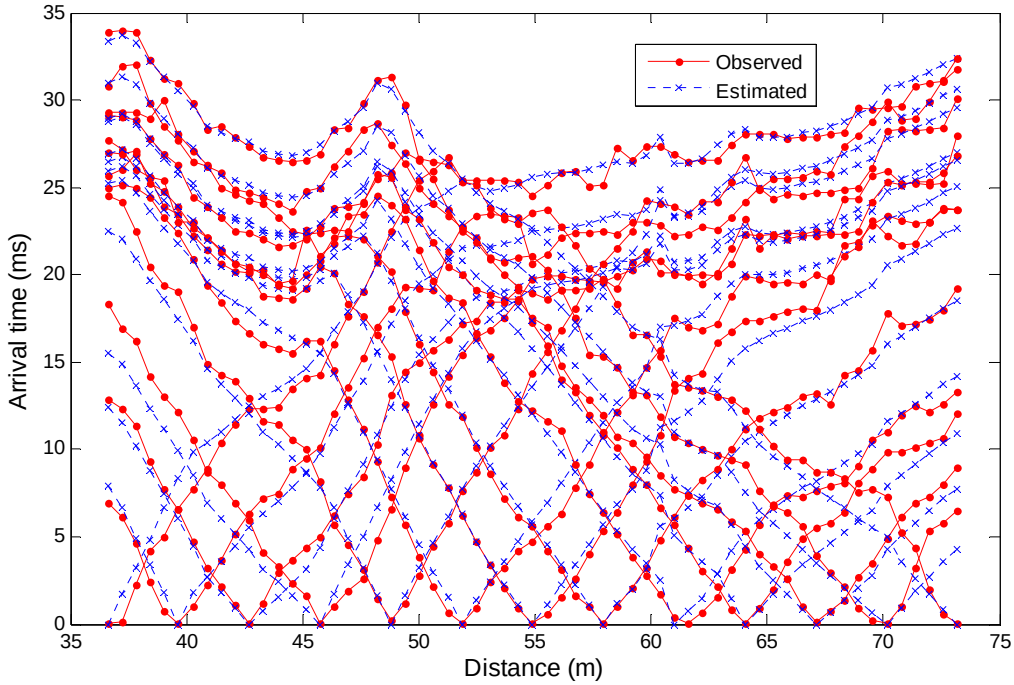

Figure 3-5. Comparison between the estimated and observed first-arrival time for the real data A_36.6-73.2

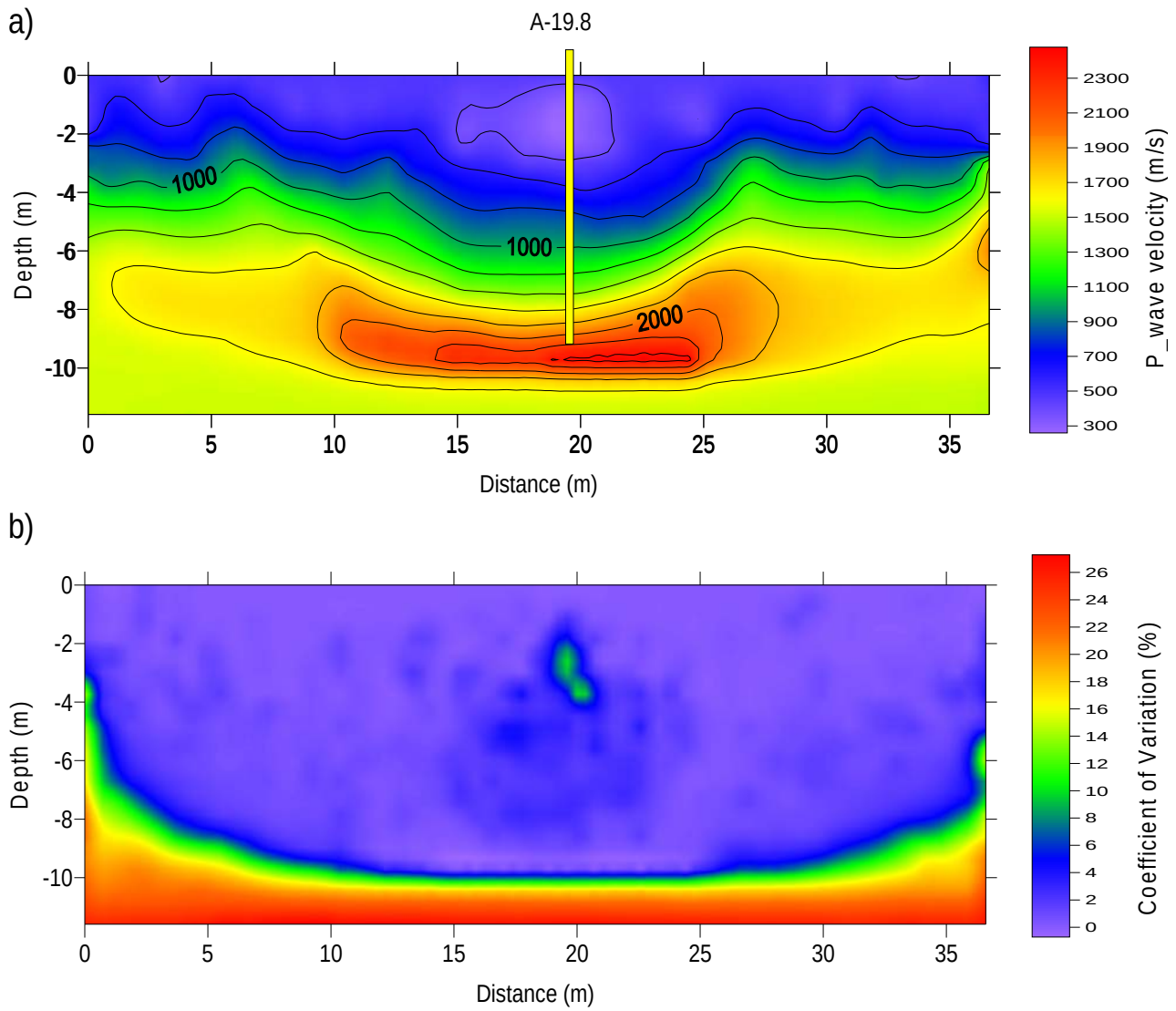

Figure 3-6. Inversion result for the real data A_0-36.6: a) inverted model, and b) uncertainty associated with the inverted model

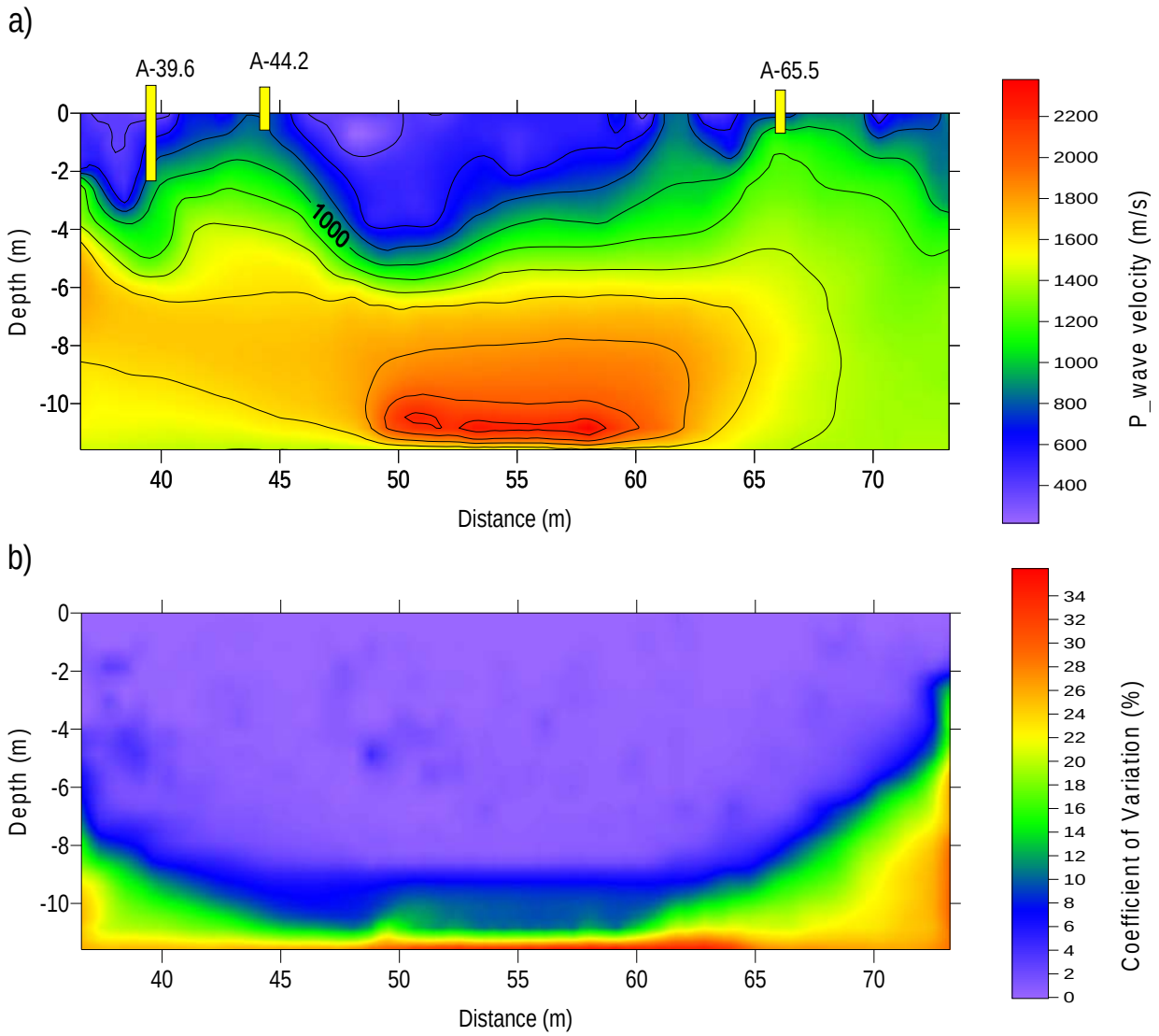

Figure 3-7. Inversion result for the real data A_36.6-73.2: a) inverted model, and b) uncertainty associated with the inverted model

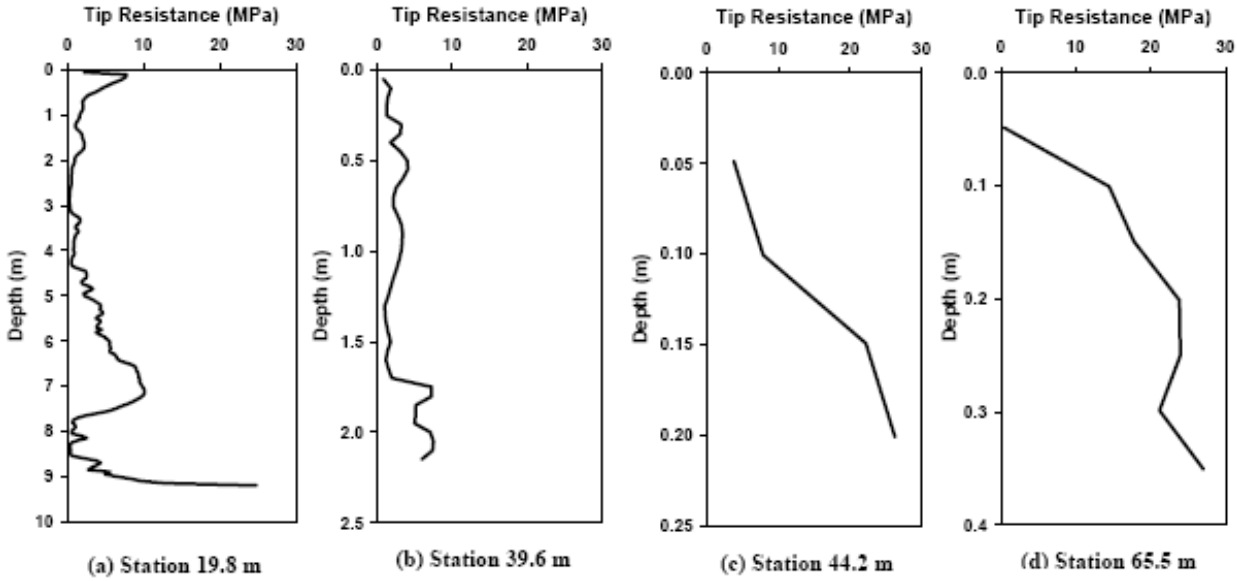

Figure 3-8. Cone penetration tip resistance, line A

CHAPTER 4
INVERSION OF COMBINED BOREHOLE AND SURFACE TRAVEL TIMES

4.1 Introduction

Site characterization for design of deep foundations is very crucial, as unanticipated site conditions still represent the most common and most significant cause of problems and disputes that occur during construction. The problem is particularly acute in karst terrain where subsurface conditions are often highly variable. The problem is further exaggerated by increased use of single, large-diameter, non-redundant drilled shafts as foundation elements. Reliance on traditional subsurface characterization methods that invasively probe and sample a very small volume of material frequently results in problems and inefficiencies. For example, such techniques often produce poor assessment of the spatial variation in subsurface conditions. This can lead to use of very conservative design parameters and produce expensive design solutions. Perhaps even worse, poor assessment of spatial variation can also result in failure to identify a significant anomaly, which can lead to substructure failure. An additional concern with traditional techniques is that they are often unreliable in characterizing the engineering parameters of soft rock. For example, the standard penetration test (SPT) can fracture soft rock during driving, producing results that are too low, and design parameters that are too conservative or construction claims for differing site conditions.

Characterizing the material to contain and surround a drilled shaft foundation could be conducted using a cross borehole tomography technique. A minimum of 3-4 boreholes would be required to develop an image. While this approach certainly has merit, it may be too costly in that multiple boreholes would be required. In this chapter, the coupling of so-called down-hole and refraction tomography technique is presented as an alternative method, which uses only one borehole. Here a string of sensors is placed both horizontally along the ground surface and down

a single borehole. The borehole sensors could be contained within another apparatus like a CPT or rock shear device. With the sensors so located, energy is created and propagated from the ground surface and then detected via the sensor strings. The combined travel times are derived by picking first-arrival signals and used for inversion to obtain the subsurface profile.

The addition of borehole data to surface data is expected to improve inversion results, thus the need to know the capability of the combined surface and borehole data is critical. To both qualitatively and quantitatively appraise the capability of the data, the global inversion scheme presented in chapter 3 is used on many synthetic and real test data sets with or without boreholes to obtain both inverted profiles and associated quantitative uncertainties. A comparison of tomograms utilizing the combined borehole and surface data against tomograms developed using just the surface data suggests that significant additional resolution of inverted profiles at depth are obtained with the addition of a borehole. The uncertainty estimates provide a quantitative assessment of the reliability of the interpreted profiles. It is also found that the quantitative uncertainties associated with the inverted profiles are significantly reduced when adding a borehole.

Refraction tomography using combined data can be utilized for site characterization of deep foundation design. It enables to provide important physical parameters of material at the socket that often carries a majority of load from deep foundations. The inversion results of the combined data enable to characterize spatial variability in geotechnical engineering physical parameters of subsurface formations useful in the design of deep foundations. This will be particularly useful in implementing the new LRFD design methodology that can explicitly account for spatial variability in design parameters. The refraction tomography using the combined data will improve the accuracy and reliability of engineering parameters determined

for design of deep foundations, and will increase the volume of material actually evaluated in a subsurface investigation. The improved characterization will lower uncertainty and risk, and reduce overall cost of subsurface construction.

4.2 Inversion of Synthetic Data

4.2.1 Synthetic Model 1

Synthetic model 1 (Figure 4-1a) was designed to illustrate the benefit of using the borehole data. It includes three layers increasing in velocity with depth and a low-velocity zone buried in layers 2 and 3. Two sets of travel time data were created from this model. The first set was calculated with 51 surface receivers at 1 m spacing and 17 shots at 3 m spacing. The second set was calculated with 51 surface receivers and 20 borehole receivers at 1 m spacing, and 16 shots at 3 m spacing. All the shots were on the surface and within the surface geophone spread (no shot at borehole location). The borehole was placed at the middle of the medium, and it runs through the low-velocity zone to the bottom of the medium. This travel time data was then used to invert the velocity structures.

To run the inversion, the medium sizes were kept the same as the true models, and discretized with a grid size of 1 m for ease in picking the first-arrival times from forward modeling. The velocity constraints were assigned by slightly increasing the maximum true value and decreasing the minimum true value, and thus the velocity was allowed to vary between 100 m/s and 5000 m/s. The initial model was specified with a constant velocity of 2000 m/s, which leads to an initial temperature of 10. Velocities of cells were then perturbed, models were updated, and temperature was reduced after each 10,000 accepted models until the criterion of convergence was satisfied. Because of the non-uniqueness of the inversion problem and to further avoid unusual artifacts, 50,000 accepted models from the last five temperature levels and

that have least-squared errors within a few percent from the smallest error are used to derive the final inverted model and the associated uncertainty.

First, consider the inverted model (Figures 4-1b) using only surface travel time data. A primary feature of refraction tomography is delineation of both vertical and horizontal changes in seismic wave velocity, e.g., detection of anomalies. Here it is observed that the inversion is able to reasonably characterize the presence, location of the low-velocity zone. However, it fails to recover the general shape and true velocity of 1000 m/s of the low-velocity zone. This is the typical limitation of refraction tomography using only surface data, because the technique can only model structures with velocity increasing with depth. In addition, refraction tomography is not able to characterize zones of material outside of the ray coverage. Here is where the uncertainty results (Figures 4-1c) are helpful. The uncertainty is low in zones with good ray coverage, such as zones near the surface, and high in zones with poor ray coverage, such as zones near the bottom corners of the medium. In zones of high uncertainty, the inversion routine simply reports the velocity as the average value from all values randomly and uniformly withdrawn between the minimum and maximum velocity constraints selected by the user. Otherwise, in the zones of low uncertainty, the inverted velocity is independent of the constraints and thus more reliable. From these results, it appears that the delineation between low and high uncertainty is reasonably established at a COV value of approximately 20%.

Here the inversion fails to provide rational information of the velocity structure below the depth of investigation of 15 m. This can be explained as follows. The half space (third layer) in this model has the highest velocity, thus the fastest rays that travel through the half space can be detected on the surface if the geophone spread is large enough. However, these fastest rays only travel with in a few meters at the top of the half space regardless how very large the geophone

spread is used. Therefore, the technique using only surface data fails to characterize the velocity structure below these few meters from the top of the half space. In this case, the borehole data is necessary. The borehole location can be decided from the inversion results of the surface data (Figures 4-1b and 4-1c), which provide the credible information of the location of the low-velocity zone. The borehole should be located at or near the low-velocity zone in order to well characterize this zone.

Second, consider the inverted model (Figure 4-1d) using combined borehole and surface data. It is observed that the presence, location, general shape, and true velocity of the low-velocity zone are well characterized. Velocity structure at depth near the borehole is well recovered. However, even using the combined data, the inverted model is not the same as the true model. Most notably, as discussed by Sheehan et al. (2005) and others, refraction tomography will always model a sharp contrast in velocity with a gradient in velocity. This reality largely accounts for the differences in the two models. In addition, from the uncertainty result (Figure 4-1e), the zone of investigation is again taken as the area having COV less than 20%.

Finally, a comparison of the tomogram (Figures 4-1d) utilizing the combined borehole and surface data against the tomogram (Figures 4-1b) developed using just the surface data suggests that significant additional resolution of inverted profiles at depth are obtained with the addition of a borehole. The borehole data help well characterize the low-velocity zone and also help to increase the depth of investigation near the borehole. Similarly, by comparing the uncertainty results (Figure 4-1c against Figure 4-1e), the uncertainty is significantly reduced at depth for the case of using the borehole data.

4.2.1 Synthetic Model 2

Synthetic model 2 (figure 2a) was designed to investigate whether a low-velocity zone can be characterize if the borehole does not run through this zone. It also includes three layers increasing velocity with depth and a low-velocity zone of 6 m by 6 m buried in layers 2 and 3. This model is 10 m deeper than model 1 and the low-velocity zone is placed nearby the borehole, which runs from the top to the bottom at the middle of the medium. Two sets of travel time data were created from this model using the same test layouts as model 1, except using 30 borehole receivers at 1 m spacing in this case.

As described for model 1 above, the inversion was conducted for both travel time data sets and the results are as follows. For the surface data only, the inversion results (not shown here) can not provide any information about the low-velocity zone. This can be explained that the low-velocity zone is buried at a significant depth compared to the surface geophone spread, and also the surface refraction tomography can only model structures with velocity increasing with depth. For the combined data, the inverted model is presented in Figure 4-2a. It is observed that the velocity structure near the borehole from the top to the bottom of the model is reasonably characterized. Particularly, the low-velocity zone is successfully recovered even though the borehole does not run through this zone. However, the inverted model and the true model are again not the same. The primary difference between the two models is due to the gradient.

Figure 4-2c presents the uncertainty associated with the inverted model. Similar to that of model 1, the uncertainty is low in zones with good ray coverage, such as zones near the borehole, and high in zones with poor ray coverage, such as zones near the bottom corners of the medium. It is interesting to note that the location and general shape of low-velocity zone also can be recognized in the uncertainty image as a high uncertainty area inside a low uncertainty zone. It is understood that the fastest rays from shots to geophones tend to avoid the low-velocity zone if no

geophones are placed in this zone. Therefore, the low-velocity zone has lower ray coverage than high-velocity zones around, and it is less defined and has higher uncertainty. The indication of low-velocity zone in the uncertainty image significantly increases the credence of a real low-velocity zone instead of an artifact of the inversion product.

4.2.1 Synthetic Model 3

Model 3 (Figure 4-3a) was designed to optimize test layouts in order to obtain a reasonable inverted profile near the borehole with the fewest possible number of shots. This model is similar to model 2, including 3 layers and a buried low-velocity zone of 4 m by 4 m, and the borehole is placed at the middle from the top to the bottom of the medium. The focus here is to delineate the velocity structure at depth within 5 meters around the borehole and it is expected the goal can be achieved by using only a few shots on the ground surface. To optimize the number of shots, three cases were tested using three sets of combined data created with the number of surface shots as 2, 4, and 6. For the first case, 2 shots were placed 5 m each side away from the borehole. And for other cases, shots were placed at both sides of the borehole at every 3m away from the borehole. Receivers were placed both on the surface within the shot spread and in the borehole at 1m spacing. The inversion results of the three cases are as follows:

First, the inversion results using 2 shots are presented in Figures 4-3b and 4-3c. Here the inversion enables to characterize the velocity of the three layers but it fails to provide any information of the low-velocity zone. This may be explained that there are not enough rays through the low-velocity zone if using only one shot each side of the borehole. Second, consider the inversion results using 4 shots (Figures 4-3d to 4-3e). It is observed that the velocity structure near the borehole is reasonably characterized. With respect to the low-velocity zone, the location and the true velocity of are well inverted. However its general shape is not fully recovered. Last,

the inversion results using 6 shots are presented in Figures 4-3f and 4-3g. The velocity structure near the borehole is well characterized; especially the low-velocity zone is well recovered.

From the inversion results for cases of model 3, it is possible to utilize just a few shot locations on the ground surface within a few meters around the borehole, surface geophones within this few meters, and a string of borehole geophones to reliably assess the subsurface properties at depth near the borehole. This is a significant reduction in test effort in comparison to full surface arrays such as those used in models 1 and 2.

4.3 Inversion of Real Test Data

4.3.1 Newberry Test Site

The description of the Newberry test site was provided in section 3.3.2. For the case presented here, the test was conducted on line K to measure both surface and borehole data. The surface data were measured with vertical geophones equally spaced at every 1 m, for a total of 37 measurements. The borehole data were measured in a borehole installed at the station 18 m with down-hole geophones at 1 m spacing, for a total of 17 measurements. Seismic energy was generated by vertically striking a metal ground plate with a sledgehammer, thus producing compression wave (P-wave) first arrivals. Shot locations were placed at 3 m spacing along 36 m and starting from 0 m, for a total of 13 shots.

First consider the surface data only (Figure 4-4). To run the inversion, the velocity constraints and the medium depth need to be established. Similar to surface data sets in chapter 3, the minimum and maximum velocities were determined as 300 m/s and 3000 m/s, respectively and the depth of the medium was simply taken as 1/2 of the geophone spread.

Second, for the case of the combined surface and borehole data (Figure 4-5), the velocity constraints are assigned the same as those for the case of the surface data only. The depth of the medium is simply taken the same as the depth of the borehole because it is expected that the

measured data does not provide any information of the structure below the tip of the borehole. In addition, because of the influence of borehole casing, the data from the shot at the borehole location is excluded from the combined data. Thus, only 12 shots are used in this case instead of 13.

In the inversion process of the two cases, the medium was discretized with a grid size equal to the geophone spacing of 1 m. The initial model was selected with a constant velocity of 1000 m/s, velocities of cells were perturbed by randomly assigning values between the constraints, models were updated, and the temperature was reduced after every 10,000 accepted models until the criterion of convergence was reached. The criterion of convergence was not satisfied until the estimated first-arrival times from the final accepted model were very close to the observed travel times (shown in Figures 4-4 and 4-5).

Because of noise, subjective judgments in manually picking first arrival times, and non-uniqueness of inverted solutions, there is no guarantee that the model corresponding to the smallest error is closest to the true model. Therefore, the inversion results should be inferred from many accepted models clustering around the global minimum and having similar errors, instead of from only one model that has the smallest error. Similar to synthetic model cases, last 50,000 accepted models were used to derive the inverted profiles and the associated uncertainties.

Figure 4-6a presents the two-dimensional compression (P) wave refraction tomogram determined from test data collected along the surface. This tomogram indicates that the P-wave velocity generally increases with depth within the investigation area. Figure 6b shows the uncertainty associated with the inverted P-wave profile. Again, the uncertainty is consistent to expectation, low uncertainty in zones with good ray coverage and high uncertainty in zones with

poor ray coverage. With the confidence gained from running synthetic models, the depth of investigation is about 10 m where the COV from surface to that depth is less than 20 percent.

Figure 4-7a presents the two-dimensional P-wave refraction tomogram determined from test combined data collected both along the surface and down the borehole. It is observed that a slightly low-velocity zone is found near the tip of the borehole. The position of this zone is also shown as the high value area in the uncertainty image (Figure 4-7b). Also based on the low uncertainty zone, the inverted structure velocity is credible near the borehole at depth.

Comparing the velocity profiles, Figure 4-6a against Figure 4-7a, the profiles are similar at shallow depth. This similarity is understandable because the shallow structure is mainly determined by the surface data, which is the same in both inversion runs. At deeper depth, the profiles are very different because only the profile from the combined data is determined from the test measurement; the other is simply reported by inversion as an average of the minimum and maximum constraints. Similarly, a comparison of uncertainty results (Figure 4-6b against Figure 4-7b) indicates that the uncertainty is significantly reduced at depth for the case of using a borehole. Thus, for deep foundation design, the inversion results of the combined data provide credible information of material at the socket, and also partially detect anomalies embedded near the socket. This is very important because the material at and near the socket will carry a majority of load from foundations.

4.3.2 Ocala Test Site

The test site is located near Ft. McCoy, Florida. The test was conducted to measure both surface and borehole data. The surface data were measured with vertical geophones equally spaced at every 1 m from 0 m to 30 m, for a total of 31 measurements. The borehole data were measured in a borehole installed at station 15 m with borehole geophones equally placed at every 1 m from 4 m to 18 m depth, for a total of 15 measurements. Seismic energy was generated by

vertically striking a metal ground plate with a sledgehammer, thus producing compression wave (P-wave) first arrivals. Shot locations were placed from 1 m to 3 m spacing along 30 m on the surface and starting from 0 m, for a total of 20 shots. The shot spacing was 1 m for shots close to the borehole, 2 m for shots farther, and 3 m for shots at both ends.

In a fashion similar to the Newberry data, two inversions were run for the surface data and the combined data. For both runs, the depth of medium was selected as 18 m, equal to the depth of the deepest borehole geophone, and the minimum and maximum velocities were 200 m/s and 3000 m/s, respectively. The inversions converged when the estimated first-arrival times from the final accepted model were very close to the observed travel times (shown in Figures 4-8 and 4-9).

Figures 4-10a and 4-10b present the two-dimensional P-wave refraction tomogram determined from test data collected along the surface and the associated uncertainty. Here, it is determined that the depth of investigation is about 10 m, and the velocity structure in the characterized zone increases with depth. Figures 4-11a and 4-11b show the P-wave tomogram and the associated uncertainty determined from combined test data collected along the surface and in the borehole. It is observed that the addition of a borehole significantly improves the resolution of inverted profile, reduces the associated uncertainty, and thus increases the depth of investigation. Again, the credible information of the bedrock is only obtained from the inversion of the combined data, and it is particularly useful for deep foundation design.

4.4 Conclusion for Chapter 4

The global inversion scheme presented in chapter 3 is used on many synthetic and real test data sets with or without a borehole to obtain both inverted profiles and associated quantitative uncertainties. A comparison of inversion results utilizing the combined borehole and surface data

against inversion results developed using just the surface data suggests that significant additional resolution of inverted profiles at depth are obtained, and uncertainties are significantly reduced with the addition of a borehole.

Employed for site characterization of deep foundation design, refraction tomography using combined surface and borehole data provides credible information of material at the socket and partially detects anomalies near the socket. This becomes very important because the material at and near the socket often carries a majority of load from foundations. The inversion results of the combined data, including inverted profiles and associated uncertainties, enable to characterize spatial variability in geotechnical engineering physical parameters of subsurface formations useful in the design of deep foundations. This will be particularly useful in implementing the new LRFD design methodology that can explicitly account for spatial variability and uncertainty in design parameters.

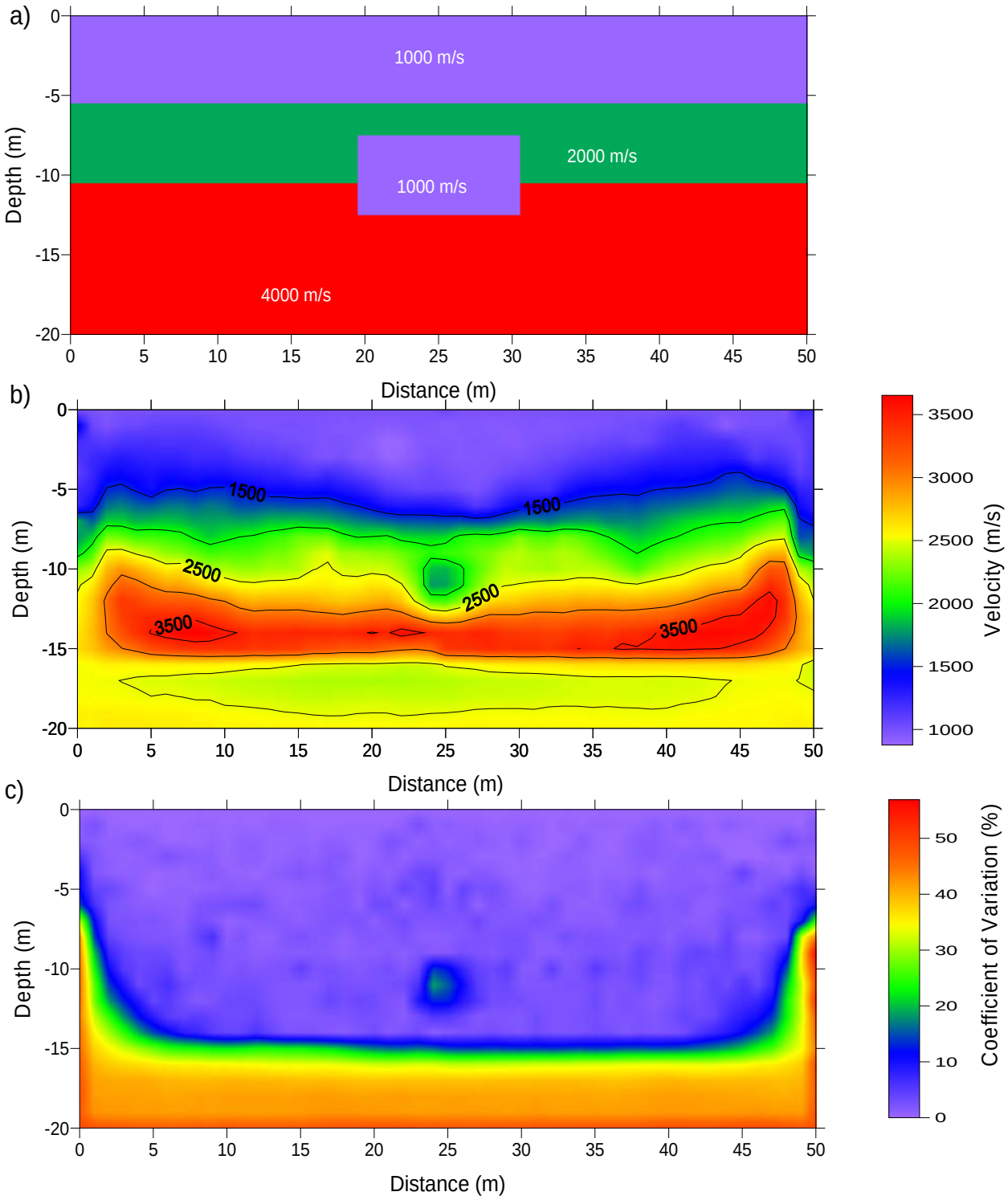

(Figure 4-1 is continued in the next page)

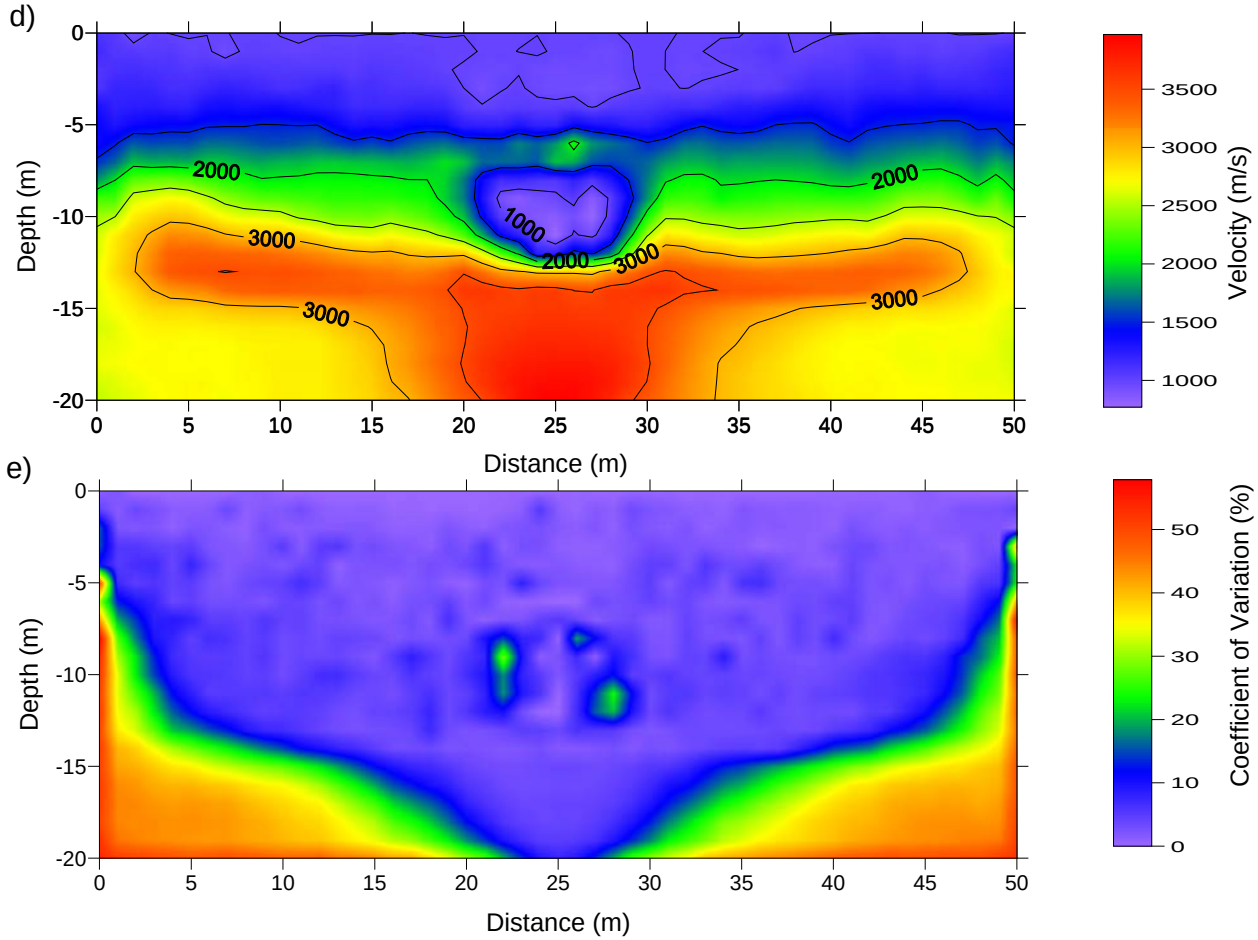

Figure 4-1. Synthetic model 1: a) true model, b) inverted model of the surface data, c) uncertainty associated with the inverted model in figure b, d) inverted model of the combined data, and e) uncertainty associated with the inverted model in figure d.

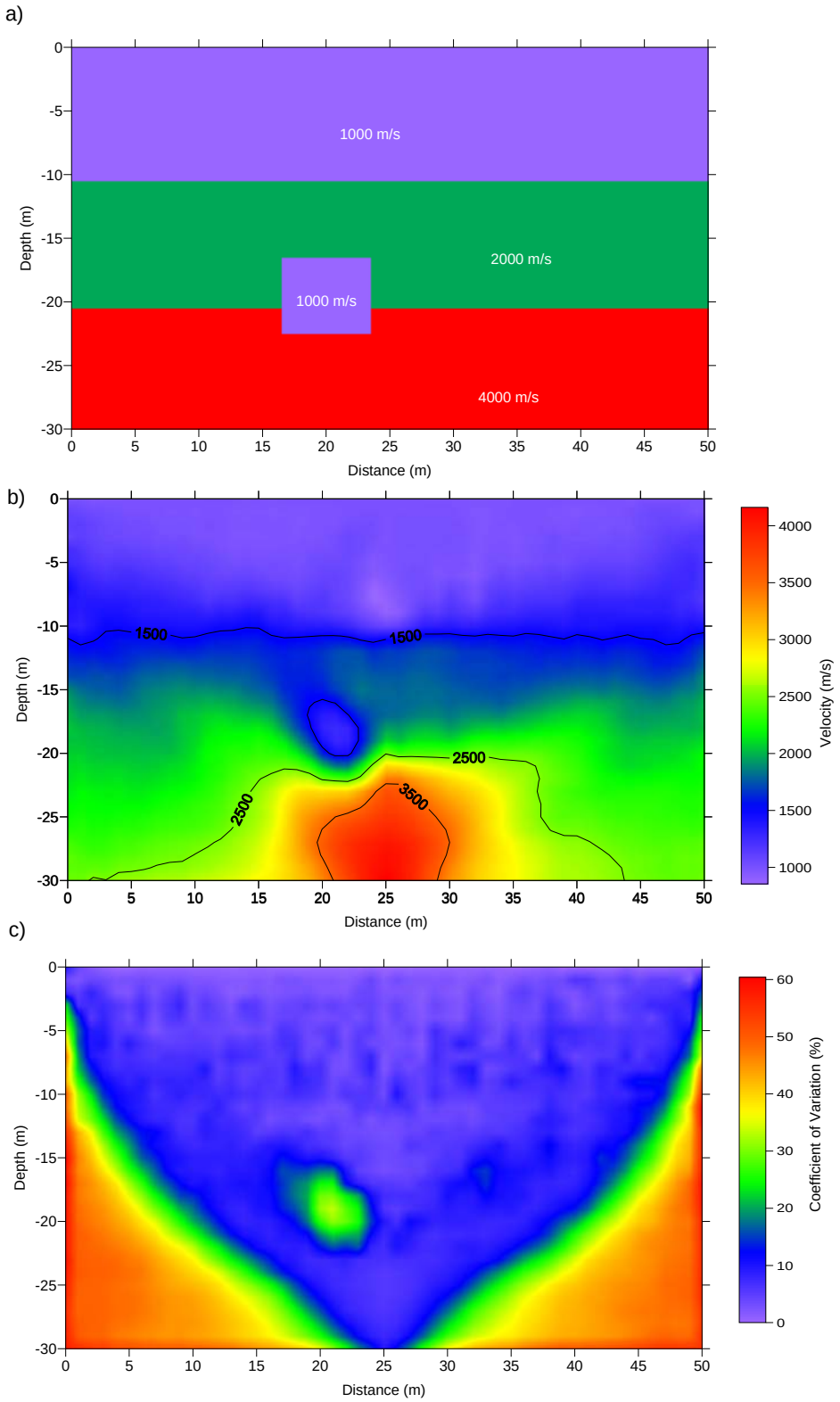

Figure 4-2. Synthetic model 2: a) true model, b) inverted model c) uncertainty associated with the inverted model

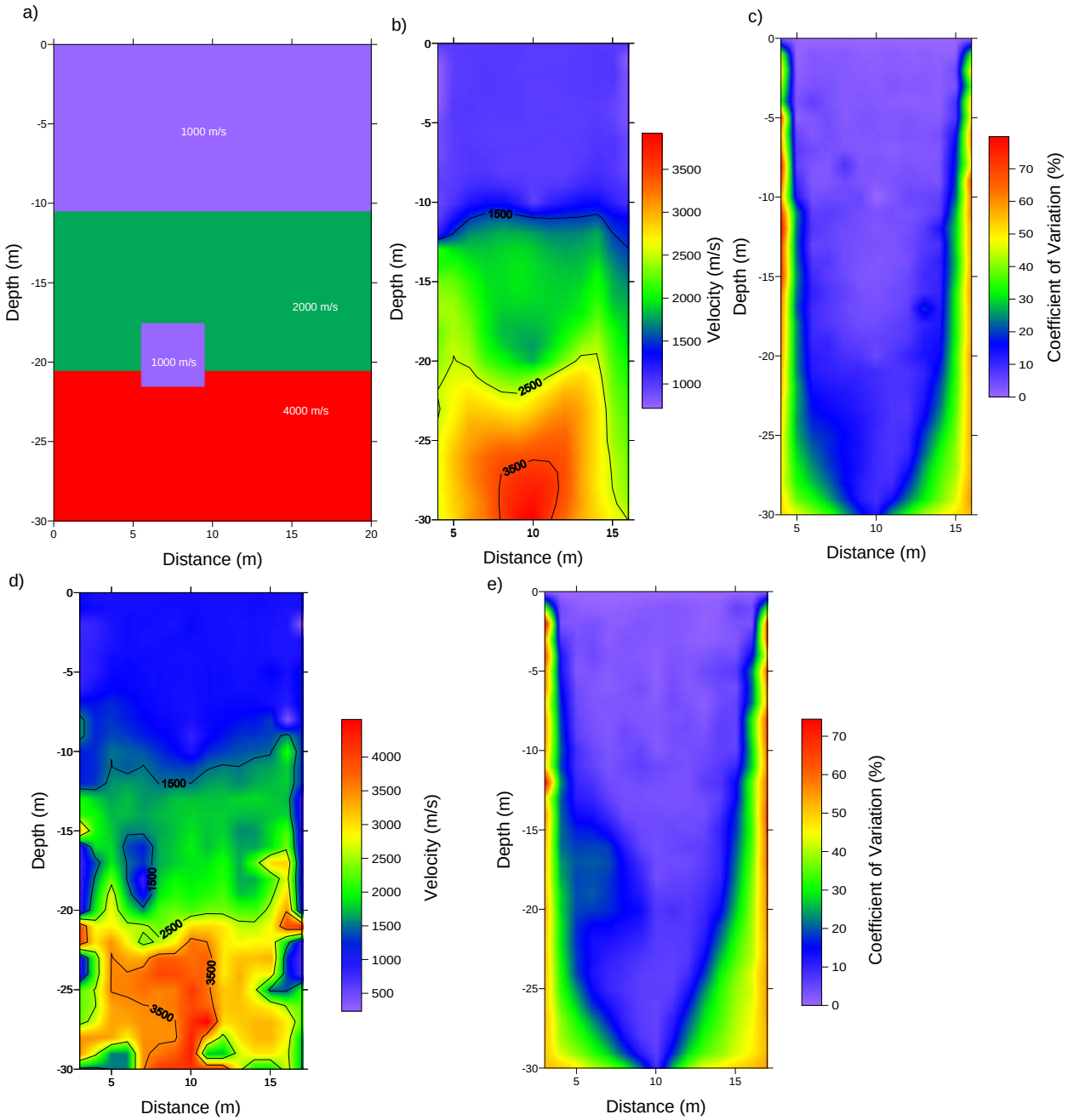

(Figure 4-3 is continued in the next page)

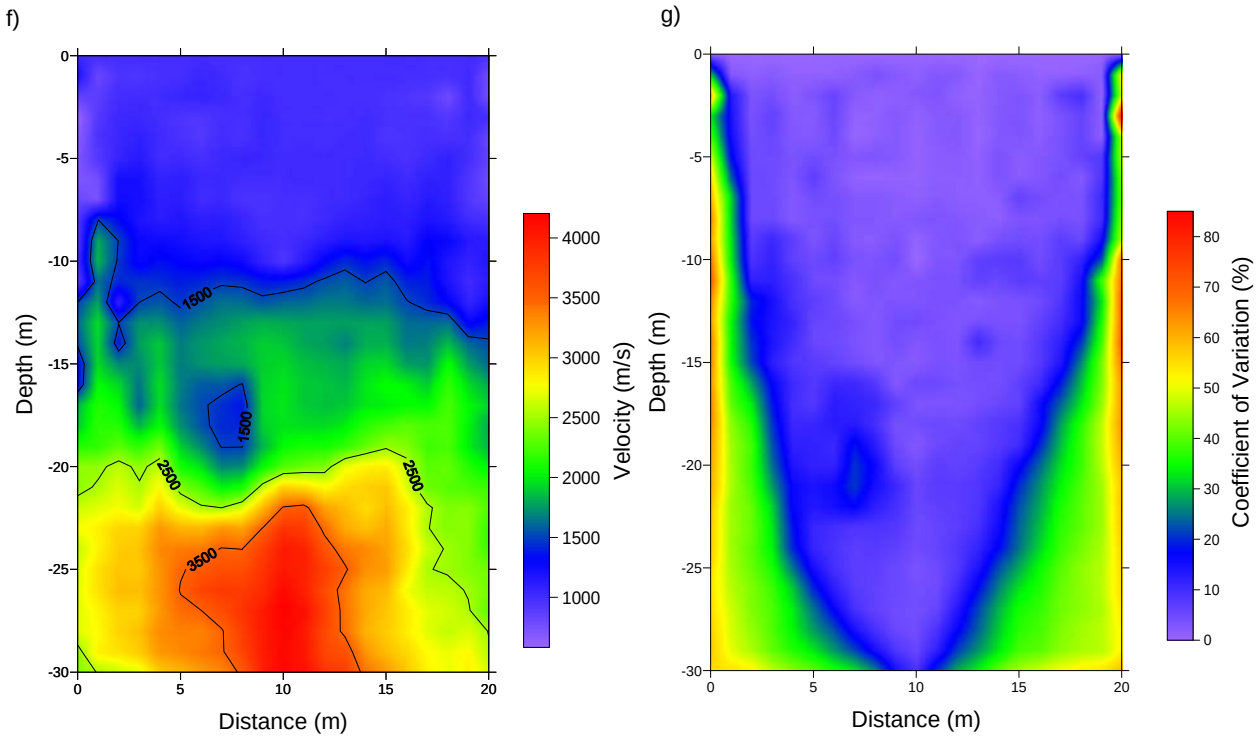

Figure 4-3. Synthetic model 3: a) true model, b and c) inverted model and uncertainty using 2 shots, d and e) inverted model and uncertainty using 4 shots, f and g) inverted model and uncertainty using 6 shots

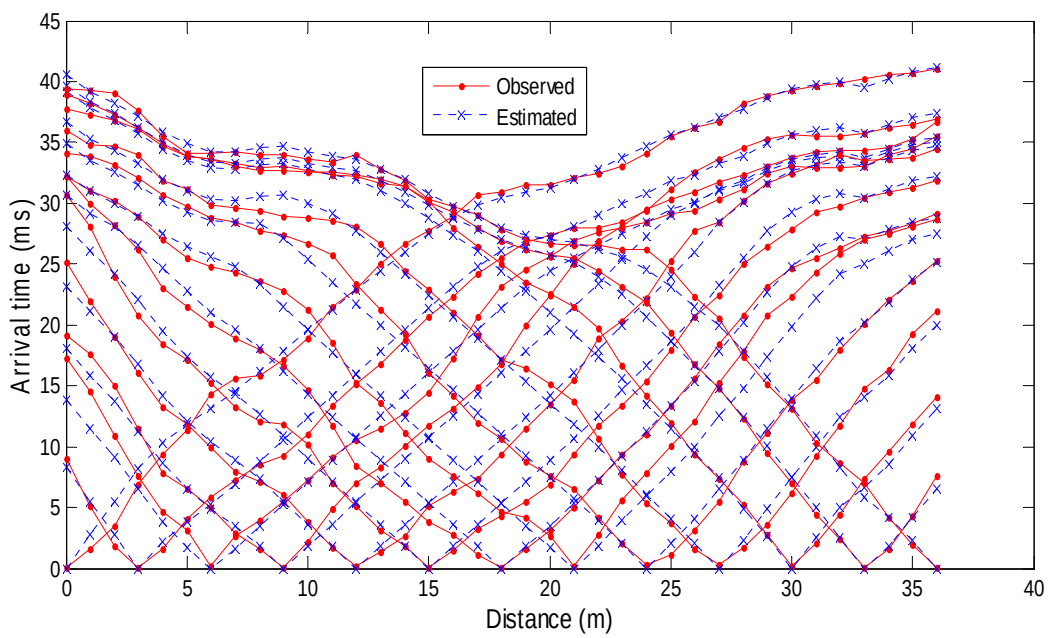

Figure 4-4. Comparison between the observed and estimated first-arrival times for Newberry surface data

a)

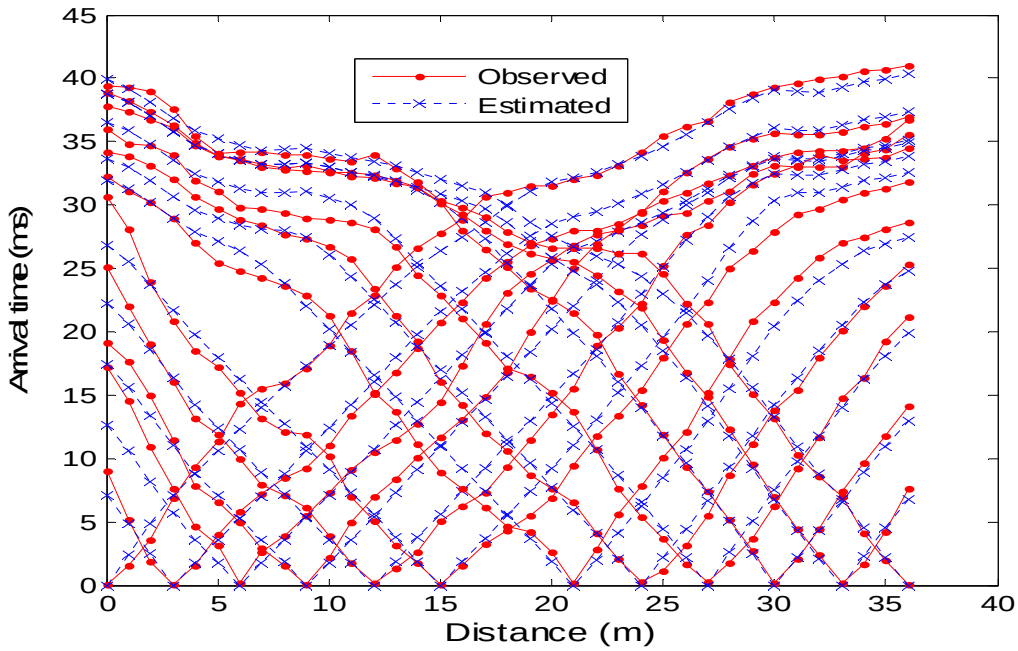

b)

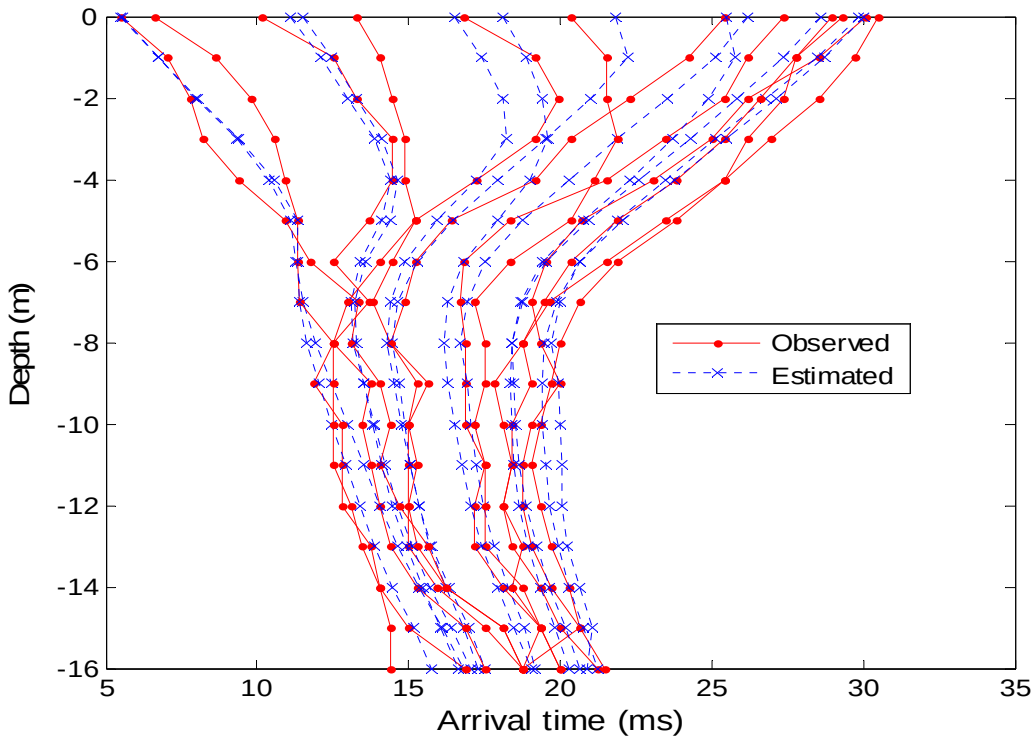

Figure 4-5. Comparison between the observed and estimated first-arrival times for Newberry combined data: a) surface data, and b) borehole data

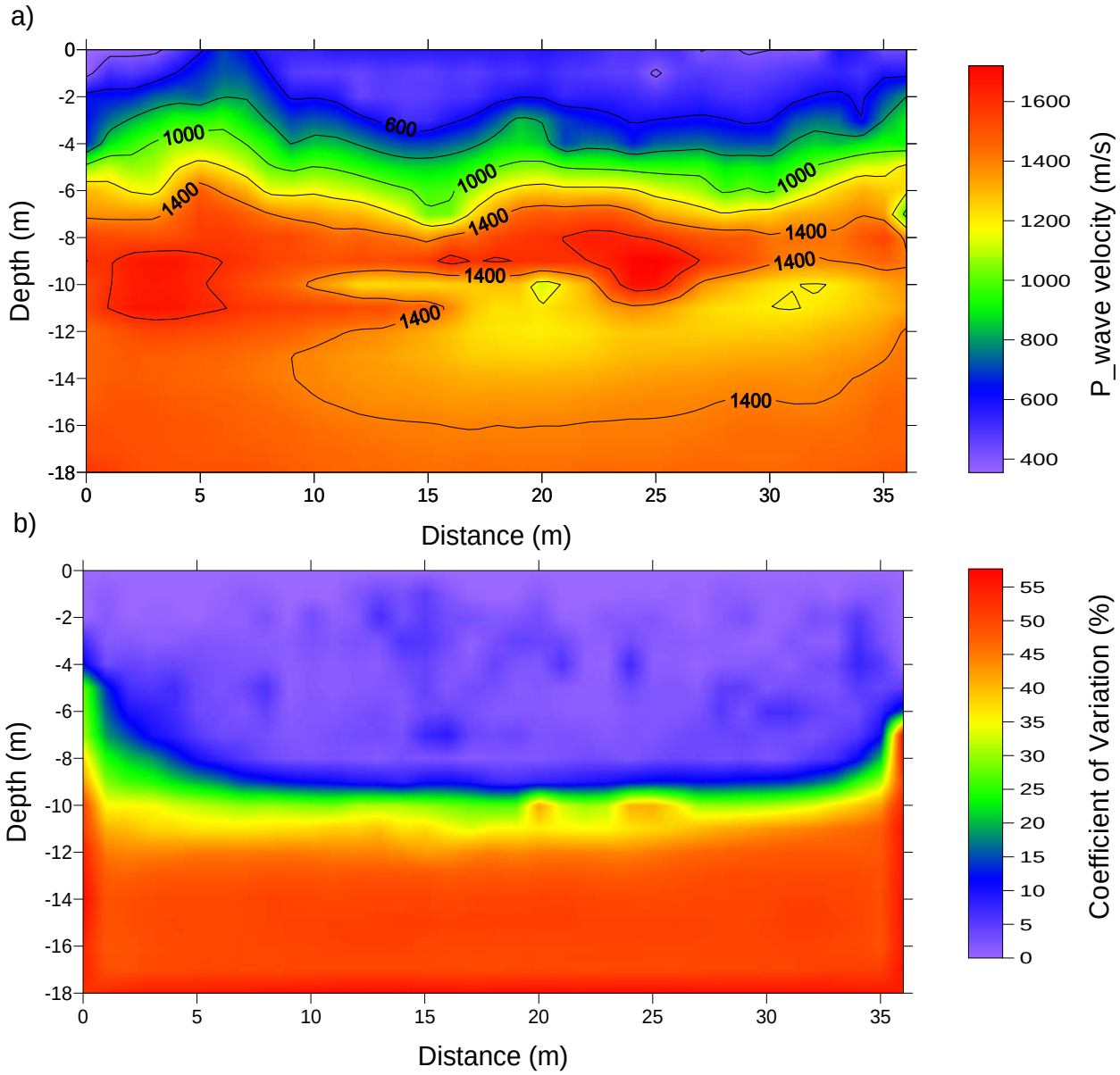

Figure 4-6. Newberry surface data: a) inverted model, and b) uncertainty

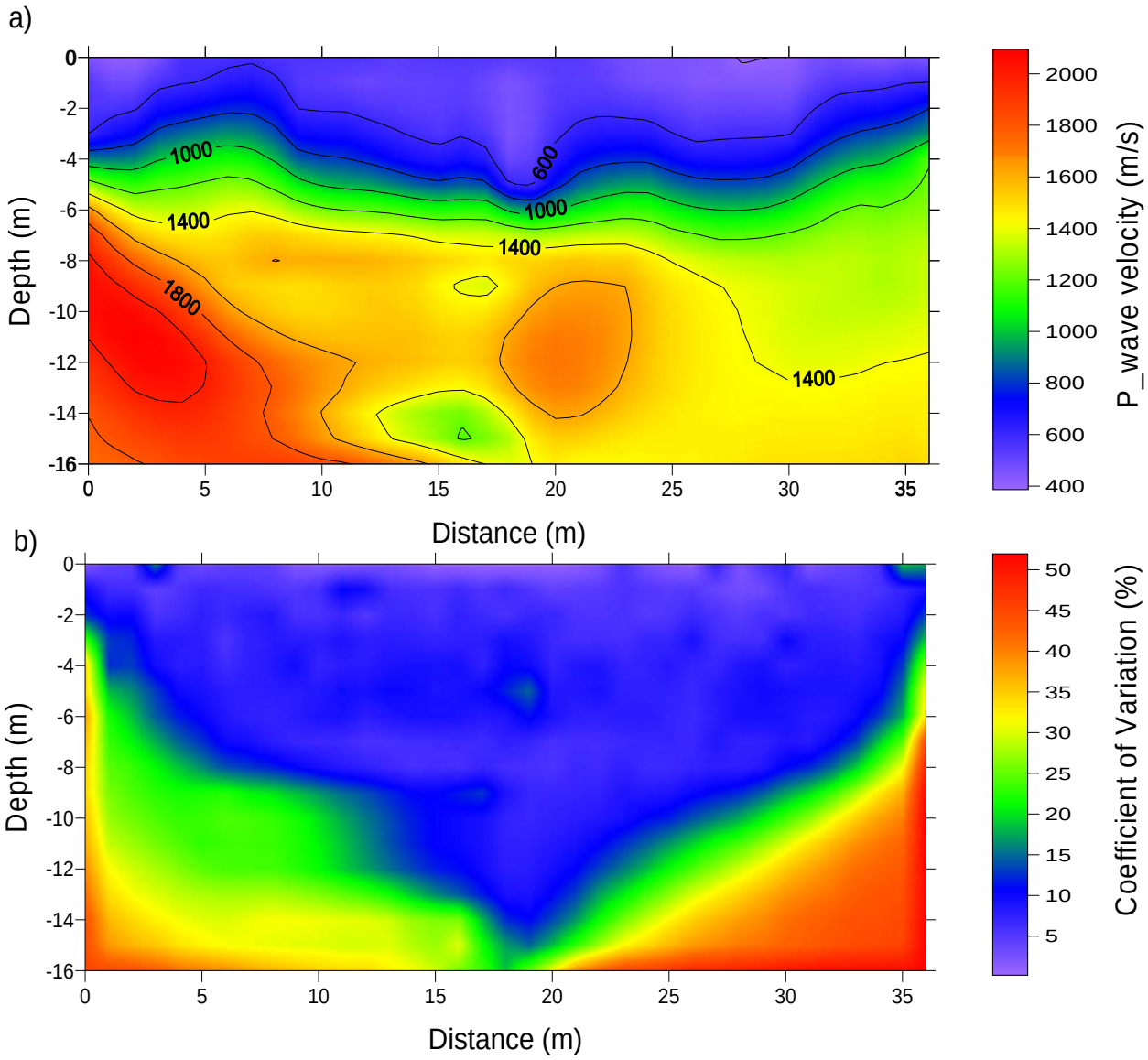

Figure 4-7. Newberry combined data: a) inverted model, and b) uncertainty

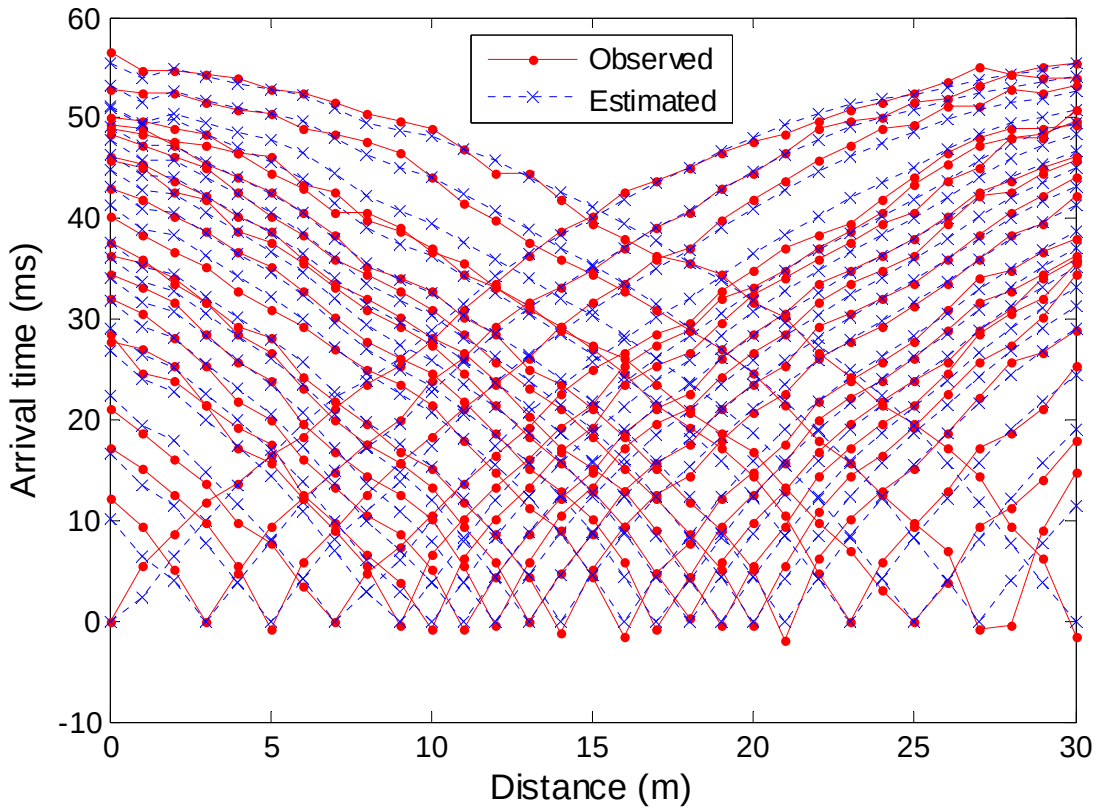

Figure 4-8. Comparison between the observed and estimated first-arrival time for Ocala surface data

a)

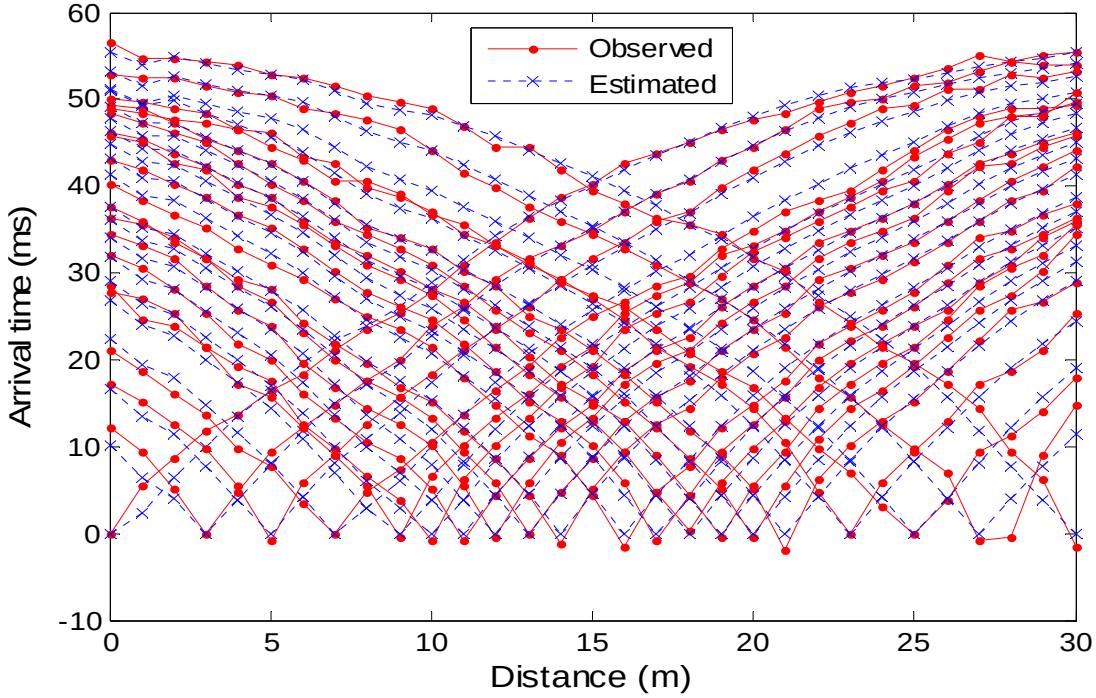

b)

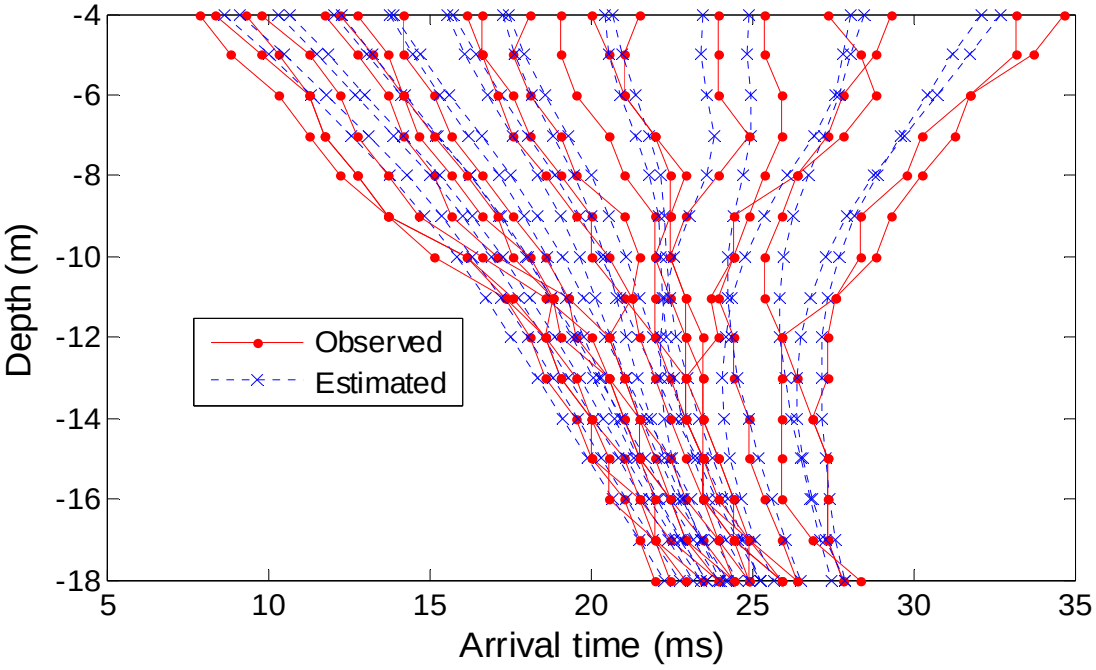

Figure 4-9. Comparison between the observed and estimated first-arrival time for Ocala combined data: a) surface data, and b) borehole data.

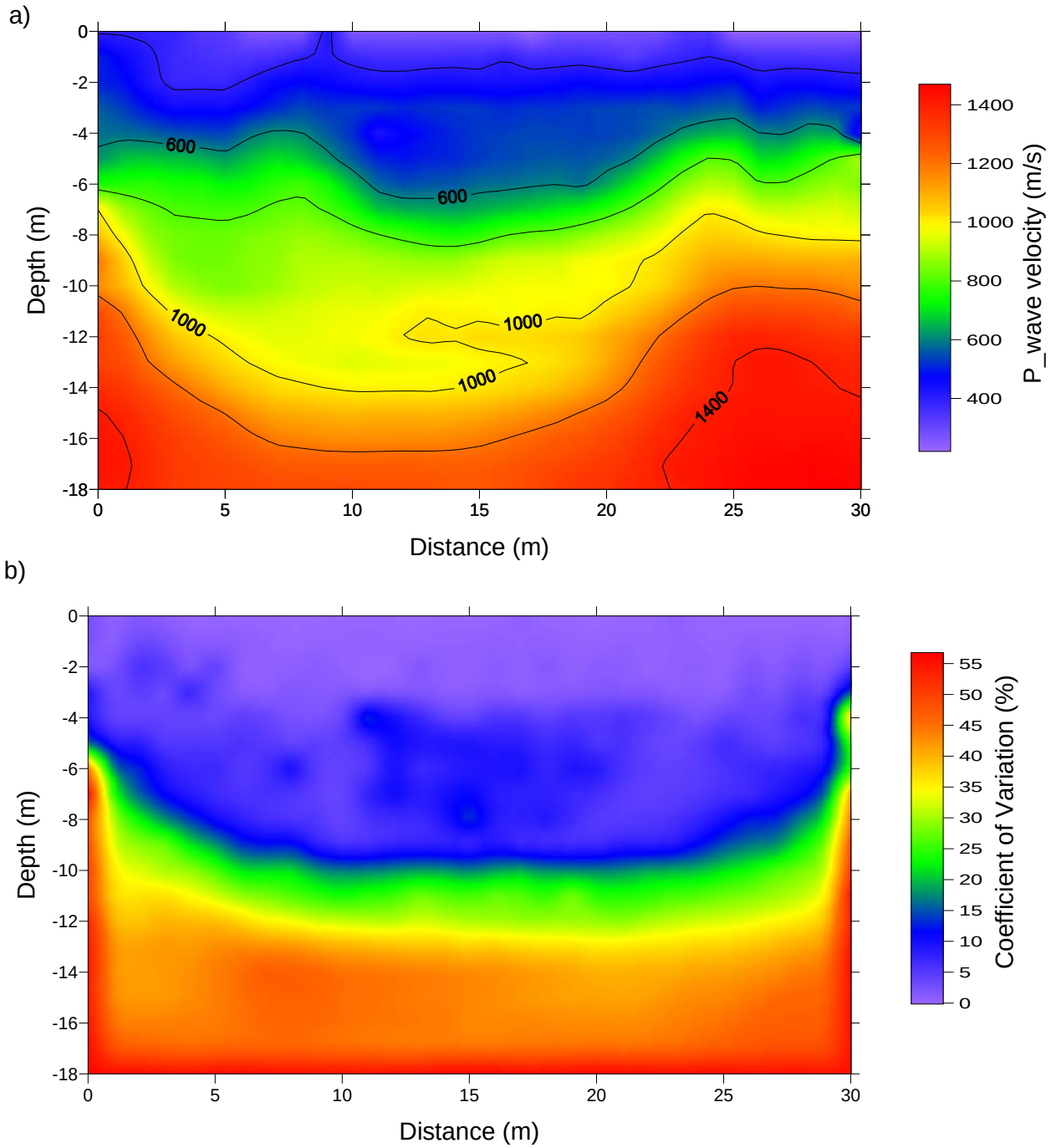

Figure 4-10. Ocala surface data: a) inverted model, and b) uncertainty

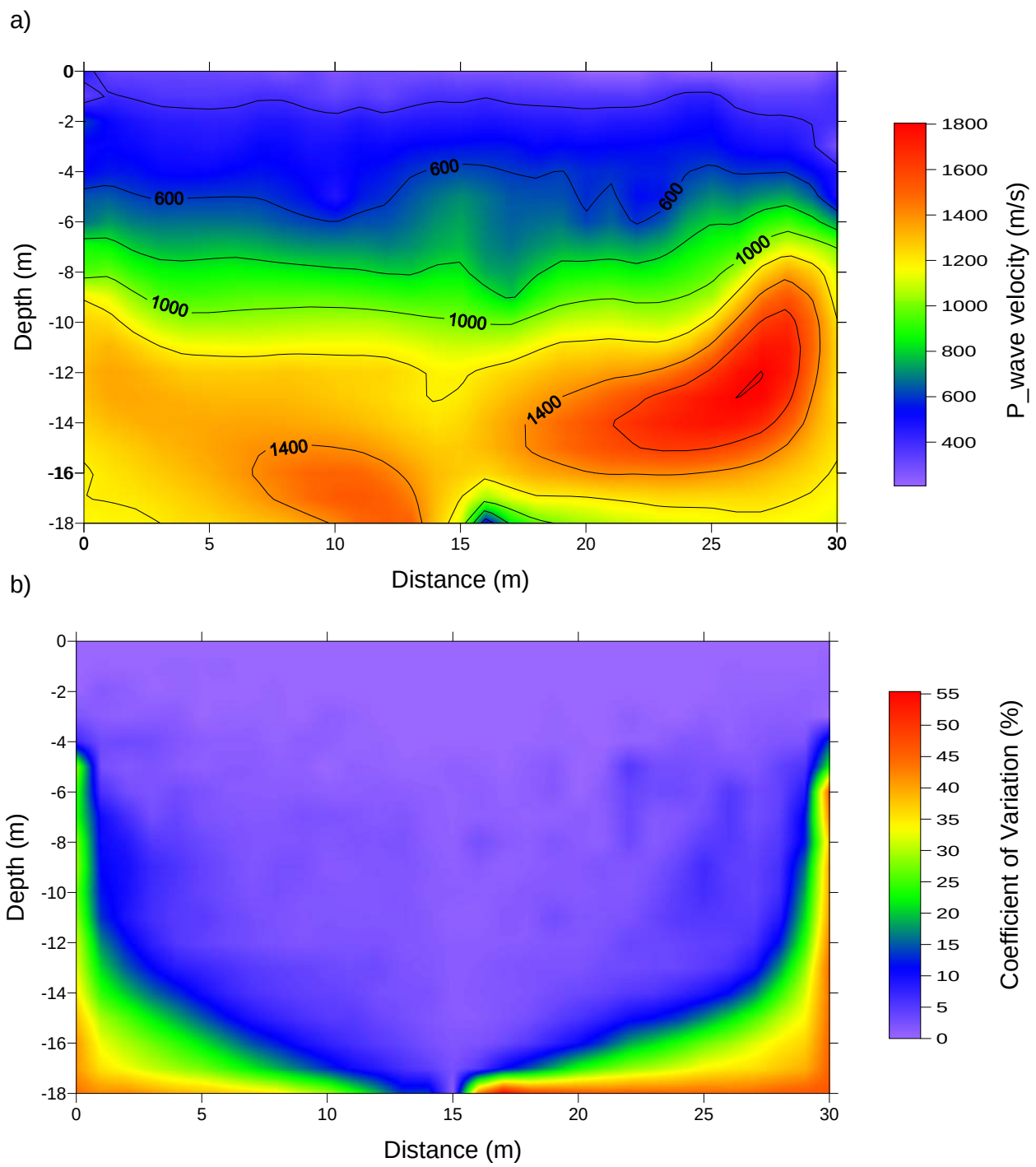

Figure 4-11. Ocala combined data: a) inverted model, and b) uncertainty

CHAPTER 5
TWO-DIMENSIONAL INVERSION OF FULL WAVEFORMS USING SIMULATED ANNEALING

5.1 Introduction

The technique using combined travel times presented in chapter 4 demonstrates a great capability of characterizing anomalies in subsurface profiles. However, it requires the borehole data, which is not always available. The question here is how do we solve problems of 2-D reverse models with only surface data? This chapter suggests a possible solution by using an inversion of full waveforms. The full waveform has been used by authors for the deep (> 1 km) subsurface investigation, in both the time domain (Shipp and Singh [2002], Sheen et al. [2006]) and the frequency domain (Pratt [1999]). In all of these applications, body waves are dominant components in wave fields used for inversion. Unlike these methods, the technique of full waveform inversion presented in this chapter uses Rayleigh waves as dominant components in wave fields. Because, Rayleigh waves are more sensitive to shear wave velocity and less sensitive to Poison's ratio or density of a medium, they are useful for geotechnical applications where the shear wave velocity primarily controls properties of soil particles.

The presented technique is based on a finite-difference solution of 2-D elastic wave equation in the time distance domain. The strength of this approach is the ability to generate all possible wave types (body waves and surface waves) and thus to simulate and accurately model complex seismic wave fields that are then compared with observed data to infer complex subsurface properties. The technique uses full information of elastic wave fields to increase resolution of inversion results, especially dealing with reverse models. It also employs a global inversion technique, simulated annealing, to invert the full wave fields for near-surface velocity profiles.

Unlike local inversion techniques, simulated annealing attempts to find the global minimum of the misfit function by searching over a large parameter space and uses more global information to update the current position, thus it likely converges to the global minimum. In addition, simulated annealing provides a suite of final models clustering around the global solution and having comparable least-square error. This allows getting the inversion result by averaging all of these models to mitigate the influence of noise and the non-uniqueness of the inversion solutions.

The most important advantage of simulated annealing is to avoid being trapped in local minima, and thus to allow final inversion results to be independent of the initial model. However, this technique can require significant computer time, especially if the model contains a large number of model parameters. This disadvantage is reduced herein by using a fast forwarding model solution, and by assuming that interfaces within a medium are multi-linear in order to limit the number of model parameters.

The technique is first tested on many different synthetic data sets created from challenging reverse models with high-velocity and low-velocity layers at different depths that are hardly inverted by traditional inversion methods using only dispersion property of Rayleigh waves. Then it is applied to real experimental data sets, and the inversion results are compared to invasive test results including those of cross-hole, SPT N-value, and material log, or compared to results of independent refraction tests. Inversion results from both synthetic and experimental data show superiority of this technique over the traditional methods via its accuracy.

5.2 Methodology

5.2.1 Forward Modeling

Virieux (1986) presented a finite-difference scheme to solve the first-order linear partial differential equation describing elastic wave propagation on a staggered grid. For 2-D case, the following two sets of equations are solved:

Equations governing particle velocity:

$$\begin{cases} \dfrac{\partial v_x}{\partial t} = \dfrac{1}{\rho}\left(\dfrac{\partial \sigma_{xx}}{\partial x} + \dfrac{\partial \sigma_{zx}}{\partial z}\right) \\ \dfrac{\partial v_z}{\partial t} = \dfrac{1}{\rho}\left(\dfrac{\partial \sigma_{zx}}{\partial x} + \dfrac{\partial \sigma_{zz}}{\partial z}\right) \end{cases} \tag{5.1}$$

Equations governing stress tensor:

$$\begin{cases} \dfrac{\partial \sigma_{xx}}{\partial t} = (\lambda + 2\mu)\dfrac{\partial v_x}{\partial x} + \lambda \dfrac{\partial v_z}{\partial z} \\ \dfrac{\partial \sigma_{zz}}{\partial t} = (\lambda + 2\mu)\dfrac{\partial v_z}{\partial z} + \lambda \dfrac{\partial v_x}{\partial x} \\ \dfrac{\partial \sigma_{zx}}{\partial t} = \mu\left(\dfrac{\partial v_x}{\partial z} + \dfrac{\partial v_z}{\partial x}\right) \end{cases} \tag{5.2}$$

In these equations, (v_x, v_z) is the particle velocity vector, (σ_{xx}, σ_{zz}, σ_{xz}) is the stress tensor, ρ is the density and μ, λ are Lame' coefficients.

Because of the need of a fast forwarding model solution for the global optimization method, some special boundary conditions are employed in this study to allow limiting medium to the smallest possible size. These boundary conditions are as follows:

Free-surface condition on top:

$$\begin{cases} \sigma_{zx} = 0 \\ \sigma_{zz} = 0 \end{cases} \tag{5.3}$$

or equivalently from equation (5.2) and (5.3):

$$\begin{cases} \dfrac{\partial v_x}{\partial z} = -\dfrac{\partial v_z}{\partial x} \\ \dfrac{\partial v_z}{\partial z} = -\dfrac{\lambda}{\lambda + 2\mu}\dfrac{\partial v_x}{\partial x} \end{cases} \tag{5.4}$$

Symmetrical condition at left hand side (load line)

$$\begin{cases} \sigma_{zx} = 0 \\ v_x = 0 \end{cases} \tag{5.5}$$

Absorbing condition A1 (Clayton and Engquist, 1977) at bottom

$$\begin{cases} \dfrac{\partial v_x}{\partial t} + Vs\dfrac{\partial v_x}{\partial z} = 0 \\ \dfrac{\partial v_z}{\partial t} + Vp\dfrac{\partial v_z}{\partial z} = 0 \end{cases} \tag{5.6}$$

and at right hand side

$$\begin{cases} \dfrac{\partial v_x}{\partial t} + Vs\dfrac{\partial v_x}{\partial x} = 0 \\ \dfrac{\partial v_z}{\partial t} + Vp\dfrac{\partial v_z}{\partial x} = 0 \end{cases} \tag{5.7}$$

where Vs, Vp are shear and P-wave velocities.

Derivatives are discretized by using center finite-differences. Assuming equations are verified at nodes, discretization leads to a unique staggered grid, as shown at Figure 5.1.

The explicit numerical scheme (Virieux, 1986), equivalent to the systems (5.1) and (5.2) is:

$$U_{i,j}^{k+1/2} = U_{i,j}^{k-1/2} + B_{i,j}\frac{\Delta t}{\Delta x}\left(Txx_{i+1/2,j}^{k} - Txx_{i-1/2,j}^{k}\right) + B_{i,j}\frac{\Delta t}{\Delta z}\left(Txz_{i,j+1/2}^{k} - Txz_{i,j-1/2}^{k}\right)$$

$$V_{i+1/2,j+1/2}^{k+1/2} = V_{i+1/2,j+1/2}^{k-1/2} + B_{i+1/2,j+1/2}\frac{\Delta t}{\Delta x}\left(Txz_{i+1,j+1/2}^{k} - Txz_{i,j+1/2}^{k}\right)$$
$$+ B_{i+1/2,j+1/2}\frac{\Delta t}{\Delta z}\left(Tzz_{i+1/2,j+1}^{k} - Txz_{i+1/2,j}^{k}\right)$$

$$Txx_{i+1/2,j}^{k+1} = Txx_{i+1/2,j}^{k} + (L+2M)_{i+1/2,j} \frac{\Delta t}{\Delta x}\left(U_{i+1,j}^{k+1/2} - U_{i,j}^{k+1/2}\right)$$
$$+ L_{i+1/2,j} \frac{\Delta t}{\Delta z}\left(V_{i+1/2,j+1/2}^{k+1/2} - U_{i+1/2,j-1/2}^{k+1/2}\right) \tag{5.8}$$

$$Tzz_{i+1/2,j}^{k+1} = Tzz_{i+1/2,j}^{k} + (L+2M)_{i+1/2,j} \frac{\Delta t}{\Delta z}\left(V_{i+1/2,j+1/2}^{k+1/2} - V_{i+1/2,j-1/2}^{k+1/2}\right)$$
$$+ L_{i+1/2,j} \frac{\Delta t}{\Delta x}\left(U_{i+1,j}^{k+1/2} - U_{i,j}^{k+1/2}\right)$$

$$Txz_{i,j+1/2}^{k+1} = Txz_{i,j+1/2}^{k} + M_{i,j+1/2} \frac{\Delta t}{\Delta z}\left(U_{i,j+1}^{k+1/2} - U_{i,j}^{k+1/2}\right) + M_{i,j+1/2} \frac{\Delta t}{\Delta x}\left(V_{i+1/2,j+1/2}^{k+1/2} - V_{i-1/2,j+1/2}^{k+1/2}\right)$$

In these equations, k, i, and j are the indices for time, x-axis, and z-axis discretization. Δt, Δx, and Δz are grid steps for time, x-axis, z-axis, respectively. Numerical velocity (U,V)=(v_x,v_z) at time (k+1/2) Δt, and numerical stress (Txx, Tzz, Txz)= (σ_{xx}, σ_{zz}, σ_{xz}) at time (k+1) Δt, are computed explicitly from velocity at time (k-1/2) Δt and stress at time k Δt. B is $1/\rho$ and M, L are Lame' coefficients (μ, λ).

For free-surface condition, the geometry is chosen so that the free surface is located exactly through the upper part of the staggered grid-points at z=0, that is, σ_{xx}, σ_{zz}, and v_x are located on the free surface. To update the wave field in the proximity of the free surface, both vertical velocity v_z and shear stress σ_{xz} of one row above the surface are required. By imaging σ_{xz} as an odd function around the free surface, it is assured that σ_{xz} =0 there. From equation (5.4), the v_z above surface can be obtained as:

$$V_{i+1/2,1/2}^{k+1/2} = V_{i+1/2,3/2}^{k+1/2} + \frac{L_{i+1/2,1}}{(L+2M)_{i+1/2,1}} \frac{\Delta z}{\Delta x}\left(U_{i+1,1}^{k+1/2} - U_{i,1}^{k+1/2}\right) . \tag{5.9}$$

Similarly, assuming σ_{xz} and v_x are odd functions around the symmetrical line to update the wave field in the proximity of left hand side boundary. For absorbing boundary conditions (5.6) and (5.7), backward finite-difference scheme is used in both spatial and time directions to update

velocity components v_x, v_z at vertical gridlines Nx, Nx-1/2 for right hand side boundary, and at horizontal gridlines Nz, Nz-1/2 for the bottom boundary.

The initial conditions are set to satisfy equilibrium at time t=0, i.e., stress and velocity are zero everywhere in the medium. Then the medium is perturbed by changing vertical stress σ_{zz} at source that is often modeled as a triangle wavelet (Figure 5-4a) or a Ricker wavelet R(t) (Figure 5-4b):

$$R(t) = \left(1 - 2\pi^2 f_c^2 (t - t_0)^2\right) \cdot \exp\left(-\pi^2 f_c^2 (t - t_0)^2\right), \tag{5.10}$$

where f_c is the center of frequency band and t_0 is time shift.

For homogeneous media, the numerical stability condition for this explicit scheme:

$$V_p \Delta t \sqrt{\frac{1}{\Delta x^2 + \Delta z^2}} \leq 1, \tag{5.11}$$

and for heterogeneous cases, *Vp* value in the equation (5.11) should be the maximum P-wave velocity in the media. Δx and Δz need to be selected to satisfy at least ten points per minimum expected wavelength to avoid numerical dispersion, and then Δt is selected from the stability condition. In inversion process, Δt is supposed to change due to different input *Vp* values, thus the wave fields are interpolated to a fixed time interval for comparing to measured wave fields.

The code is developed in Matlab in which all stresses and particle velocities are calculated in matrix forms at each time step and then advanced along time direction. The accuracy of this finite-difference method (FDM) is verified by comparing its wave field to that generated by a finite element method (FEM) that is available in commercial software Plaxis2D. Figure 5.2 shows the results from two methods are almost identical. By using FDM, computer time can be saved significantly. On the same standard computer, FDM needs less than 1 second, while FEM needs a few minutes to generate the wave field shown in the Figure 5.2. This fast finite

difference solution brings possibility of being applied to the global optimization method for inversion presented in next section.

5.2.2 Optimization Method

Rather than discussing the analogy of simulated annealing that has been well described by Sen and Stoffa (1995), a brief description of the process used in this technique is presented herein.

1. Select an initial model P so that each component P_i to satisfy $P_i^{\min} \le P_i \le P_i^{\max}$ and then calculate the least-squared error E as:

$$E = \frac{1}{N}\sum_{k=1}^{N}\left[d_k - g_k(P)\right]^2 , \tag{5.12}$$

   where d_k and g_k are the *kth* observed and computed responses, respectively, and N is the number of observation points, equal to the number of receivers times the number of time steps.

2. Following the idea of Ingber (1989, 1993), randomly select one parameter (say *ith* parameter) and perturb it according to the Cauchy probability distribution. The updating factor y_i for the *ith* parameter is computed from the equation:

$$y_i = \mathrm{sgn}(u_i - 0.5)\frac{T}{T_0}\left[\left(1+\frac{T_0}{T}\right)^{|2u_i-1|} - 1\right] . \tag{5.13}$$

   In the above equation, y_i varies between -1 and +1, u_i is a random number between 0 and 1, T is the current temperature, and T_0 is the initial temperature. Thus, the parameter P_i is updated to P_i^{j+1} from its previous value P_i^j by:

$$P_i^{j+1} = P_i^j + y_i(P_i^{\max} - P_i^{\min}) . \tag{5.14}$$

   The random number u_i sometimes needs to be reselected to guarantee that the value P_i^{j+1} from equation (5.14) satisfies the constraint $P_i^{\min} \le P_i^{j+1} \le P_i^{\max}$. Following the process described, the new model is now obtained and then the least-squared error corresponding to this new model is calculated.

3. The new model is unconditionally accepted if its least-squared error is smaller than that from the previous model, and conditionally accepted if its least-squared error is bigger with the following probability:

$$p = \exp\left(-\frac{\Delta E}{T}\right), \tag{5.15}$$

   where ΔE is the positive difference between the least-squared errors of the two models.

4. Repeat steps 2 and 3 until a desired number of accepted models is completed, then reduce the temperature to the next level according to a schedule:

$$T(k) = \frac{T(k-1)}{2} \ , \tag{5.16}$$

where *T(k)* is the temperature at the *kth* level.

The criterion for convergence requires that the relative difference between the maximum and minimum least-squared errors from all accepted models at a particular temperature to become very small (empirically say between 0.5% and 1%). If the criterion for convergence is not satisfied, the temperature is reduced to the next level. At a sufficiently low temperature, the accepted models are in the vicinity of the global minimum and the optimization converges.

The selection of a correct initial temperature is very important. Selecting a very high value leads to unnecessary computations, whereas starting from a low value leads to a local solution. In this study, the initial temperature is taken as the nearest lower power of ten to the least-squared error; for example, if the least-squared error is 0.35 then the initial value is 0.1. In this way, the initial temperature is usually higher than the critical temperature and any bias in the initial model will be destroyed.

The cooling schedule is another important parameter in the global optimization using simulated annealing. Many schedules have been tested for inversion problems with the number of model parameters up to 40, and it is found that the number of accepted models at each temperature level should be at least 200 times of the number of model parameters, and the temperature needs to reach to a very low value to obtain the global solution. In this study, the final temperature is about 10^{-4} to 10^{-5} when the initial temperature is 0.1. When the number of model parameters increases, the procedure needs a slower schedule and hence the time of computation increases in order to get the global solution. Therefore, the cooling schedule should be selected with care, particularly when dealing with a large number of model parameters.

5.3 Applications

5.3.1 Applications on Synthetic Data

Synthetic models refer to earth models whose velocity profile is assumed or known a priori. Using a known velocity structure, wave field data is calculated for an assumed test layout. This wave field data is then input to the inversion program as if it were data collected from a field test ("observed" data), and velocity structure (inverted model) is calculated from the observed data. By comparison of the inverted model against the true model, the capability of the inversion technique is appraised.

5.3.1.1 One-dimensional synthetic models

Two 1-D synthetic challenging models (models 1 and 2) that include high- and low-velocity layers are presented in this section. They are from Tokimatsu et al. (1992) and were previously used for studies of inversion using surface wave velocity dispersion by O'Neill (2003).

Synthetic model 1

Model 1 consists of a buried low-velocity layer (second layer) between two high-velocity layers, followed by a half space (Figure 5-3a). The observed wave field was generated in Plaxis2D using 10 receivers at 4 m spacing on the surface, and an active source placed 4 m away from the first receiver. The active source was modeled as a triangle impulsive load (Figure 5-4a), and such a source produced a wave field with dominant components between 10 Hz and 30 Hz. The observed wave field (at 10 points from A to J) is presented in Figure 5-5. It shows that the magnitude of the wave field is decayed significantly from point A (closest to the source), to point J (farthest from the source) due to damping. In order to increase the contribution of the far field signals, the receivers were treated equally by normalizing the maximum magnitude of measured

signals at each receiver to unity before being used for inversion, thus removing all kinds of damping (material and radiation) in wave propagation.

Before running inversion, constraints, medium sizes, and the grid size need to be specified. For velocity constraints, S-wave velocities were allowed to vary between 50 m/s and 300 m/s for the 3 layers, and between 200 m/s and 500 m/s for the half space. For thickness constraints, thicknesses were allowed to vary between 1 m and 5 m for layers 1 and 2, and between 5 m and 10 m for layer 3. For the medium sizes, the medium was selected as 20 m depth and 60 m width. The width was extended 20 m horizontally from the last receiver to limit the boundary affect during forward modeling. Finally, based on the receiver spacing and the minimum true S-wave velocity, the grid size was specified as 0.5 m, which can accurately model the maximum frequency of about 30 Hz at which the criterion of 10 mesh points per wavelength is satisfied.

To run inversion, Poisson's ratio and the medium density were kept the same as those used to generate the observed data to limit the number of model parameters to 7 (3 thicknesses and 4 velocities). The inversion began with the initial model of a constant S-wave velocity of 200 m/s and all thicknesses of 5 m, model parameters were perturbed within the constraints, models were updated, and the temperature was reduced after every 1400 (200 times of the number of model parameters) accepted models until the criterion of convergence was satisfied. The convergence was only found when the estimated data was very close to the observed (Figure 5-6), and the least-squared error was reduced from the initial value of 0.2087 to the final value of 0.0240.

Figure 5-6 presents a comparison between the observed and the estimated data. A good match is achieved at every channel along the whole range of the offset. Figure 5-7 presents velocity histograms of all accepted models at all temperature levels. At high temperatures, the accepted models are located over a large model space, and thus accepted velocities are any

random values between the constraints. Otherwise, at low temperatures, the accepted models cluster around the global minimum, and thus the mode values of the histograms are close to those of the true model. Similarly, Figure 5-8 presents thickness histograms of all accepted models, and again the mode values are observed to be close to those of the true model.

Figure 5-9 compares the inverted S-wave profile against the true model. It is found that the true model is well recovered. The differences of velocities and thicknesses between the true and the inverted models are less than 15%. These differences may be due to the incomparability of numerical methods used to generate the observed data (FEM) and the estimated data (FDM).

O'Neill (2003) did inversion studies on this model using dispersion data and a local inversion scheme. Even though the same synthetic modeling methods were used for the observed and estimated dispersion data, he found that the true model was hardly recovered. It was relatively recovered if the true depth of the half space was fixed during the inversion, and the initial model was close enough to the true model, such as the initial model having the true depth interfaces and a reasonable shear wave velocity.

It is clear that the technique presented here requires much less prior information to invert the true model. The superiority of the technique is attributed to the full waveform data used for inversion that is more sensitive to a low-velocity layer (LVL) than the dispersion data, and the advantage of the global inversion scheme that is independent of the initial model.

Synthetic model 2

Model 2 consists of a buried high-velocity layer (second layer) between two low-velocity layers, followed by a half space (Figure 5-3b). Similar to model 1, the observed wave field (Figure 5-10) was generated in Plaxis2D using 10 receivers at 4 m spacing on the surface, and an impulsive source (Figure 5-4a) placed 4 m away from the first receiver.

In the same manner of model 1, an inversion was conducted using the observed data of model 2. During the inversion, the least-squared error decreased from 0.2025 for an initial model of a constant velocity of 200 m/s to 0.0378 for the final accepted model. Again, the final inverted model (Figure 5-14) is a good recovery of the true model, correctly inverting both interfaces and velocities. The good recovery of the velocity model leads to a good match between the observed and estimated wave fields (Figure 5-11). The velocity and thickness histograms of all accepted models are also shown in Figures 5-12 and 5-13, whose mode values are close to those of the true model.

Similar to model 1, O'neil (2003) found that this true model was also hardly recovered. It was relatively recovered if the true depth of the half space was fixed during the inversion, and the initial model had the true depth interfaces and a reasonable shear wave velocity.

5.3.1.2 Two-dimensional synthetic models

Three 2-D synthetic models (models 3, 4, and 5) are presented here. The first two models only consist of linear interfaces, and they can be inverted by data from a few receivers on the surface. The two synthetic data sets from these simple configurations were generated by the commercial software Plaxis2D. The last model consists of multi-linear interfaces that require data from many receivers along the surface to recover. For convenience, the synthetic data set from this more complicated configuration was generated by the finite-difference solution.

Synthetic model 3

Model 3 consists of a buried high-velocity layer (second layer) between two low-velocity layers, followed by a half space (Figure 5-15a). The medium is extended 20 m from the last receiver to limit the boundary affect.

The observed wave field was generated in Plaxis2D using 6 receivers at 10 m spacing on the surface, and an active source placed 10 m away from the first receiver. The active source was

modeled as a triangle impulsive load (Figure 5-4a), and such a source produced a wave field with dominant components between 10 Hz and 30 Hz.

To run inversion, the medium sizes were kept the same as those used in Plaxis2D. Poisson's ratio and density were also kept the same as values used to generate the observed wave field, thus the number of model parameters is 10 (4 shear velocities, 3 left thicknesses, 3 right thicknesses). The velocities of all layers were allowed to vary between 200 m/s and 1000 m/s, and the thickness was allowed to vary between 2 m and 10 m. The medium was discretized with a grid size of 1 m, and the material property at each node was assigned based on its tributary area, i.e., the material property was interpolated when interfaces lied between grid lines. Based on the grid size and the minimum true velocity, the maximum frequency that can be model accurately in forward modeling is 30 Hz, thus both observed and predicted wave fields were low band-pass filtered to remove all signals above 30 Hz before comparing.

The inversion began with an initial model selected with a constant shear velocity of 500 m/s, and left and right thicknesses of 7.5 m. With such the initial model, the initial least–squared error was 0.1480, thus the initial temperature was taken as 0.1. During inversion, velocities and thicknesses were perturbed, models were updated, and the temperature was reduced after every 2000 accepted models until the criterion of convergence was satisfied at which the final smallest error was 0.0048. The criterion of convergence was satisfied when the difference between the observed and predicted wave fields became very small, as shown in Figure 5-16 where an excellent match is found.

Figure 5-17 presents histograms of velocities from all accepted models for all temperature levels. It demonstrates that at high temperatures, the accepted models are located over a large model space and at low temperatures, the accepted models cluster around the true model.

Therefore, the inversion result should be inferred from a suite of models that have similar least-squared error near the global minimum. The last 2000 accepted models at the final temperature are used to get an average model for the inversion result (Figure 5-15b), and it is observed that the true model is excellently recovered.

Synthetic model 4

Synthetic model 4 consists of a buried low-velocity layer (second layer) between two high-velocity layers followed by a half space as shown in Figure 5-18a. Synthetic data was generated in Plaxis2D exactly the same as model 3.

Similar to model 3, during inversion, the least-squared error decreased from 0.1088 for an initial model of constant velocity of 500 m/s to 0.0066 for the final accepted model. Again, the final inversion result (Figure 5-18b) is an excellent recovery of the true model, correctly inverting both interfaces and velocities. The excellent recovery of the velocity model leads to an excellent match between the observed and estimated wave fields (Figure 5-19). The histogram of all accepted models is also shown in Figure 5-20, whose mode values are close to the velocities of the true model.

Synthetic model 5

Model 5 consists of three low- and high-velocity layers followed by a half space, with six linear segments in each interface (Figure 5-21a). The observed wave field was generated by the finite-difference solution using 51 receivers at 1 m spacing on the surface, and an active source placed 10 m away from the first receiver. The active source was modeled as a Ricker wavelet (Figure 5-4b) having a central frequency of 15 Hz. The Ricker wavelet is typically better than the triangle wavelet for modeling an impulsive load, because a wave field generated by the Ricker wavelet has less numerical noise, and thus less filtering is required.

To run inversion, the source, Poisson's ratio, density, and the number of linear segments in each interface were kept the same as values used to generate the observed wave field, thus the number of model parameters was 25 (7 thicknesses in each layer of the 3 layers, and 4 velocities). The velocity was allowed to vary between 200 m/s and 900 m/s, and the thickness was allowed to vary between 2 m and 10 m. The inversion began with the initial model of a constant velocity of 400 m/s, parameters were perturbed, and the temperature was reduced after 5000 accepted models until convergence. The run tested more than 150,000 trial models in about half a day on a standard laptop.

Figure 5-21b presents the inverted model, which is taken as the average model from the last 5000 accepted models at the final temperature. One more time, excellent recovery of the true model is found. Both layer velocities and interfaces are accurately inverted with differences less than 10% from those of the true model.

The observed wave field, the estimated wave field associated with the last accepted model, and residuals are shown alongside in Figure 5-22. It is observed that the data has been well fit across the whole range of offsets, and the two wave fields are almost identical. The histogram of all accepted models is also shown in Figure 5-23. Again, the mode values are close to those of the true model.

The inversion result of model 5 demonstrates that it is possible using a full wave field from only one shot to characterize 2-D profiles with interfaces of linear segments of a few meters. However, one should not expect too much from just one shot, for example, dividing the medium into too many layers with interfaces of multiple small segments, or dividing the medium into many small cells. In such cases, full wave fields from multiple shots are required for characterization.

5.3.2 Applications on Real Test Data

The results from the synthetic models have shown the capability of the presented technique in dealing with reverse and high variation profiles. In the end, to gain acceptance and wide-spread application, the technique must be demonstrated that tomography results compare well with ground truth information obtained from real test sites. Here it is applied to well-documented testing sites.

5.3.2.1 TAMU test site

Data were collected at the National Geotechnical Experiment site (NGES) on the campus of Texas A & M University (TAMU). The TAMU site is well documented, and consists of an upper layer of approximately 10 m of medium dense, fine, silty sand followed by hard clay. The multi-channel test were conducted using 31 receivers at a spacing of 1.22 m, giving a total receiver spread of 36.6 m, and an active source 6 m away from the first receiver. In addition, the cross-hole test was conducted at a set of nearby cased boreholes spaced approximately 3 m apart.

Before running inversion, the velocity constraints and the medium depth need to be established. Although the technique does not require strict constraints for convergence, the computer time can be reduced significantly if they are available. To save computer time, an estimate of velocity constraints and medium sizes must be established. For the estimate of velocity constraints, a spectral analysis was employed. By applying the spectral analysis to the measured data set, the measured wave field was decomposed into components of different frequencies, and velocity of each component was determined. Figure 5-24 presents the normalized spectral obtained by using the cylindrical beamformer technique. It is observed that most energy of the measured wave field concentrates in a narrow band, and Rayleigh wave velocities are determined to vary from 120 to 500 m/s. Thus, the constraint of shear wave velocity, which is a little bit bigger than Rayleigh wave velocity, was taken as a range of 100 to

600 m/s. For the estimate of medium sizes, the depth of investigation was assumed as one half of the geophone spread.

Based on the geophone spacing and the dispersion property from the spectral analysis, the grid size was selected as 0.61 m that is sustainable to the maximum frequency of 30 Hz at which the criterion of 10 mesh points per wavelength is satisfied. Therefore, the measured data was low band-pass filtered through a bandwidth of frequencies below 30 Hz to remove high frequency signals and background noise before using for inversion. In addition, the filtered data from every receiver was treated equally by normalizing the maximum magnitude to unity, thus removing all damping in wave propagation. The central frequency of the filtered data was about 15 Hz, and it was selected to be the central frequency of a Ricker wavelet for an active source in forward modeling.

Because most of the signals in the full wave field measured on the surface are Rayleigh waves, which are not very sensitive to Poisson's ratio and density, and because the number of model parameters needs to be limited to reduce computer time, the Poisson's ratio and the density were kept constant as 0.3 and 1800 kg/m^3, respectively for the entire medium during inversion. It was assumed that the medium consists of 3 layers and a half space, and each interface was divided into five horizontally equal linear segments. Thus, six thicknesses for each layer and 4 velocities were searched; the number of model parameters was 22.

To run inversion, the shear velocity was allowed to vary between the constraints, the thickness was allowed to vary between 2 m and 8 m, and the temperature was reduced after every 4400 accepted models until the criterion of convergence was satisfied. The least-squared error decreased from 0.1560 for the initial model of constant velocity of 400 m/s, to 0.0160 for the final accepted model after searching over 120,000 trial models in about a half day on a

standard laptop. The criterion of convergence was only satisfied when the estimated full wave field from the final accepted model was very close to the observed wave field as shown in Figure 5-25, where a good match is found.

Because of noise and non-uniqueness of inversion solutions, there is no guarantee that the model corresponding to the smallest error is closest to the true model. Therefore, the inversion results should be inferred from many accepted models clustering around the global minimum and having similar errors, instead of from only one model that has the smallest error. Similar to synthetic data sets, the last 4400 accepted models at the final temperature were averaged for the inversion result.

Figure 5-26 presents the velocity histograms from all accepted models. It is observed that the first three layers are characterized better than the half space below. Figure 5-27 presents the 2-dimensional shear wave velocity within the geophone spread (0 - 36.6 m) from the full wave field inversion. The tomogram indicates that the shear wave velocity structure at the test site is a lightly reverse profile with a buried low-velocity layer (layer 3).

For comparison, the Vs profile from the inversion result at distance 10 m that is near to the boreholes used for the cross-hole test is plotted together with cross-hole measurements, SPT N-values, and material logs in Figure 5-28. It is observed that the full wave field inverted shear wave profile compares well with the cross-hole results, and the presented technique successfully detects the thin low-velocity layer that is hardly detected by traditional surface wave methods that use only dispersion property of Rayleigh waves. There also appears to be reasonable consistency between the shear wave velocity results and the SPT N-values and material log.

5.3.2.2 Newberry test site

The description of the Newberry test site is provided in section 3.3.2. For the case presented here, the full wave field measurement was conducted at line F from station 36.6 m to

73.2 m, using 31 vertical geophones at a spacing of 1.22 m, giving a total geophone spread of 36.6 m, and the wave field was generated by an active source 6 m away from the first geophone.

To run the inversion of the measured full wave field, the velocity constraints and the medium depth need to be established. For the velocity constraints, the cylindrical beam-former technique was again employed for spectral analysis of the measured data, and the minimum and maximum shear velocity constraints were determined as 100 m/s and 1200 m/s, respectively. For the medium depth, it was simply taken as 1/3 of the geophone spread.

The medium was discretized with a grid size of 0.61 m, which can accurately model the maximum frequency of 40 Hz, and thus the measured data was low band-pass filtered to remove all components above 40 Hz before using for inversion. The center frequency at 18 Hz of the filtered data was selected to be the central frequency of Ricker wavelet for the active source in forward modeling.

Similar to TAMU data, during inversion, the Poisson's ratio and the density were kept constant as 0.3 and 1800 kg/m^3, respectively, for the entire medium. It was assumed that the medium consists of 3 layers and a half space, and each interface was divided into five horizontally equal linear segments. Six thicknesses for each of three layers and 4 velocities were searched, thus the total number of model parameters was 22.

The inversion began with the initial model of a constant velocity of 500 m/s, which led to the initial least-squared error of 0.225. The model was then perturbed and updated by allowing the shear velocity to vary between the constraints, the thickness to vary between 1 m and 6 m, and the temperature was reduced after every 4400 accepted models until the criterion of convergence was satisfied. The convergence was found at the final least-squared error of 0.0360 after searching over 120,000 trial models in about a half day on a standard laptop.

The observed wave field, estimated wave field associated with the last accepted model, and residuals are set alongside in Figure 5-29. It is observed that the data has been fit relatively well across the whole range of offsets except the last few channels at both ends of the geophone array. The misfit at these channels may be explained that the laterally variable subsurface velocity structure can not be completely modeled by a 2-D multi-linear interface profile. To find a better fit wave field, more complexity of velocity profile needs to be added into the medium, such as a medium consisting of small cells with different velocities.

Figure 5-30 presents velocity histograms of all accepted models during the inversion. Again, it demonstrates that at high temperatures, the accepted models are located over a large model space and thus the velocities randomly vary between the constraints. Otherwise, at low temperatures, the accepted models cluster around the global minimum model, whose layer velocities are the mode values in these histograms.

Figure 5-31a presents the 2-dimensional shear wave (S-wave) velocity with in the geophone spread (36.6-m length) from the full wave field inversion, which is the average model from last 4400 accepted models. The tomogram indicates that the shear wave velocity structure at the test site is increased with depth. It is noted that this increased-velocity-with-depth profile can be well characterized by the seismic refraction tomography.

For comparison, the result of the seismic refraction tomography (SRT) developed by Quigley (2006) using commercial software Rayfract is also presented on Figure 5-31b. The refraction test data was measured on the same location of the full wave field test by vertical geophones spaced equally at 0.61 m, for a total of 61 measurements, and shot locations were spaced at 3.0-m intervals along the 36.6-m line, for a total of 13 shots.

The comparison of the S-wave velocity profile (Figure 5-31a) generated from the full wave field against the P-wave velocity profile (Figure 5-31b) generated from the refraction travel times is as following:

- As expected, the P-wave velocity is about twice of the S-wave velocity generally over the medium.
- There is a good agreement in depth of the top bedrock, which is about 9 m depth in both tomograms.
- The interface between layer 2 and layer 3 in Figure 5-31a is similar to the interface (contour of 1500 m/s) in Figure 5-31b.
- Slopes in interfaces at the left of the medium are found in both tomograms.
- There are some differences in velocity at shallow depth because the full wave field inversion assumes the medium consisting of layers, not consisting of cells, and the velocity of each layer is an average value of many cells.

The relatively good agreement between the inversion results of the full wave field and travel times suggests that the full waveform technique should be even applied to normal profiles that can be well characterized by the SRT for two reasons. First, the full waveform technique can characterize sharp contrasts in velocity, which SRT always models by gradient in velocity. Second, the full waveform technique requires much less effort in both field testing and manually data processing than that of SRT. The SRT usually requires many shots in data measurement, and days for data processing, e.g., manually picking the first-arrival signals.

5.4 Conclusion for Chapter 5

A global inversion technique based on simulated annealing is presented to obtain near-surface velocity profiles from full wave fields. This inversion technique does not depend on the initial model and becomes important in regions where the prior information about subsurface profiles is not available. Simulated annealing provides a suite of final models clustering around the global solution and having comparable least-square error. This allows getting the inversion

result by averaging all of these models to mitigate the influence of noise and the non-uniqueness of the inversion solutions.

The capability of the technique to accurately invert 2-D reverse models demonstrates superiority over 1-D traditional methods that use only dispersion property of Rayleigh waves. In addition, the technique though requires significant computer time for inversion; it possibly replaces the seismic refraction tomography to characterize normal profiles (increasing velocity with depth) because it requires much less effort in both site testing and manually data processing.

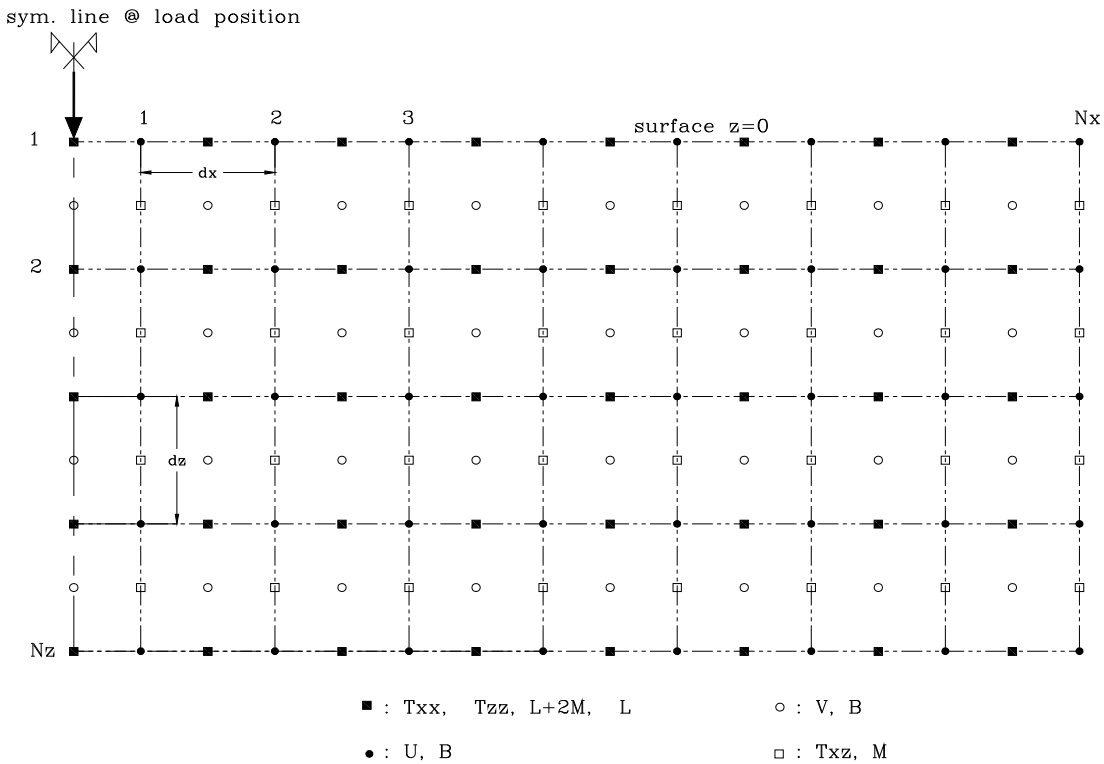

Figure 5-1. Discretization of the medium on a staggered grid.

a) b)

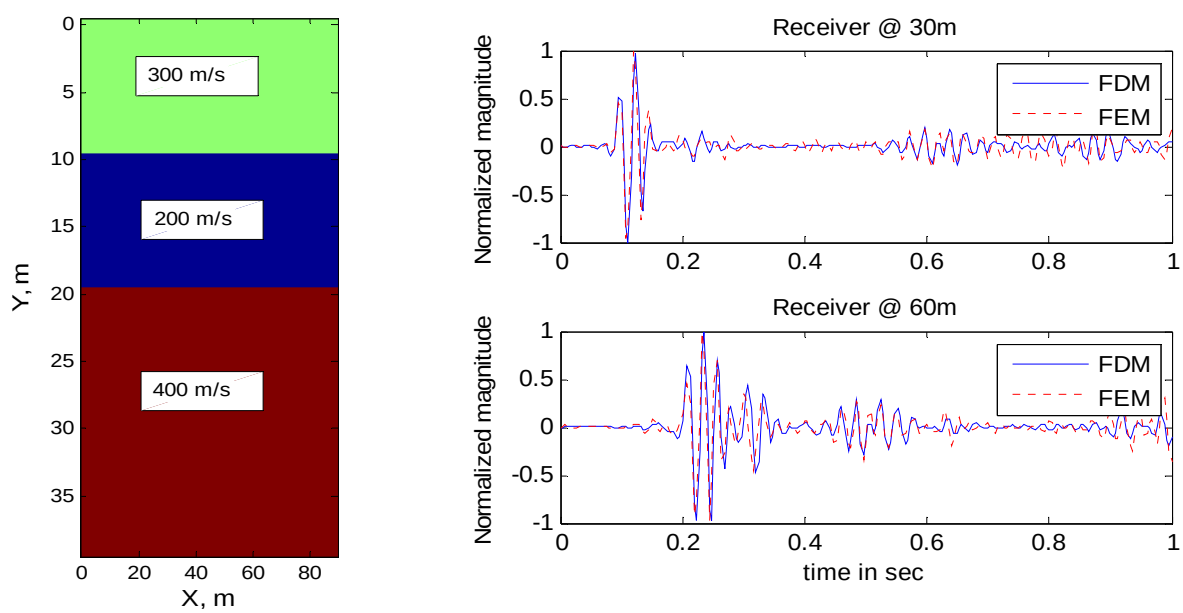

Figure 5-2. Comparison between wave fields generated by FDM and FEM: a) input model shear velocity Vs, and b) wave fields at 2 points x=30m and x=60m on the surface

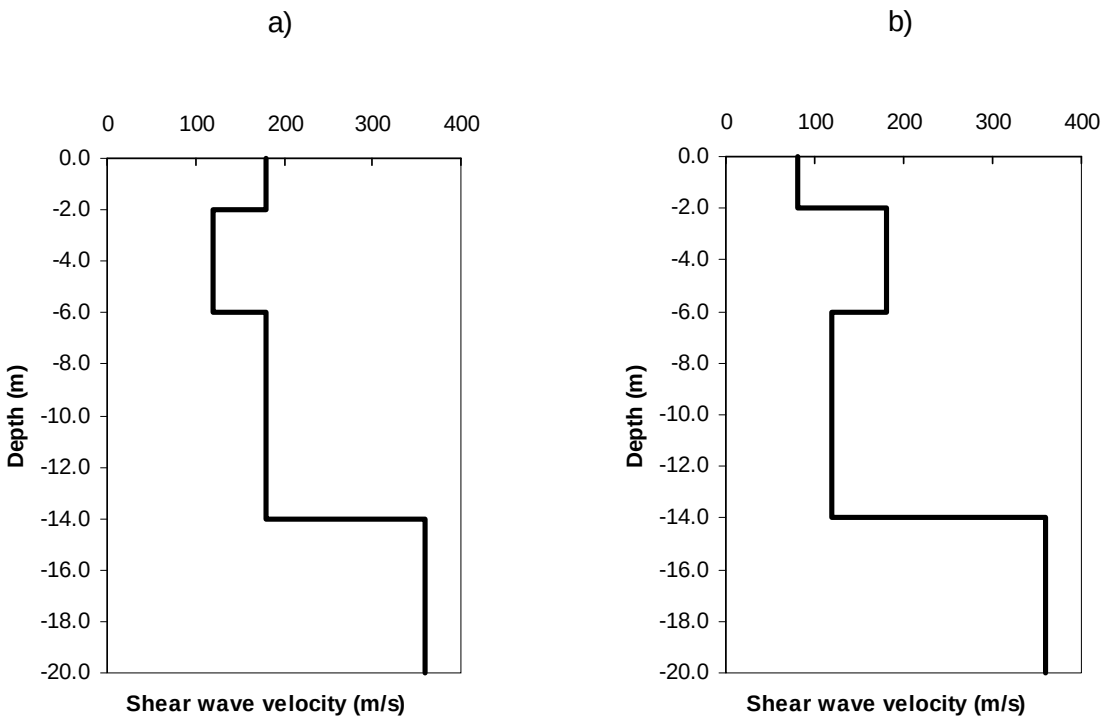

Figure 5-3. Shear wave velocity of 1-D models of Tokimatsu et. al. (1992): a) model 1 and b) model 2

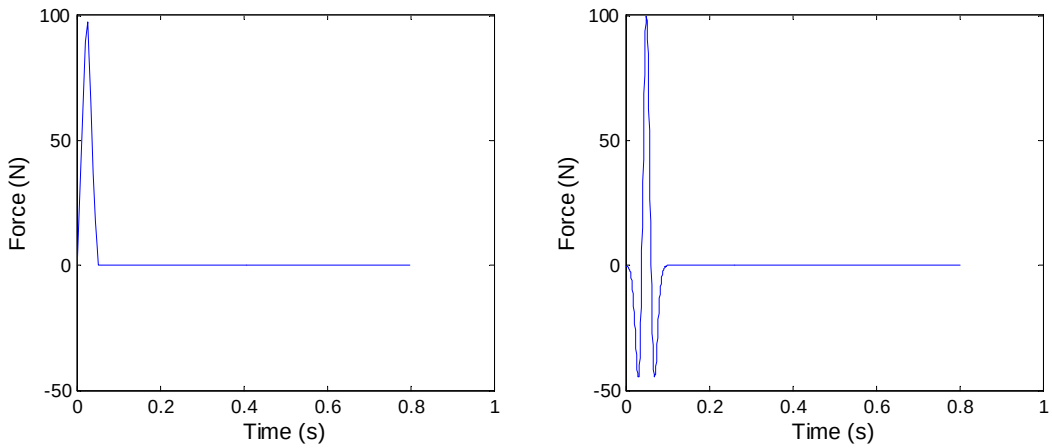

Figure 5-4. Impulsive load: a) triangle wavelet and b) Ricker wavelet

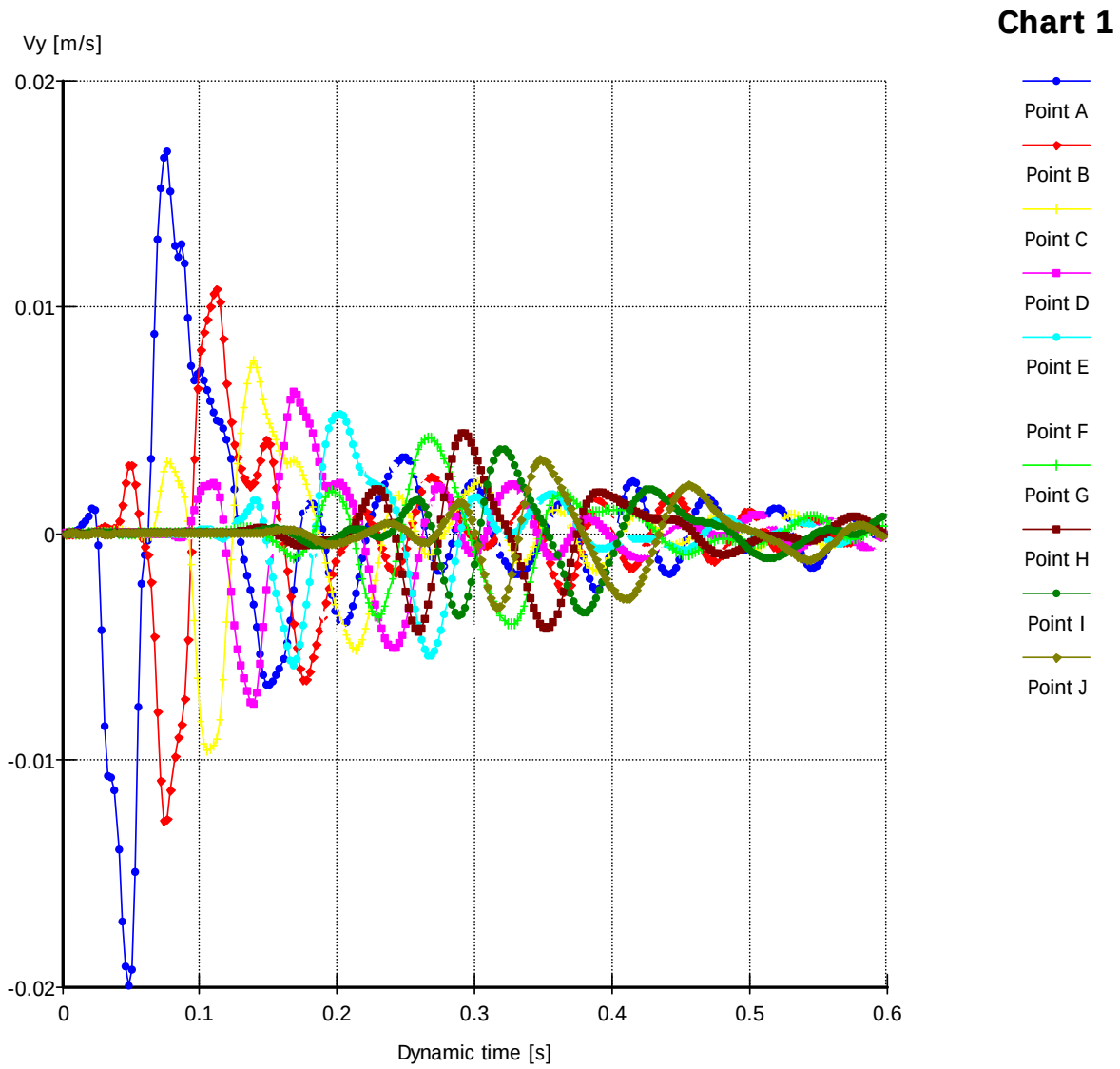

Figure 5-5. Synthetic model 1: particle velocity data from Plaxis2D observed at 10 points (A to F) spaced equally at 5 m on the surface

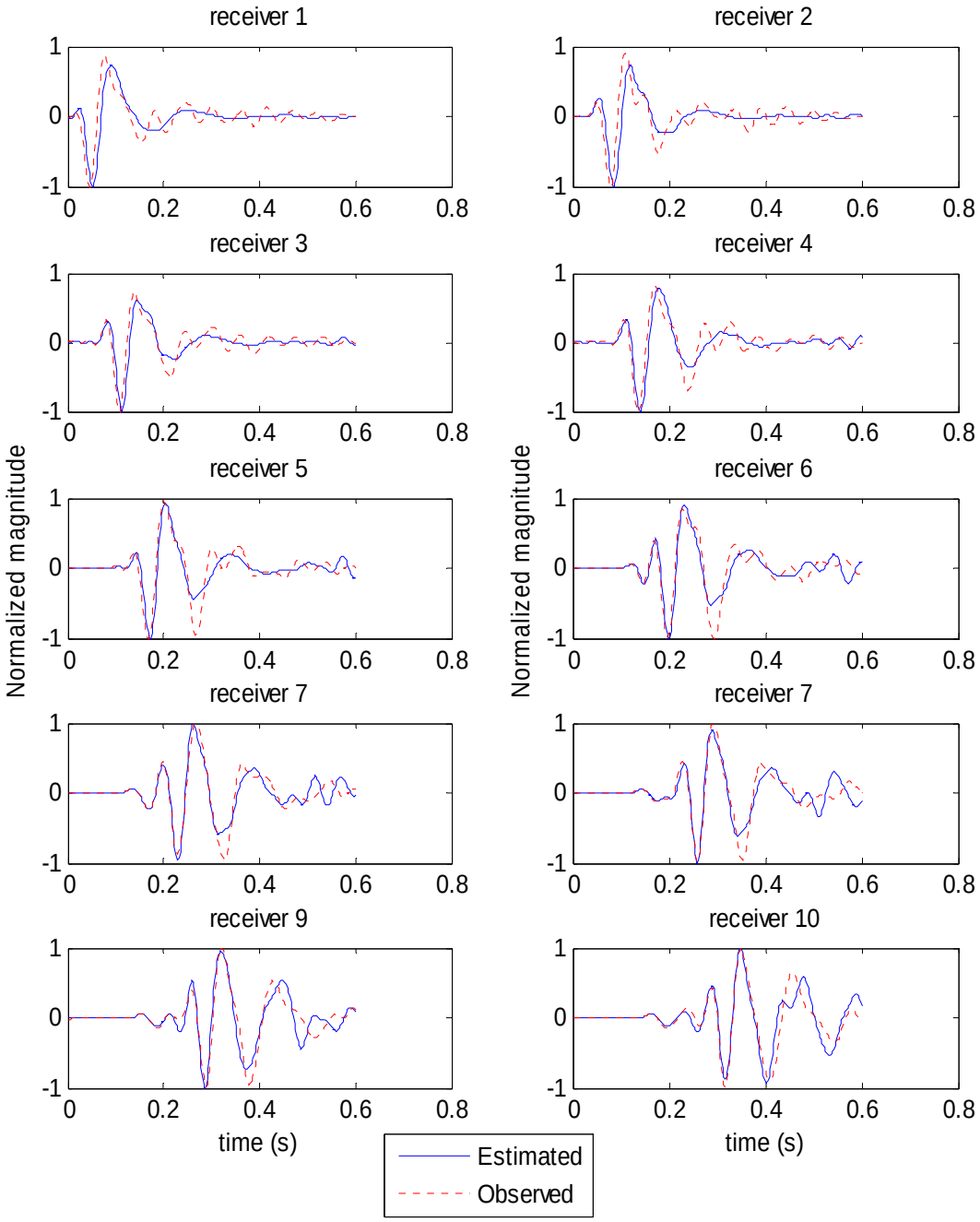

Figure 5-6. Synthetic model 1: comparison between estimated and observed wave fields.

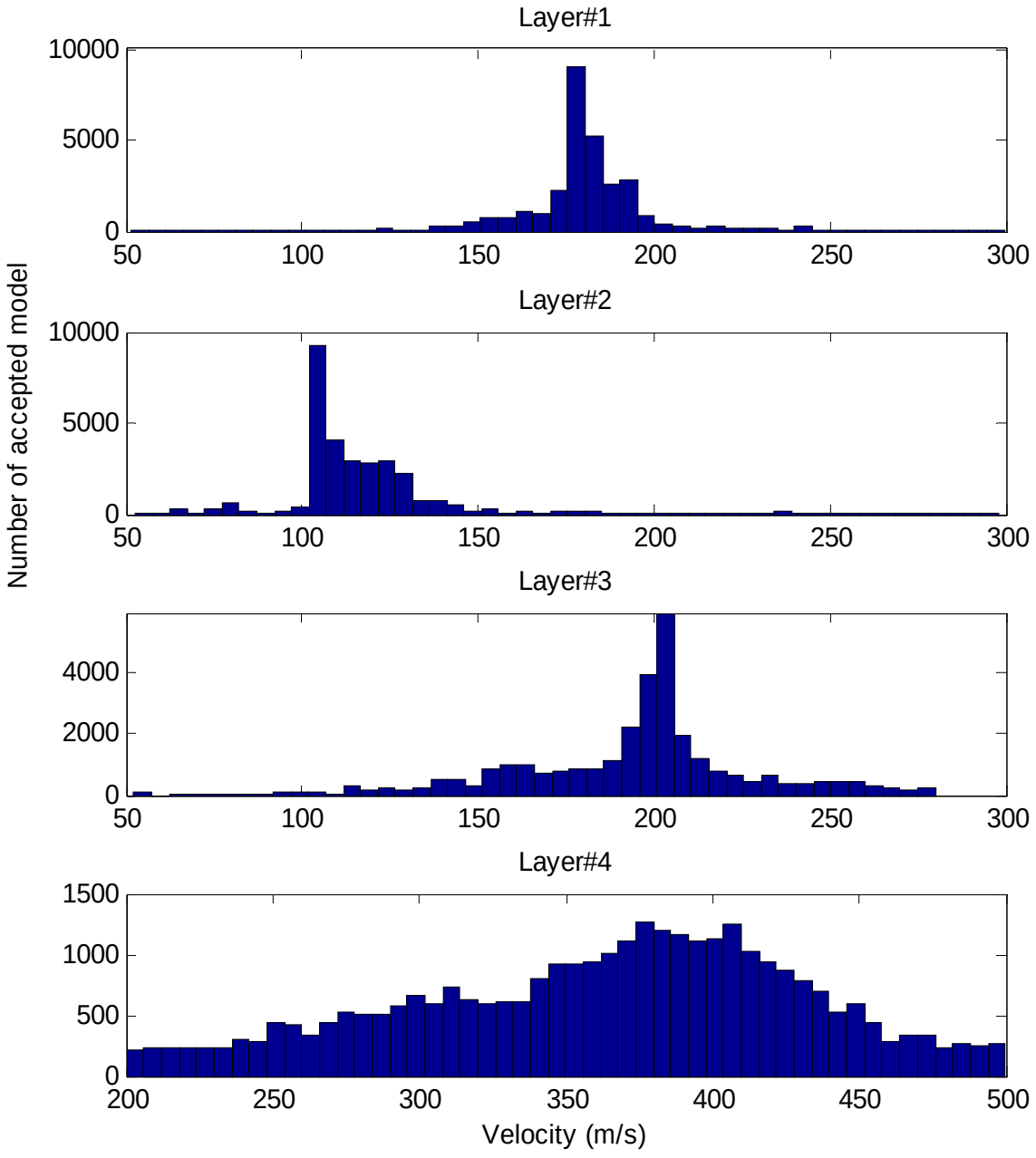

Figure 5-7. Synthetic model 1: velocity histograms from all accepted models

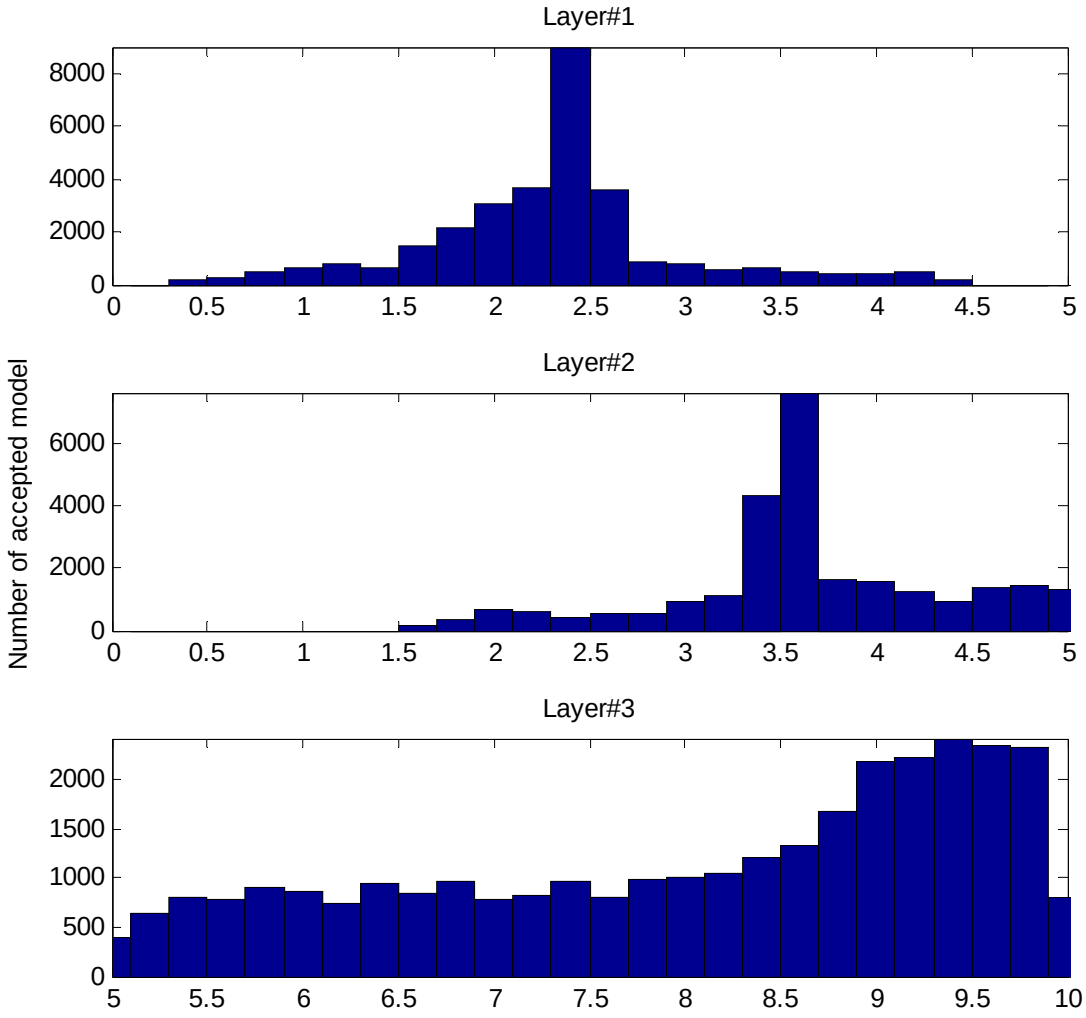

Figure 5-8. Synthetic model 1: thickness histograms from all accepted models

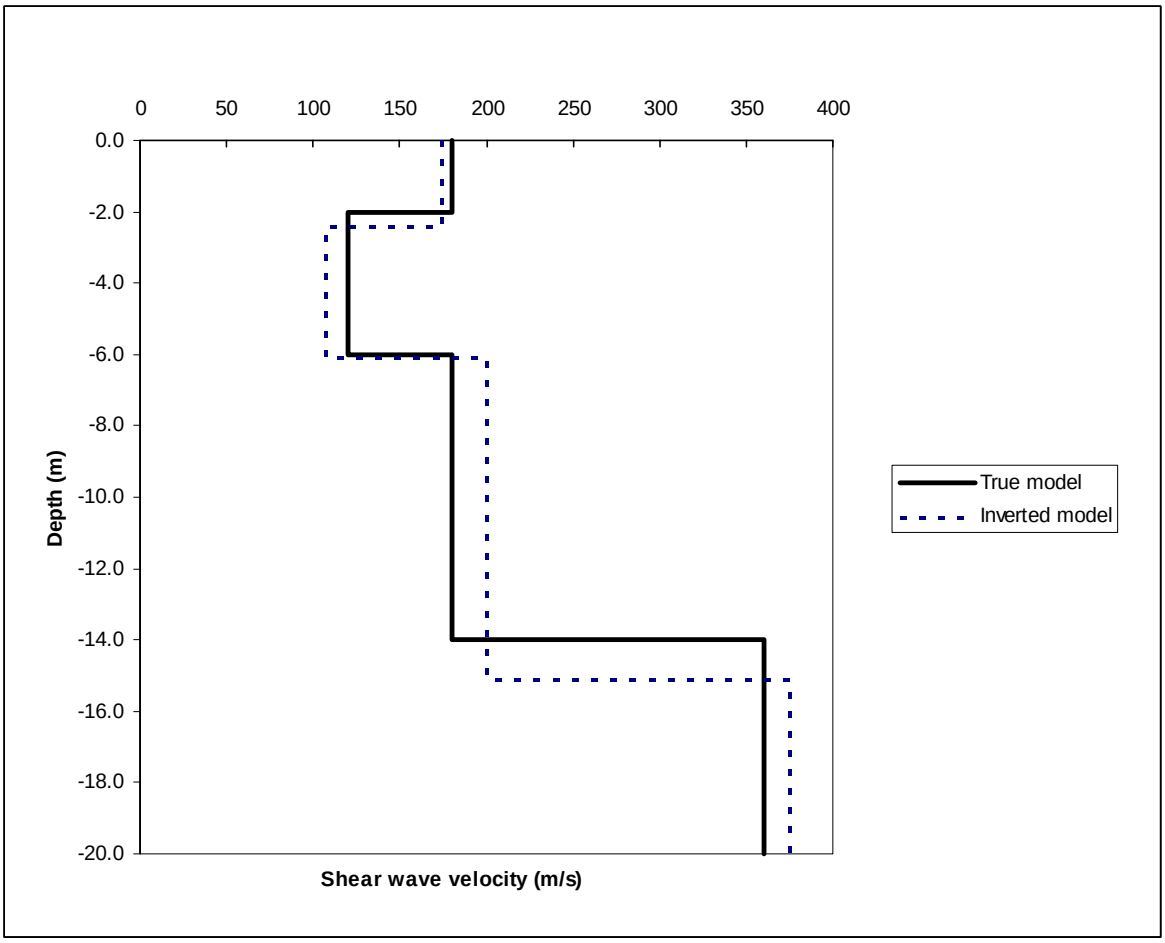

Figure 5-9. Synthetic model 1: comparison between the true and inverted models

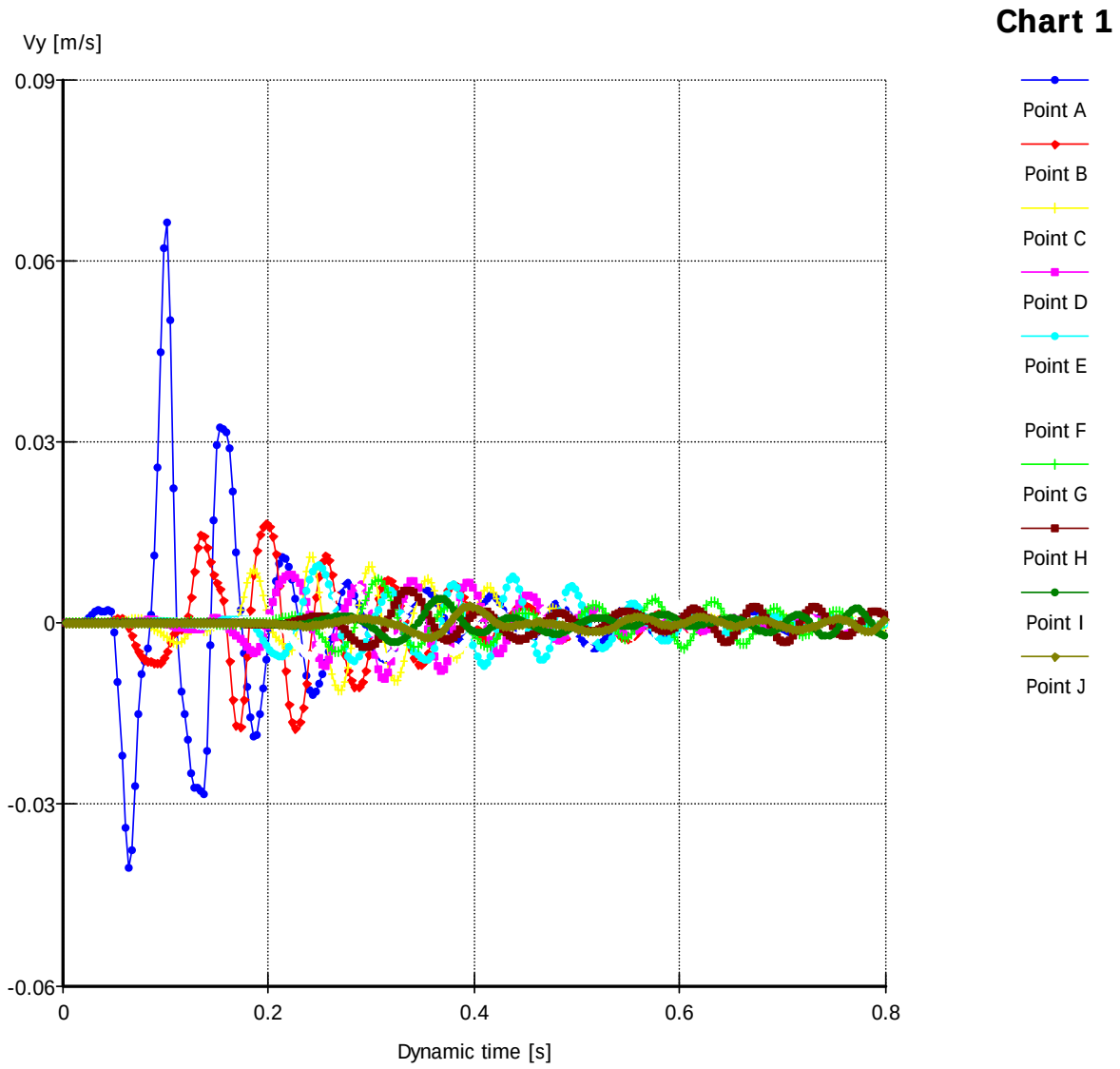

Figure 5-10. Synthetic model 2: particle velocity data from Plaxis2D observed at 10 points (A to F) spaced equally at 5 m on the surface

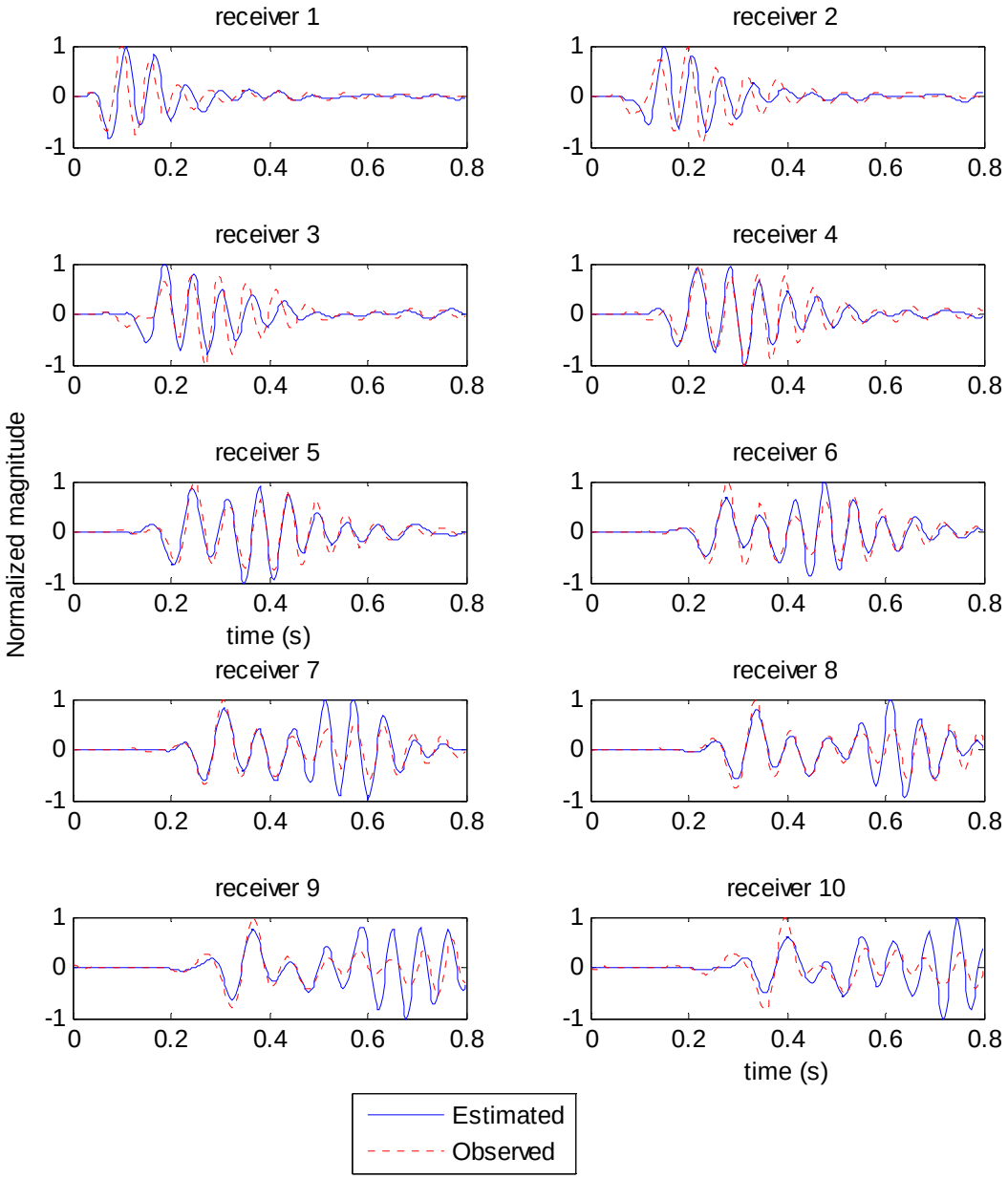

Figure 5-11. Synthetic model 2: comparison between estimated and observed wave fields.

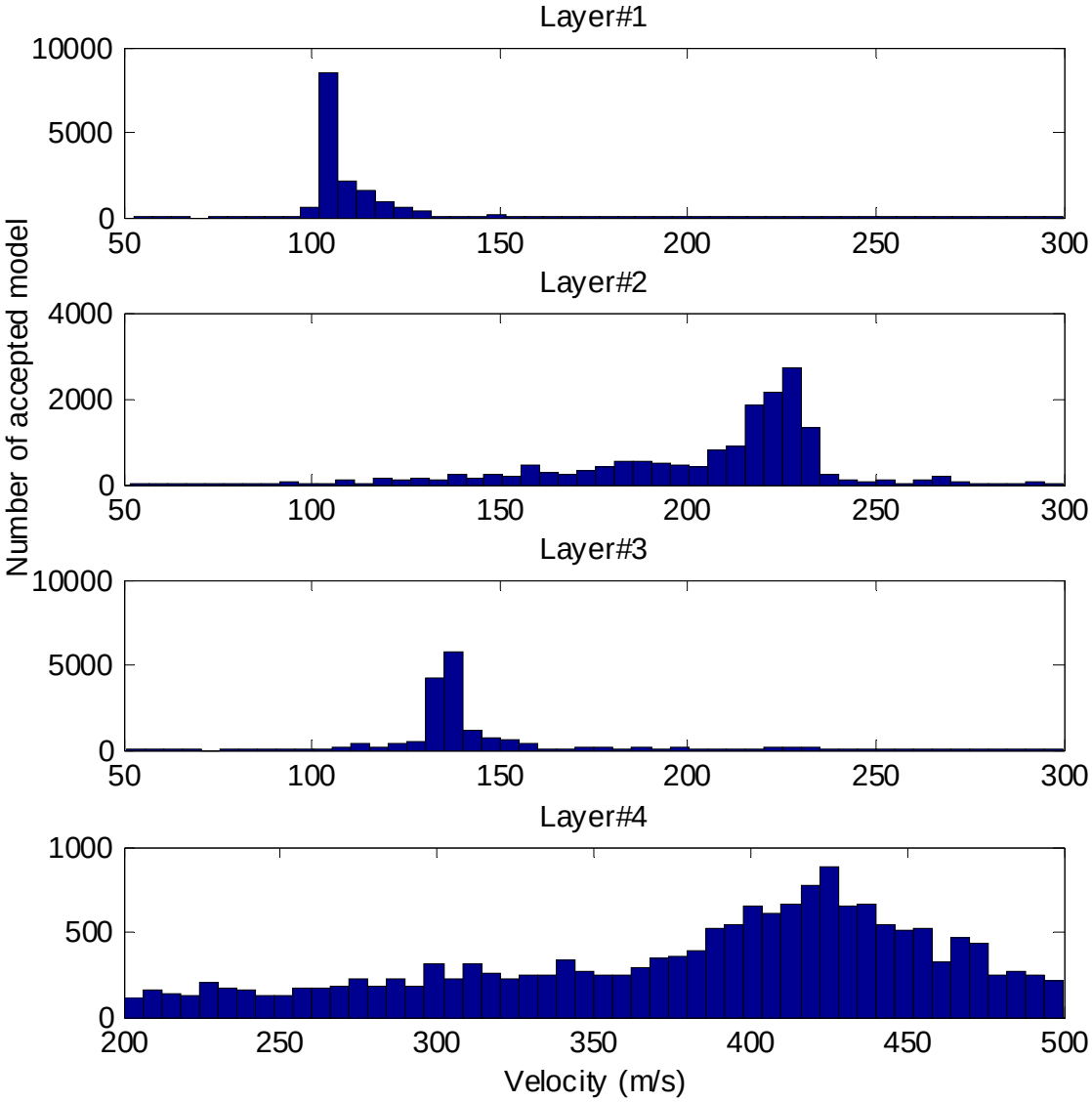

Figure 5-12. Synthetic model 2: velocity histograms from all accepted models

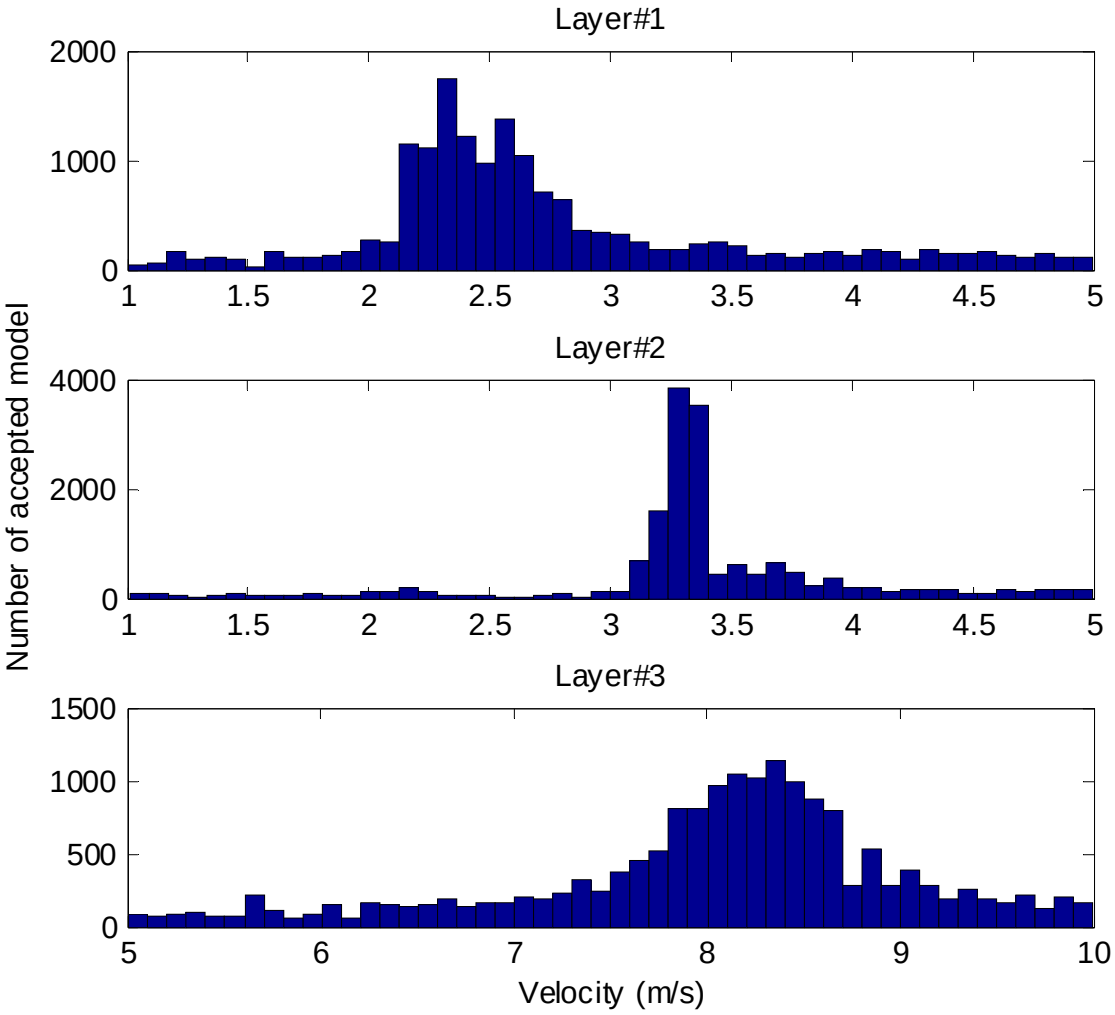

Figure 5-13. Synthetic model 2: thickness histograms from all accepted models

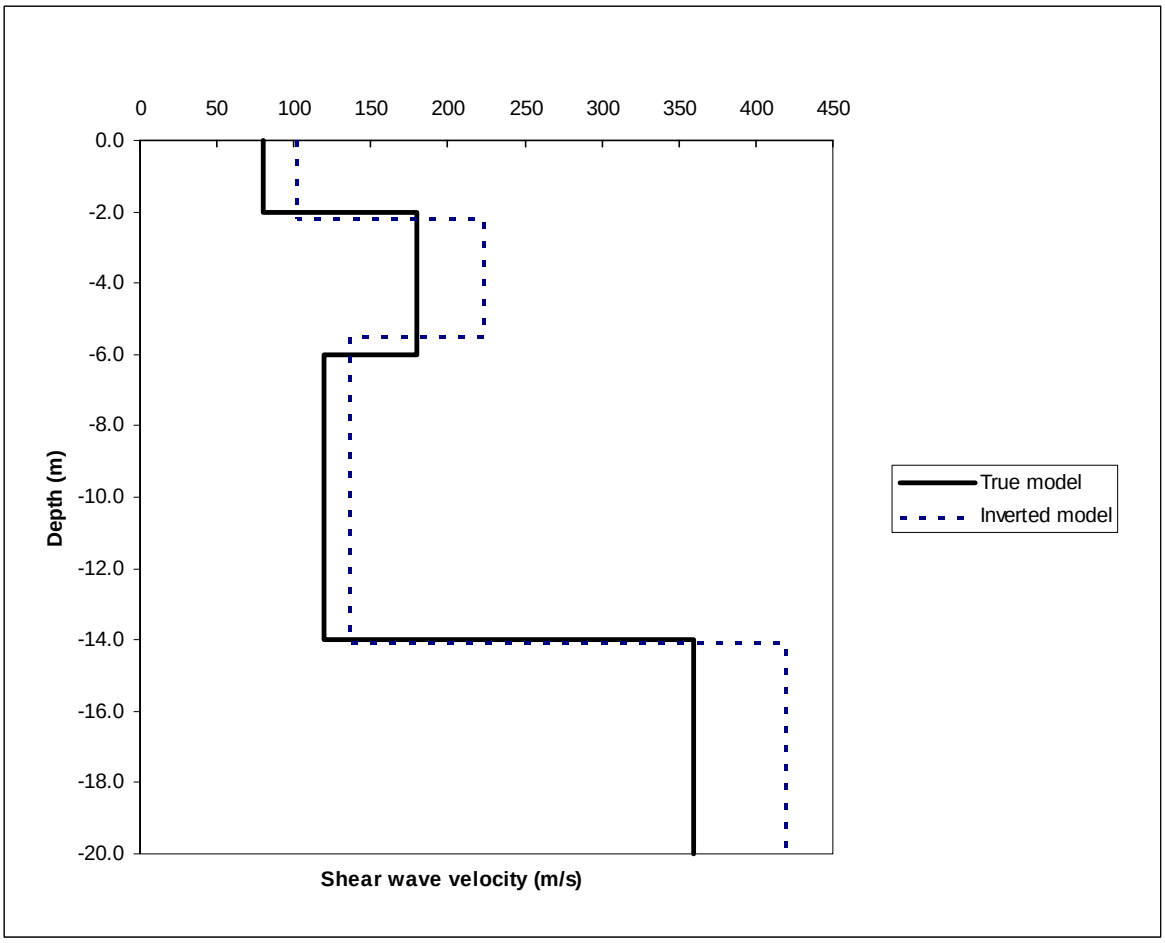

Figure 5-14. Synthetic model 2: comparison between the true and inverted models

a)

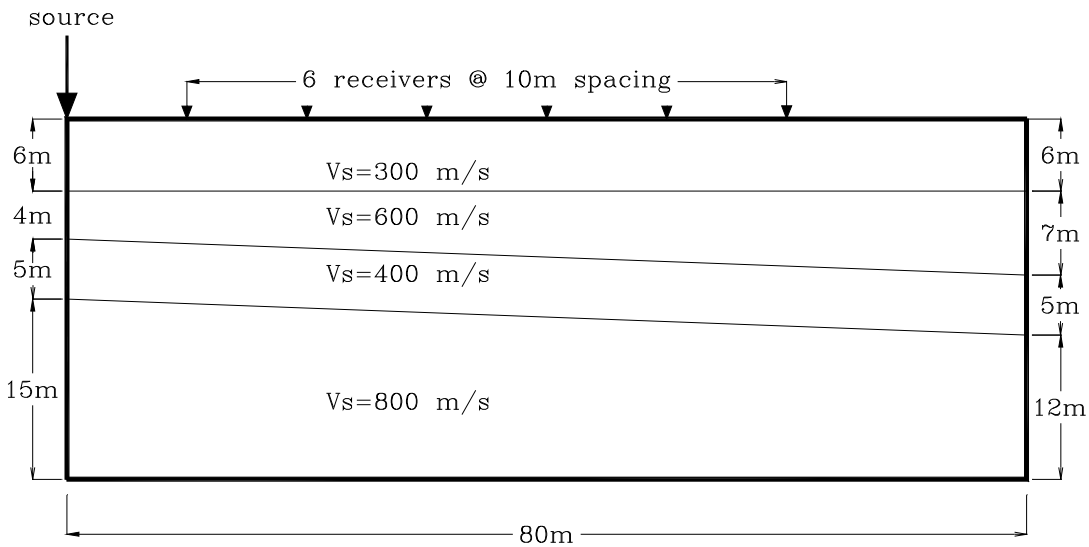

b)

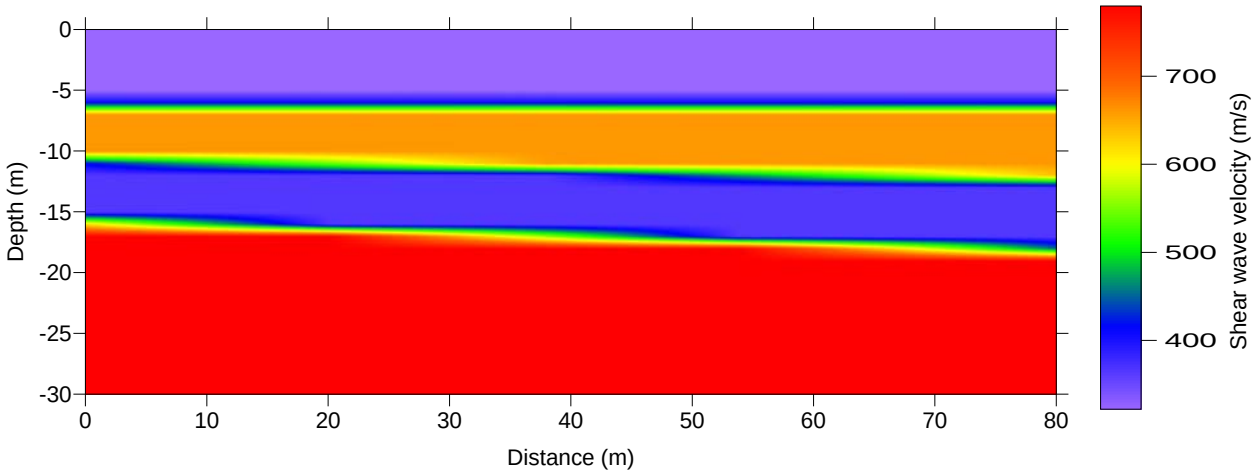

Figure 5-15. Synthetic model 3: a) true model, and b) inverted model

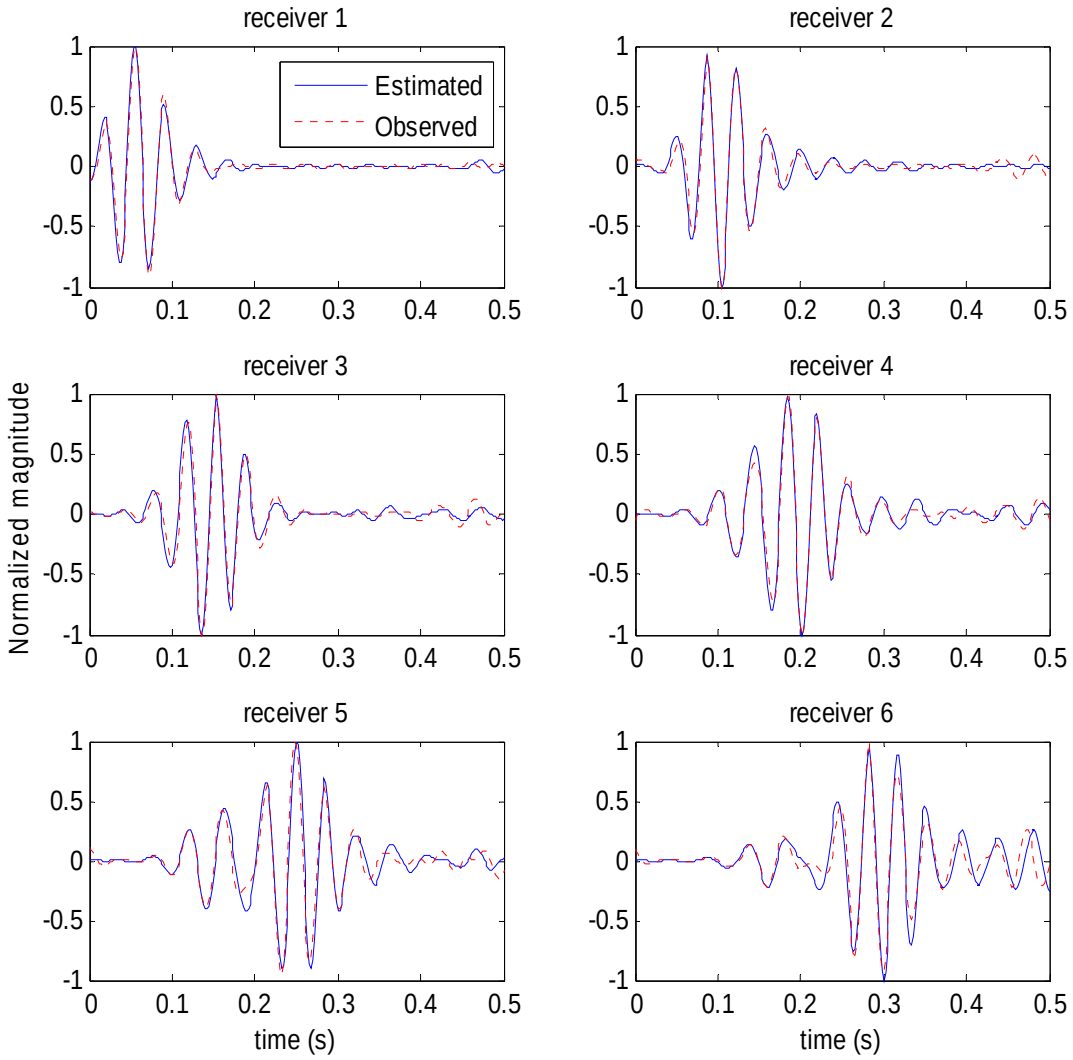

Figure 5-16. Synthetic model 3: comparison between estimated and observed wave fields

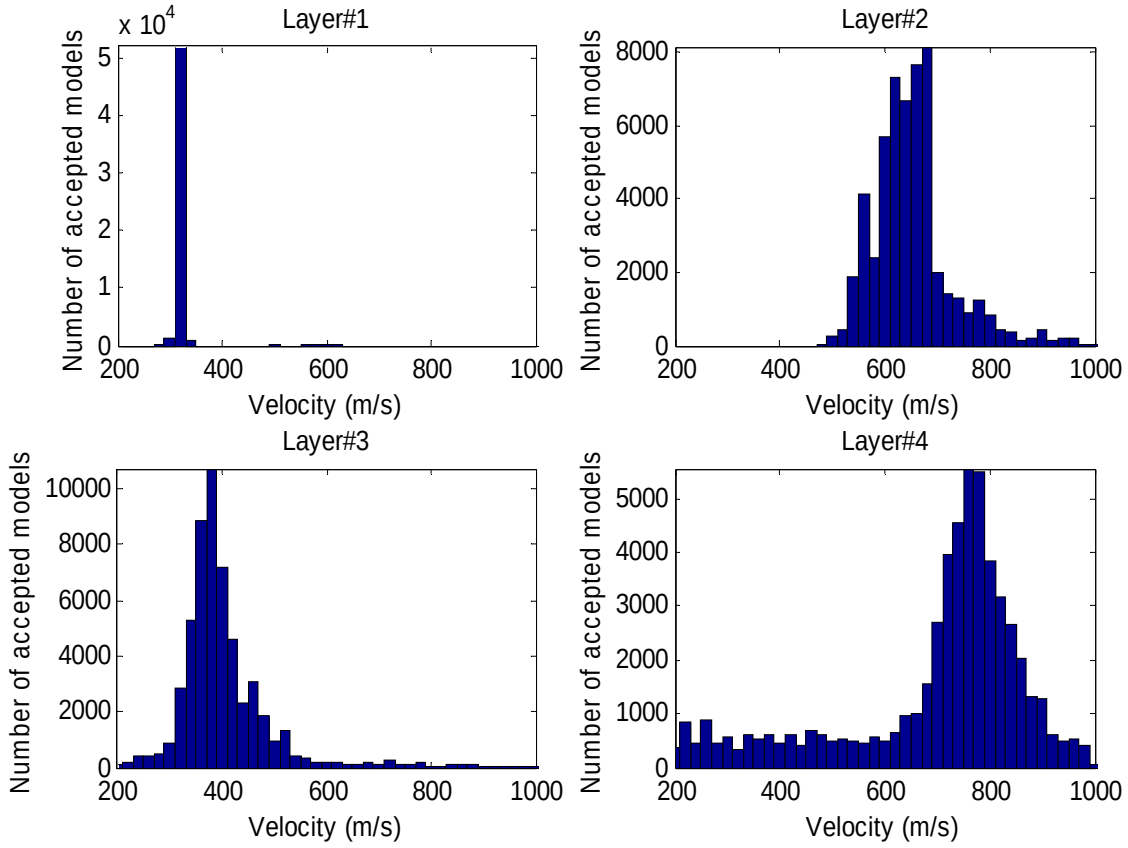

Figure 5-17. Synthetic model 3: velocity histograms from all accepted models

a)

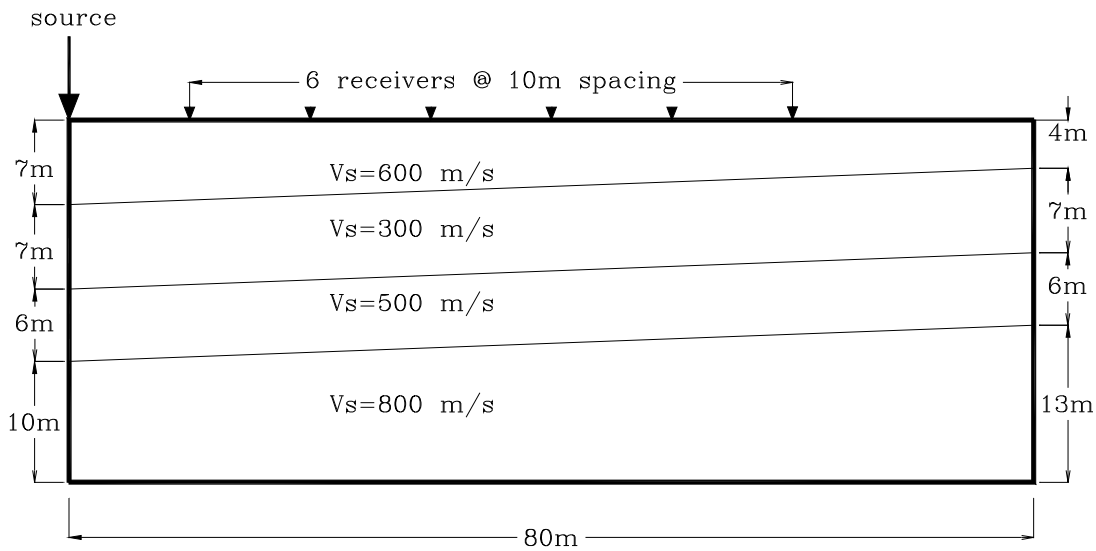

b)

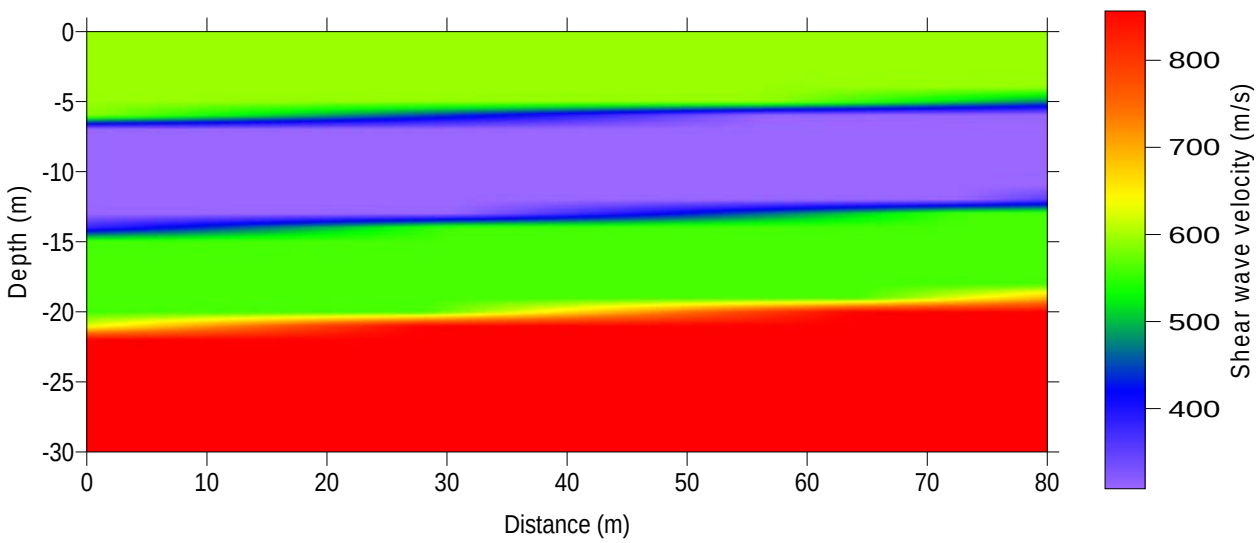

Figure 5-18. Synthetic model 4: a) true model, and b) inverted model

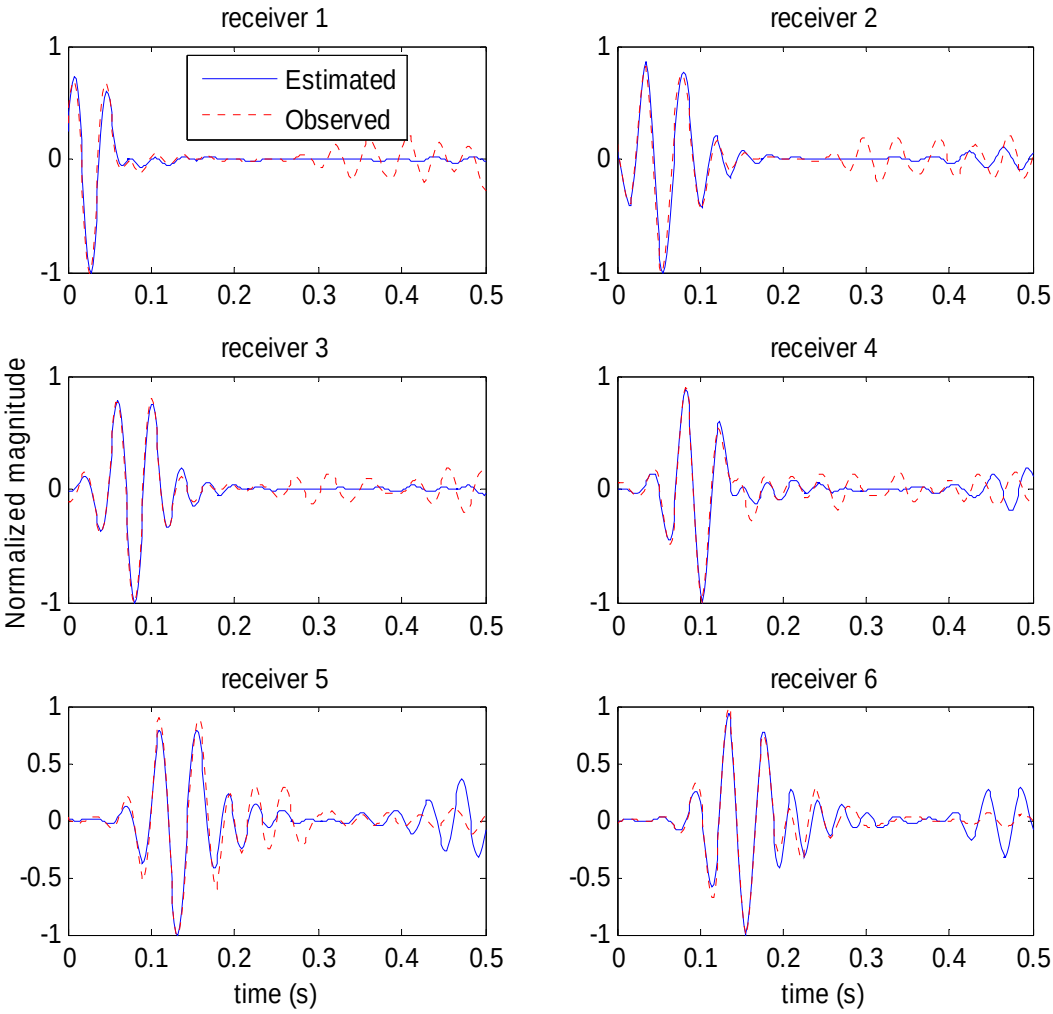

Figure 5-19. Synthetic model 4: comparison between estimated and observed wave fields

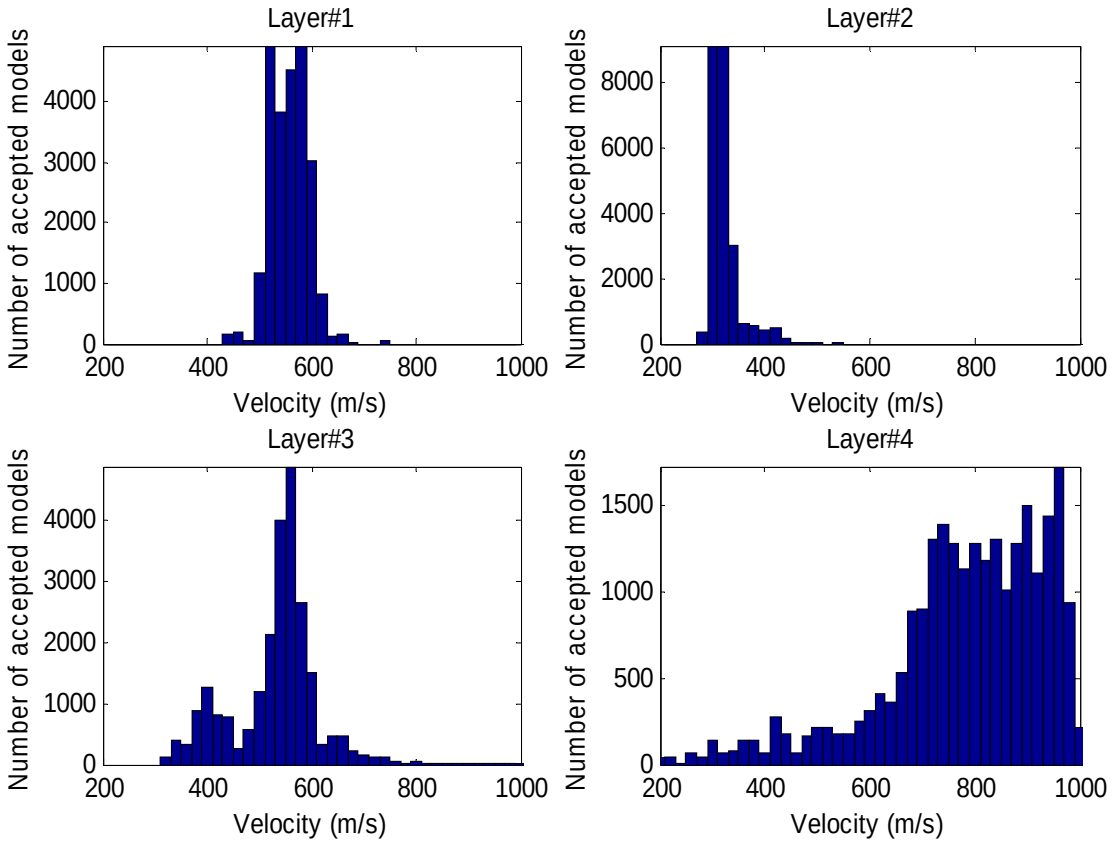

Figure 5-20. Synthetic model 4: velocity histograms from all accepted models

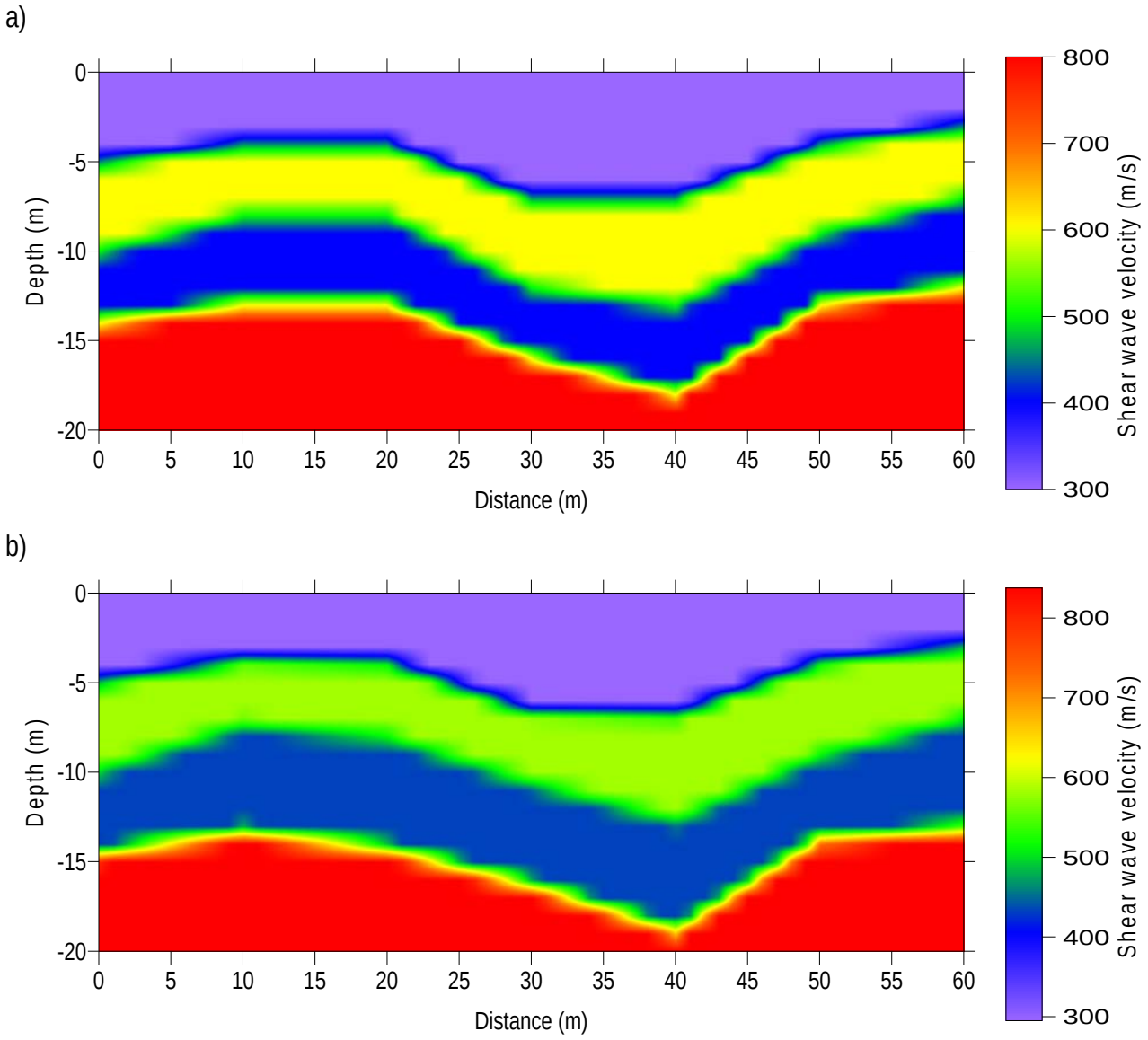

Figure 5-21. Synthetic model 5: a) true model, and b) inverted model

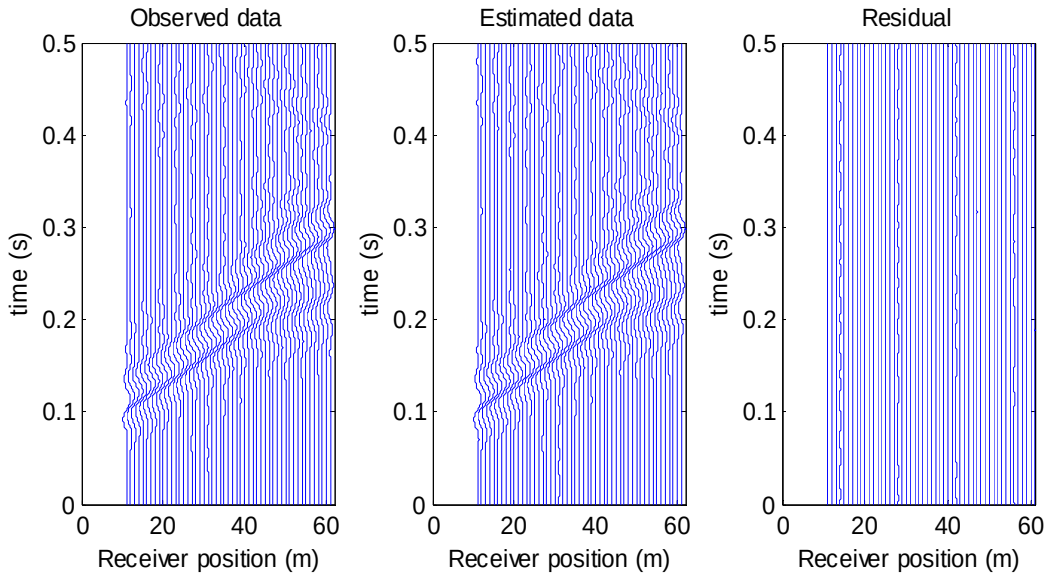

Figure 5-22. Synthetic model 5: comparison between observed and estimated wave fields

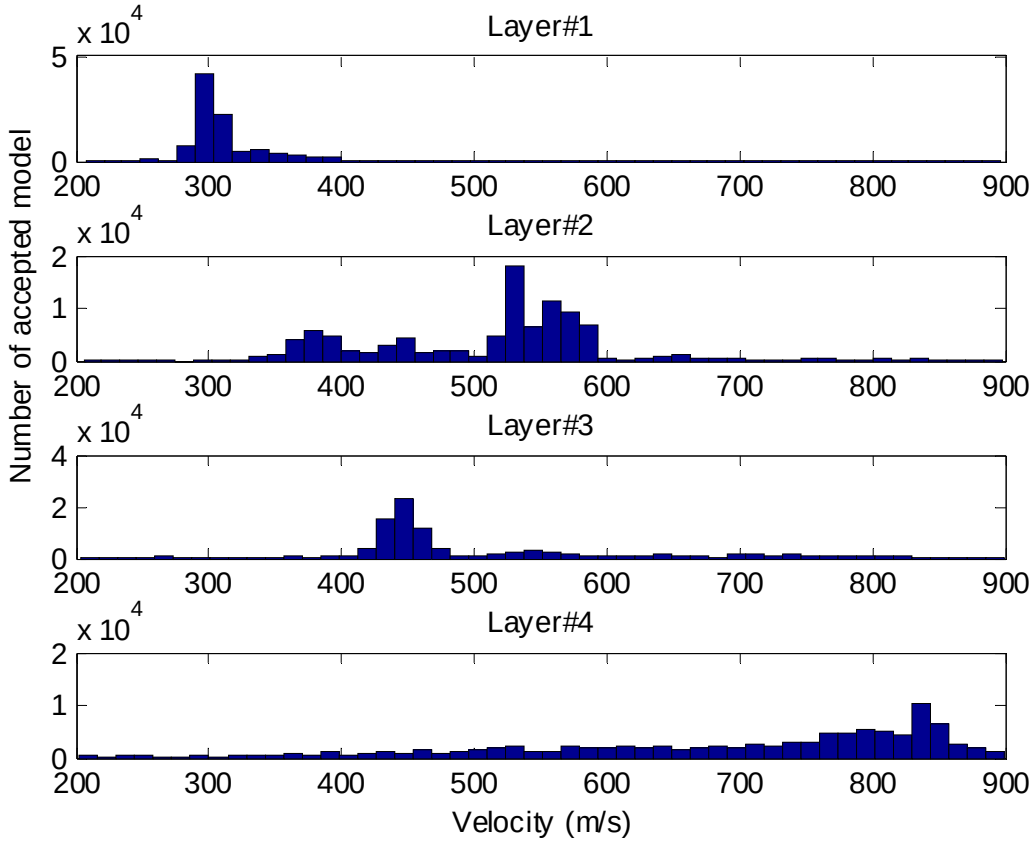

Figure 5-23. Synthetic model 5: velocity histograms from all accepted models

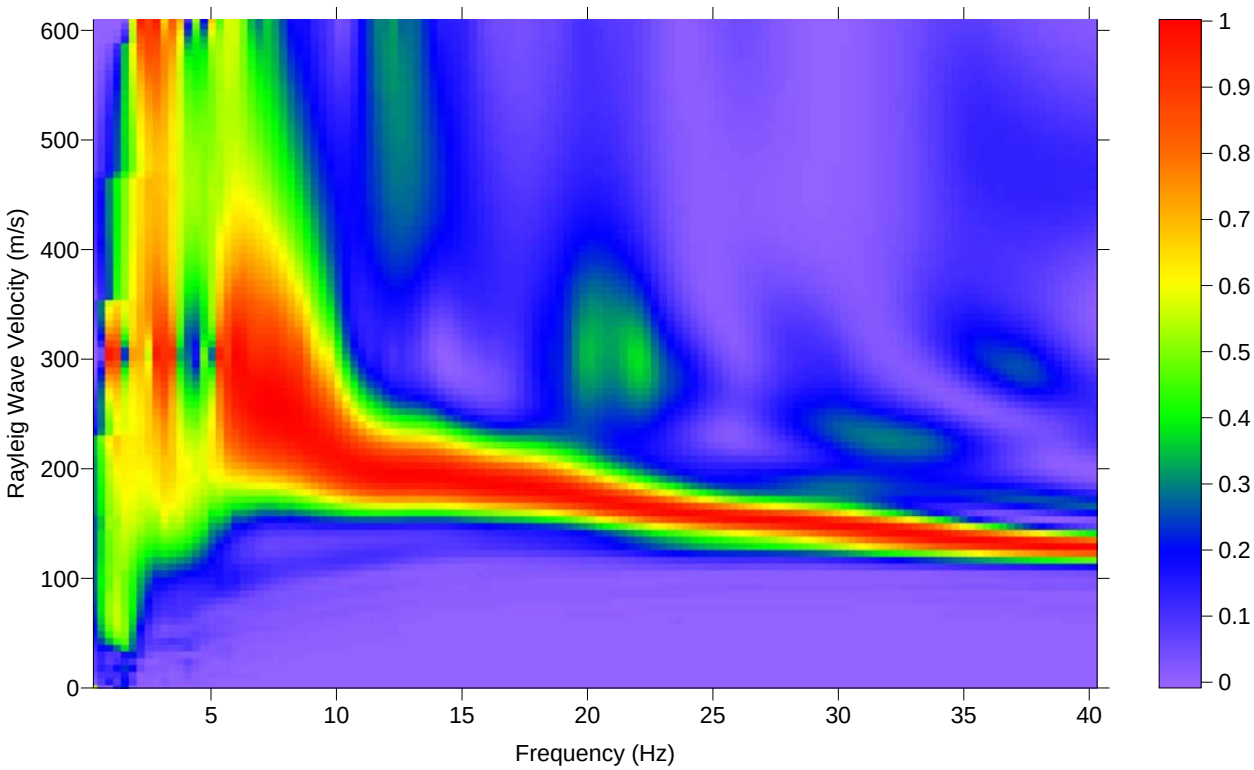

Figure 5-24. Normalized spectral of the measured data at TAMU

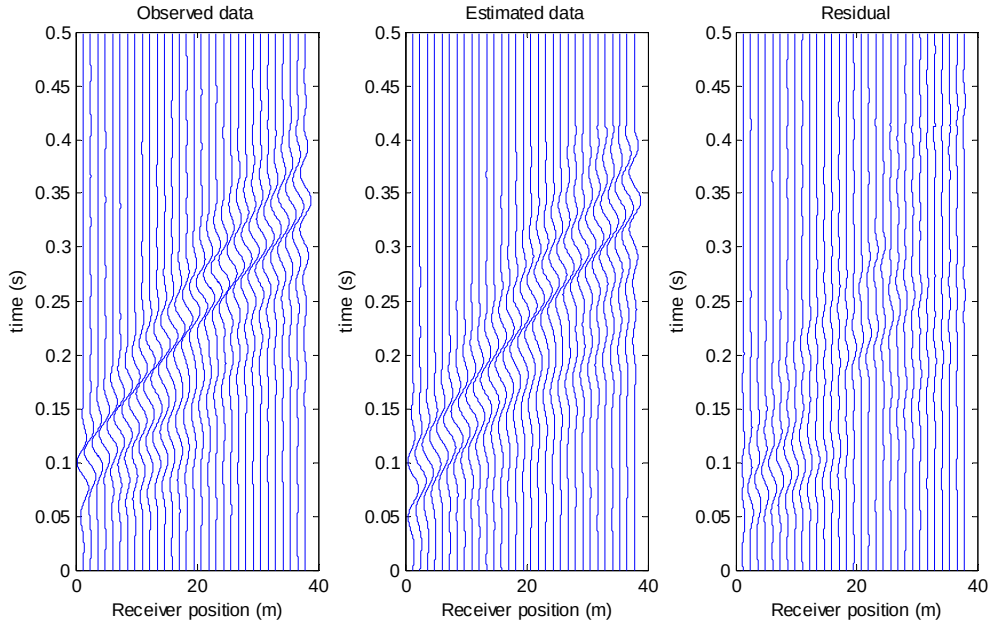

Figure 5-25. Comparison between observed wave field and estimated wave field for the real data set at TAMU.

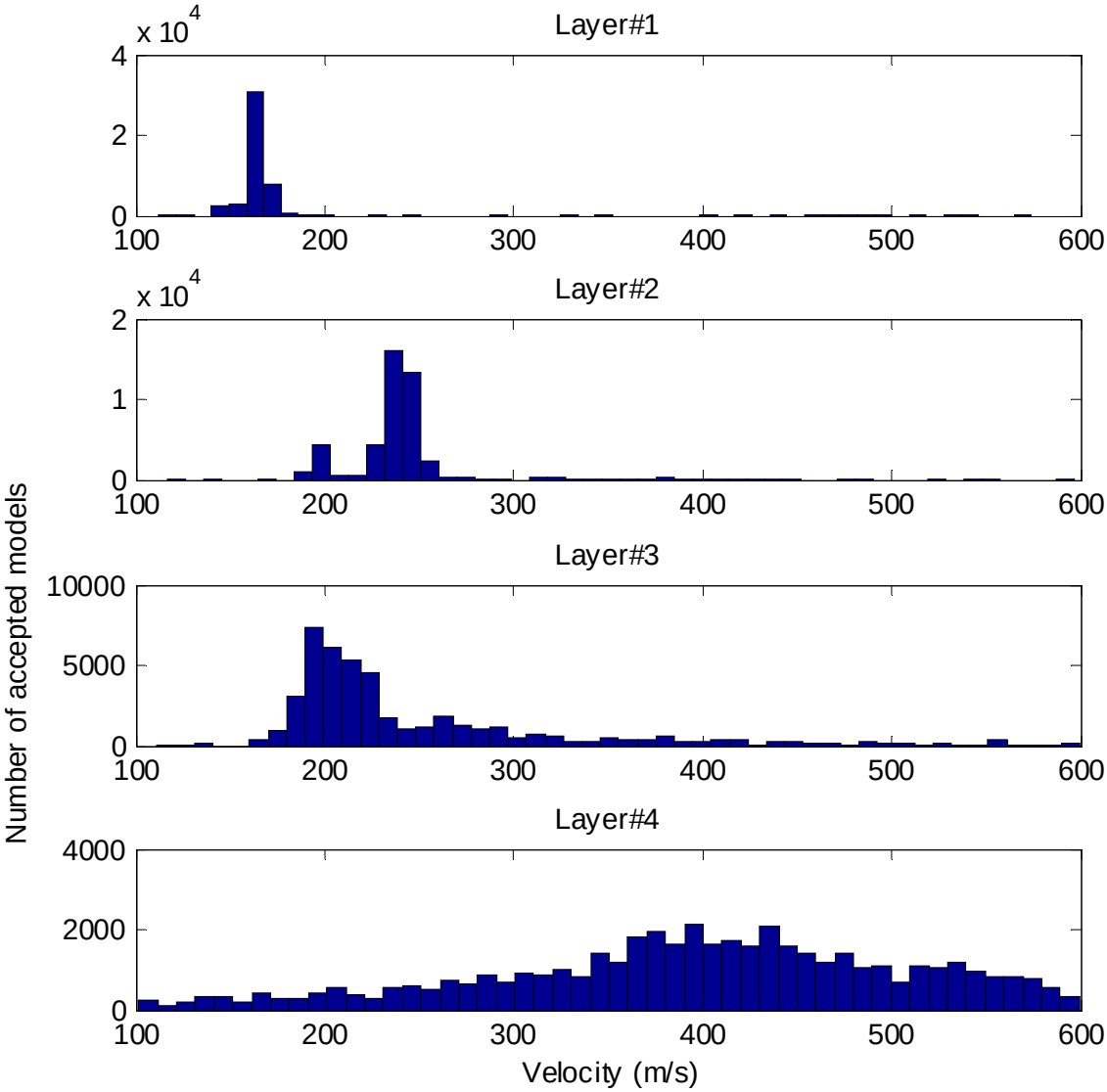

Figure 5-26. Velocity histograms from all accepted models for the real data set at TAMU.

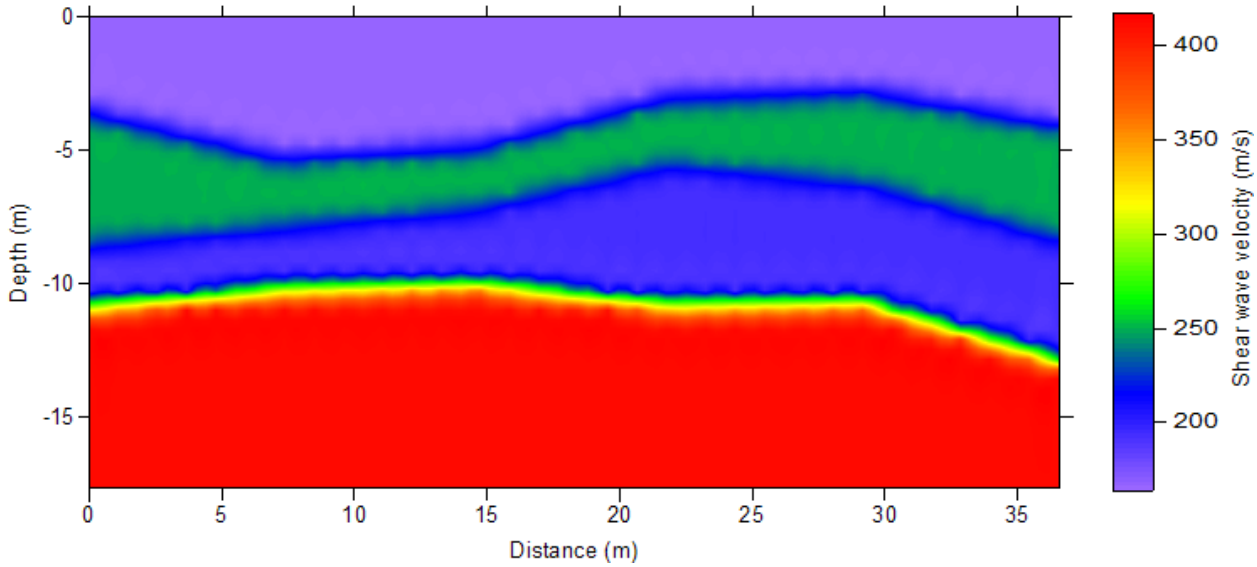

Figure 5-27. Inversion result of shear wave velocity (m/s) profile for the real data set at TAMU.

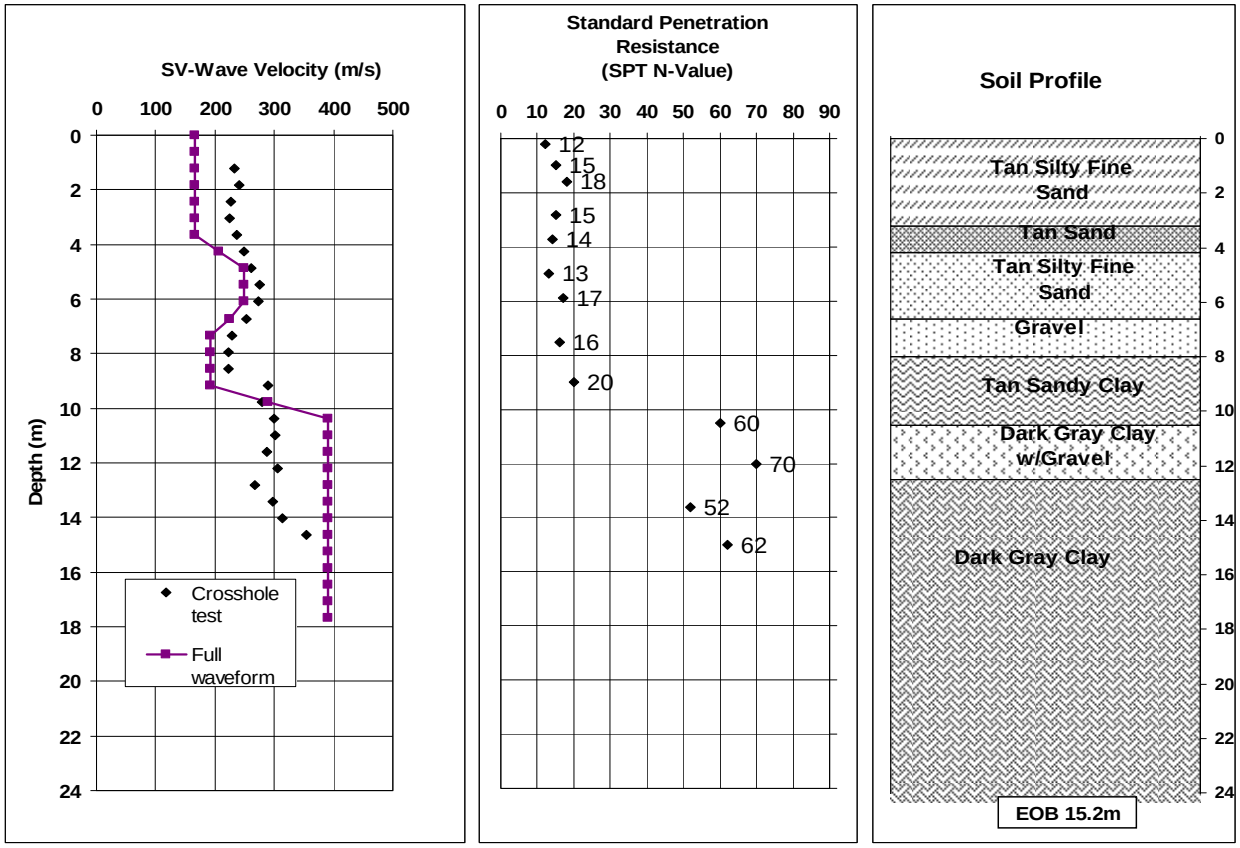

Figure 5-28. Composite soil profile of TAMU.

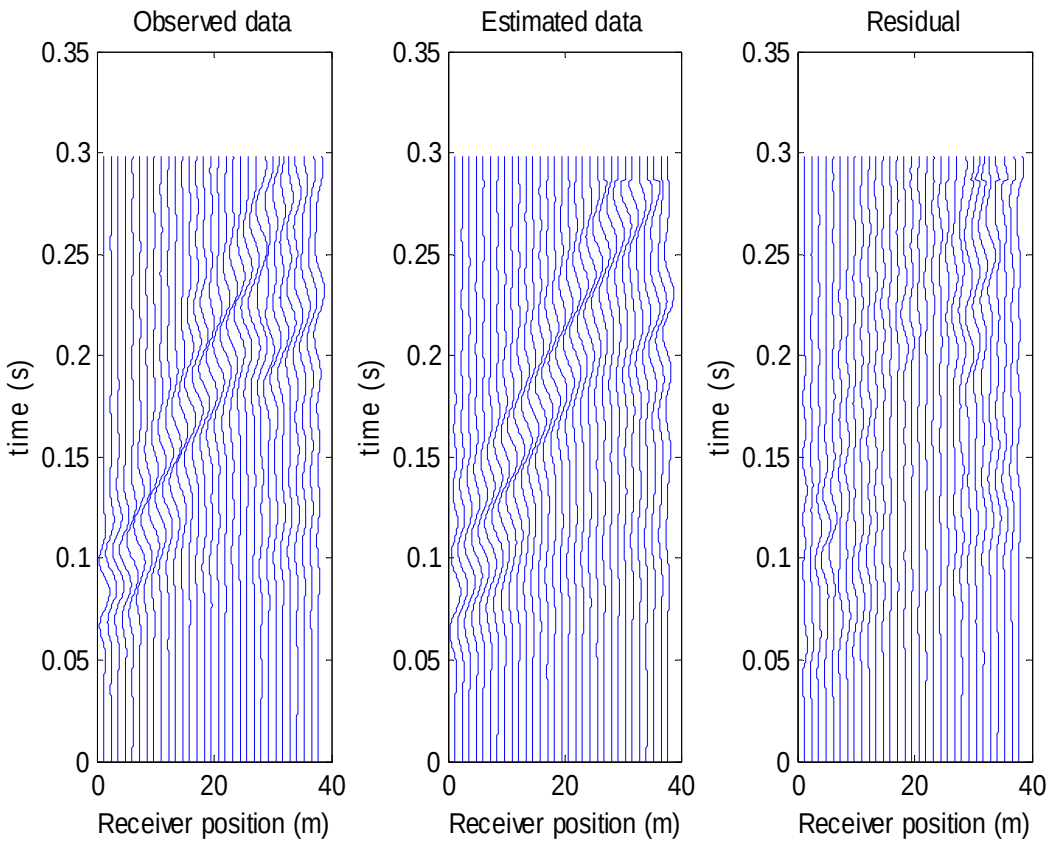

Figure 5-29. Comparison between observed wave field and estimated wave field for the real data set at Newberry.

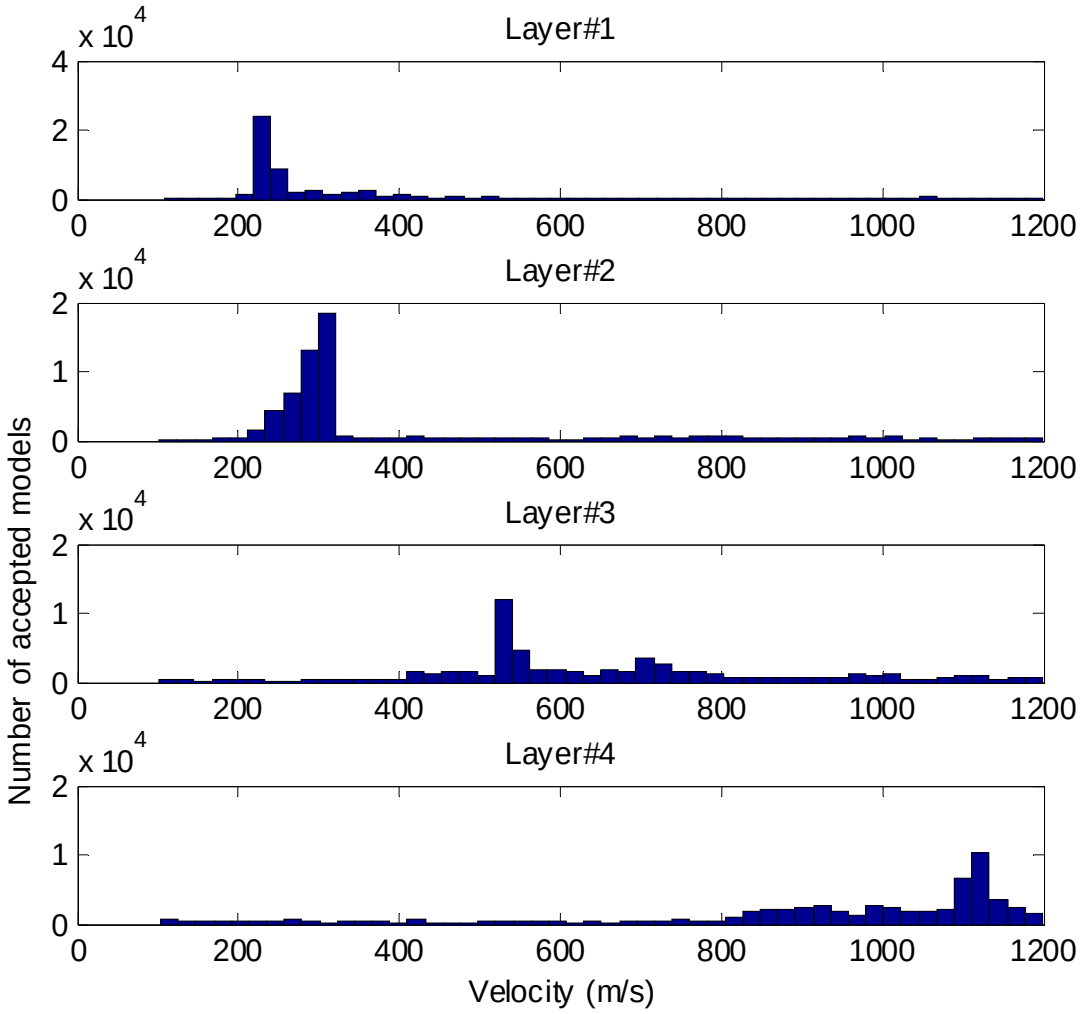

Figure 5-30. Velocity histograms from all accepted models for the real data set at Newberry.

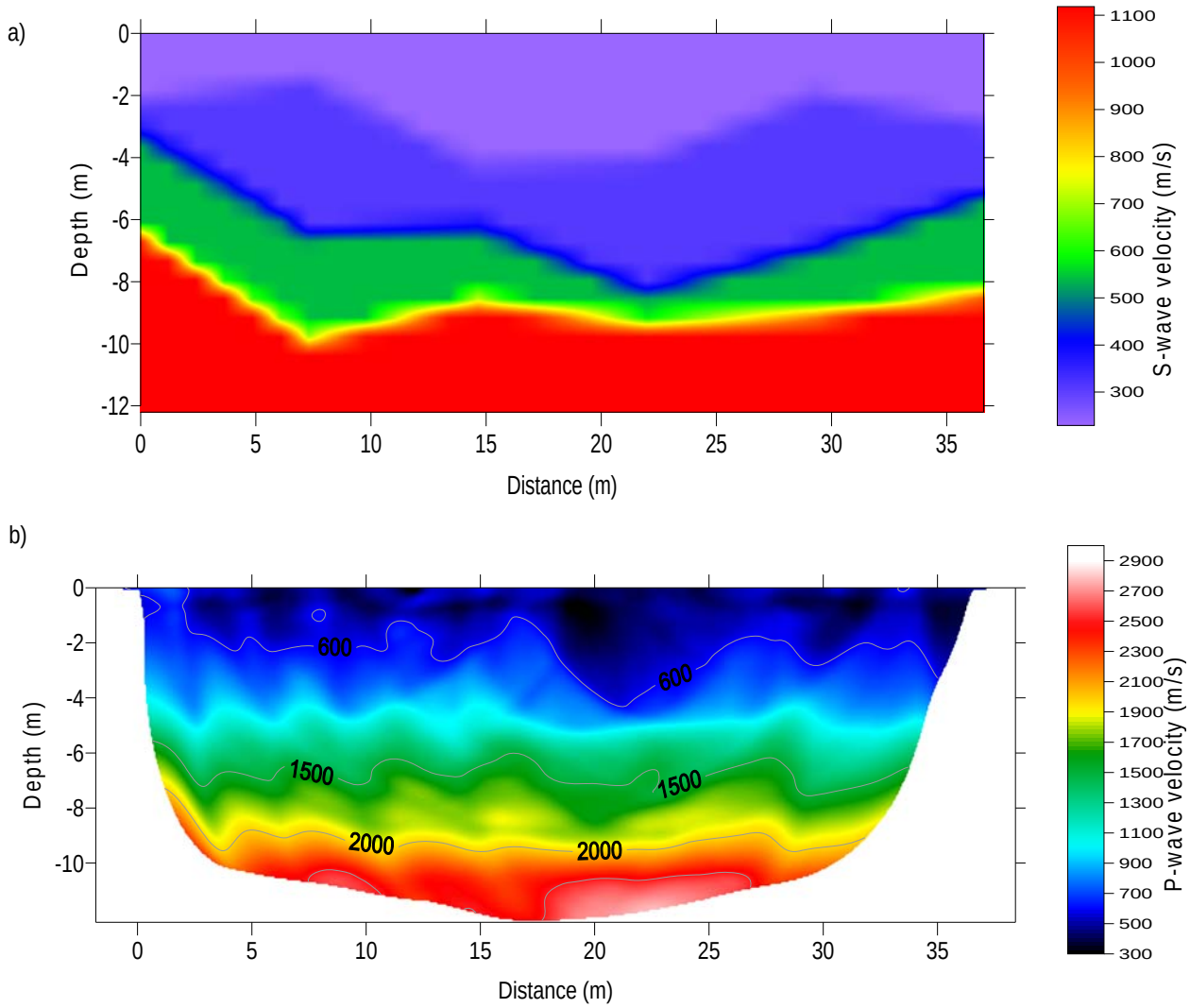

Figure 5-31. Newberry test site: a) S-wave tomogram from the full wave field, and b) P-wave tomogram from refraction travel times

CHAPTER 6
CLOSURE

6.1 Summary of Findings

Two inversion techniques using simulated annealing have been developed to invert travel times and full waveforms for wave velocity profiles. They are first tested on synthetic data and then applied to real test data. The inverted profiles from the real test data are compared to other independent test results such as those of CPT, SPT, geotechnical borings, and cross-hole test to verify the feasibilities of the techniques for geotechnical engineering applications.

6.1.1 Inversion Technique Using Travel Times

The technique using travel times is based on an extremely fast finite-difference solution of the Eikonal equation to compute the first-arrival time through the velocity models by the multi-stencils fast marching method. The core of the simulated annealing, the Metropolis sampler, is applied in cascade with respect to shots to significantly reduce computer time. This technique has been applied to surface data, and to combined surface and borehole data.

For the cases of only surface data, the following findings have been derived:

- Tested on synthetic data, the presented technique produces inverted results consistent to those from commercial codes including GeoCT-II, SeisImager, and Rayfract, and it performs better than those codes in cases of sharp contrasts in velocity.
- Applied to real test data, the presented technique produces inverted results that appear consistent to those from invasive tests including CPT, SPT, and geotechnical borings. Using surface travel times, the technique can well characterize normal profiles that increase in velocity with depth.
- Although the presented technique requires more computer time than the three mentioned commercial packages, it has several advantages. First, this inversion technique does not depend on the initial model and becomes important in regions where prior information about subsurface profiles is not available. Second, simulated annealing provides a suite of final models clustering around the global solution and having comparable least-squared error. This provides an inversion result by averaging all of these models to mitigate the influence of noise and the non-uniqueness of the inversion solutions. Last, the technique also enables to determine the uncertainties associated with inverted results.

- As a typical limitation of surface-based refraction methods, the presented technique fails to detect anomalies such as low-velocity zones and embedded cavities. It also fails to characterize velocity structure below a few meters from the top of the half space (bottom layer), because the fastest rays only travel within these few meters at the top of the half space regardless of how very large the geophone spread is used.

For the cases of combined surface and borehole data, the following findings have been derived:

- Tested on synthetic combined data, the presented technique well characterizes velocity structures at depth near the borehole. Presence, location, general shape, and true velocity of embedded low-velocity zones are well characterized.

- Also tested on synthetic combined data, the presented technique requires just a few shot locations on the ground surface within a few meters around a borehole, surface geophones within this few meters, and a string of borehole geophones to reliably assess the subsurface properties at depth near the borehole.

- Applied to real test combined data, the presented technique produces credible inverted velocity profiles. A comparison of tomograms utilizing the combined data against tomograms developed using just the surface data suggests that significant additional resolution of inverted profiles at depth are obtained with the addition of a borehole. It is also found that the quantitative uncertainties associated with the inverted profiles are significantly reduced when adding a borehole.

- Employed for site characterization of deep foundation design, refraction tomography using combined surface and borehole data provides credible information of material at the socket and partially detect anomalies near the socket. This becomes very important because the material at and near the socket often carries a majority of load from foundations. The inversion results of the combined data, including inverted profiles and associated uncertainties, enable to characterize spatial variability in geotechnical engineering physical parameters of subsurface formations useful in the design of deep foundations. This will be particularly useful in implementing the new LRFD design methodology that can explicitly account for spatial variability and uncertainty in design parameters.

6.1.2 Inversion Technique Using Full Waveforms

The technique using full waveforms is based on a finite-difference solution of 2-D elastic wave equation in the time distance domain. It uses full information of elastic wave fields to increase resolution of inversion results, especially dealing with reverse models. It also employs a global inversion technique, simulated annealing, to invert the full wave fields for near-surface velocity profiles. The technique is first tested on many different synthetic data sets created from

challenging reverse models with high-velocity and low-velocity layers at different depths. Then it is applied to experimental data sets, and the inversion results are compared to invasive test results including cross-hole, SPT N-value, and material log, or compared to results of independent refraction tests. The following findings about the technique have been derived:

- Tested on 1-D synthetic models, the presented technique performs well on reverse models and shows superiority over the traditional techniques using Rayleigh wave velocity dispersion.
- Tested on 2-D synthetic models, the presented technique shows that 2-D profiles with multi-linear interfaces of a few meter segments can be characterized using a full wave field from only one source.
- Applied to real full waveform data, the presented technique produces inverted results that appear consistent to those from invasive tests including SPT, cross-hole test, and geotechnical borings. The inverted results from the full waveform data also appear consistent to the inverted results from the refraction travel times.
- Besides its superiority over the traditional methods in dealing with reverse profiles, the presented technique possibly replaces the seismic refraction tomography to characterize normal profiles (increasing velocity with depth) because it requires much less effort in both site testing and manual data processing.
- The presented technique does not depend on the initial model and becomes important in regions where prior information about subsurface profiles is not available. Simulated annealing provides a suite of final models clustering around the global solution and having comparable least-squared error. This provides an inversion result by averaging all of these models to mitigate the influence of noise and the non-uniqueness of the inversion solutions.

6.2 Conclusions

Based on the findings outlined above, the following conclusions are made. First, the technique using travel times can well characterize normal profiles (increasing in velocity with depth) using only surface data and it also well characterize profiles with embedded anomalies using combined surface and borehole data. The inverted results from travel times appear consistent to those from invasive tests including CPT, SPT, and geotechnical borings. Second, the technique using full waveforms can accurately characterize challenging reverse models

including high- and low-velocity layers with only surface data. The inverted results from full waveforms are consistent with those from invasive tests including SPT, cross-hole test, and geotechnical borings. The inverted results also appear consistent to the inverted results from the refraction travel times. Last, both inversion techniques do not depend on the initial model and become important in regions where prior information about subsurface profiles is not available. Simulated annealing provides a suite of final models clustering around the global solution and having comparable least-squared error. This provides an inversion result by averaging all of these models to mitigate the influence of noise and the non-uniqueness of the inversion solutions.

6.3 Recommendations

The following recommendations are suggested after reviewing all of the findings and conclusions previously discussed:

- The developed inversion techniques should be applied in commercial software.
- Full waveform inversion technique should be investigated more. For example, using data from multiple shots to increase the resolution of inverted profiles, in such a case, the medium can be divided into many small cells and velocity of each cell is determined independently.
- Guidelines for array design and depth of investigation of the full waveform technique are needed.
- The global inversion techniques could be followed by a local inversion technique in order to save computer time.

LIST OF REFERENCES

Burger, H. R. (1992). "Exploration geophysics of the shallow subsurface." Prentice-Hall, Inc., Englewood Cliffs, New Jersey.

Carpenter, P. J., Higuera-Diaz, I. C., Thompson, M. D., Atre, S., and Mandell, W. (2003). "Accuracy of seismic refraction tomography codes at karst sites." *Geophysical Site Characterization: Seeing Beneath the Surface, Proceedings of a Symposium on the Application of Geophysics to Engineering and Environmental Problems, San Antonio, Texas, April 6-10*, 832-840.

Chopp, D.L. (2001). "Some improvements on fast marching method." *SIAM J. Scientific Computing*, 23(1), 230-244.

Clayton, R. and Engquist, B. (1977). "Absorbing boundary condition for acoustic and elastic waves." *Bull. Seimol. Soc. Am.*, 67(6), 1529-1540.

Dijkstra, E.W. (1959). "A note on two problems in connection with graphs." *Numer. Math. J.* , 1, 269-271.

Doyle H. (1995). "Seismology." J. Wiley & sons, Chichester.

Foti S. (2000). "Multistation methods for geotechnical characterization using surface waves." Ph.D. dissertation, Politecnico di Torino.

Hassouna, M.S. and Farag, A.A. (2007). "Multistencils fast marching methods: a highly accurate solution to the eikonal equation on cartesian domains," *IEEE Trans. Patt. Anal. Mach. Int.*, 29(9), 1-12.

Hiltunen, D. R. and Cramer, B. J. (2008). "Application of seismic refraction tomography in karst terrane." *Journal of Geotechnical and Geoenvironmental Engineering,* 134(7), 938-948.

Ingber, L. (1989). "Very fast simulated reannealing." *Math. Comput. Modeling*, 12(8), 967-993.

Ingber, L. (1993). "Simulated annealing: practice versus theory." *Math. Comput. Modeling*, 18(11), 29-57.

Jin, X., Luke B., and Calderon-Macias C. (2009). "Role of forward model in surface-wave studies to delineate a buried high-velocity layer." *Journal of Environmental and Engineering Geophysics,* 14(1), 1-14.

Kim, S. (1999). "ENO-DNO-PS: A stable, second-order accuracy eikonal solver." *Soc. Exploration Geophysicists*, 1747-1750.

Li J. (2008). "Study of surface wave methods for deep shear wave velocity profiling applied in the upper mississippi embayment." Ph.D. dissertation, University of Missouri – Columbia.

Louie, J. N. (2001). “Faster, better, shear-wave velocity to 100 meters depth from refraction microtremor arrays.” *Bulletin of Seismological Society of America*, 91(2), 347-364.

Metropolis, N., Rosenbluth A., Rosenbluth M., Teller A., and Teller E., (1953). “ Equation of State Calculations by Fast Computing Machines.” *J. Chem. Phys.*, 21(6), 1087-1092.

Moser, T.J. (1991). “Shortest path calculation of seismic rays.” *Geophysics*, 56, 59-67.

Nakanishi, J. and Yamaguchi, K. (1986). “A numerical experiment on non-linear image reconstruction from first arrival times for two-dimensional island structure.” *J. Phys. Earth*, 34, 195-201.

Nazarian, S. (1984). “In situ determination of elastic moduli of soil deposits and pavement systems by spectral-analysis-of-surface-waves method.” Ph.D. Dissertation, The University of Texas at Austin.

Nichols, D.E. (1996). “Maximum energy travel times calculated in seismic frequency band,” *Geophysics*, 61, 253-263.

O’neil, A. (2003). “Full-waveform reflectivity for modeling, inversion, and appraisal of seismic surface wave dispersion in shallow site investigations.” Ph.D. dissertation, The University of Western Australia.

Park, C. B., Miller, R. D., and Xia, J. (1999), “Multi-channel analysis of surface wave (MASW),” *Geophysics*, 64(3), 800-808.

Pratt, R. G. (1998). “Seismic waveform inversion in the frequency domain, part 1: theory and verification in a physical scale model.” *Geophysics*, 64(3), 888-901.

Pullammanappallil, S.K. and Louie, J.N. (1994). “A generalized simulated annealing optimization for inversion of first arrival time.” *Bull. Seimol. Soc. Am.*, 84(5), 1397-1409.

Quigley, T. P. (2006). “Ground proving seismic refraction tomography (SRT) in laterally variable karstic limestone terrain.” Master’s Thesis, University of Florida.

Redpath, B. B. (1973). “Seismic refraction exploration for engineering site investigations.” *Technical Report TR E –73-4*, U. S. Army Engineer Waterways Experiment Station Explosive Excavation Research Laboratory, Livermore, California, May.

Sambridge M. and Mosegaard K. (2000). “Monte carlo methods in geophysical inverse problems,” *Reviews of Geophysics*, 40(3).

Sharma, S.P. and Kaikkonen, P. (1998). “Two-dimensional non-linear inversion of VLF-R data using simulated annealing.” *Geophysics J, Int.*, 133, 649-668.

Sheehan, J.R., Doll, W.E., and Mandell, W.A. (2005). “An evaluation of methods and available software for seismic refraction tomography analysis.” *Journal of Environmental and Engineering Geophysics*, 10, 21-34.

Sheen, D. H., Tuncay, K., Baag, C. E., and Ortoleva1, P. J. (2006). "Time domain Gauss–Newton seismic waveform inversion in elastic media." *Geophysical Journal International*, 167, 1373-1384.

Shipp, R. M. and Singh, S. C. (2002). "Two-dimensional full wavefield inversion of wide-aperture marine seismic streamer data." *Geophysical Journal International*, 151, 325-344.

Sen, M.K. and Stoffa, P.L. (1991). "Nonlinear one-dimensional seismic waveform inversion using simulated annealing," *Geophysics*, 56, 1624-1638.

Sen, M.K. and Stoffa, P.L. (1995). "Global optimization methods in geophysical inversion," *Adv. Explor. Geophysics*, 4, Elsevier Sci., New York.

Sethian, J.A. (1996a), "Fast marching set level method for monotonically advancing fronts," *Pro. Nat. Acad. Sci.*, 93.

Sethian, J.A. (1999). "Level set methods and fast marching methods," second ed. Campridge Univ. Press.

Tokimatsu, K., Tamura, S., and Kojima, H. (1992). "Effects of multiple modes on Rayleigh wave dispersion characteristics." *J. Geotech. Eng.*, 118 (2), 1529–1543.

Thomson W.T. (1950). "Transmission of elastic waves through a stratified solid medium." *J. Applied Physics*, 21(1), 89-93.

Van Trier, J. and Symes, W. (1991). "Upwind finite-difference calculation of travel times." *Geophysics*, 56, 812-821.

Vidale, J.E. (1988). "Finite-difference travel time calculation." *Bull. Seis. Soc. Am.*, 78, 2062-2076.

Virieux, J. (1986). "P-SV wave propagation in heterogeneous media: velocity-stress finite-difference method." *Geophysics*, 51(4), 889-901.

Zhang, J. and Toksoz, M.N., (1998). "Nonlinear refraction traveltime tomography." *Geophysics*, 63(5), 1726-1737.

BIOGRAPHICAL SKETCH

Khiem Tat Tran was born in 1978 in Thanh Hoa, Vietnam, and remained in Thanh Hoa until he graduated from Lam Son High School in 1996. He enrolled in Hanoi University of Civil Engineering, and graduated with a Bachelor of Science in civil engineering in spring 2001. He decided that it would be most beneficial to gain a few years of work experience before continuing on with graduate studies so he worked for five years in Vietnam until he moved to United States for studying. He enrolled at the University of Florida in Gainesville, FL in August of 2006 where he worked as a graduate research assistant under Dr. Dennis Hiltunen. He completed his Master of Science in May of 2008 and Doctor of Philosophy in August of 2010.